The Dissertation Committee for Jingjing Sun Certifies that this is the approved version of the following dissertation:

Quantitative Body Shape Analysis for Obesity Evaluation

Committee:

Bugao Xu, Supervisor

Mia K. Markey

Christopher A. Jolly

Pengyu Ren

Thomas E. Milner

Quantitative Body Shape Analysis for Obesity Evaluation

by

Jingjing Sun, B.E.; M.S.T.A.T; M.E.

Dissertation

Presented to the Faculty of the Graduate School of

The University of Texas at Austin

in Partial Fulfillment

of the Requirements

for the Degree of

DOCTOR OF PHILOSOPHY

The University of Texas at Austin

May 2016

Dedication

To my dear parents Li Sun and Jinyong Liu,

And to my wonderful husband Tianyi Wang.

Acknowledgements

I would like to express my special appreciation and thanks to my supervisor, Professor Bugao Xu, for his continuous support and encouragement throughout my whole PhD study. It is he who brought me into this research area, inspired me to freely express my ideas and explore my interests, and provided me with insightful advices and suggestions guiding me to my research goals. I will always remember the guidance and inspiration he provided in every step of my research.

My sincere gratitude is reserved for my committee members at the University of Texas at Austin who always supported me: Drs. Mia K. Markey, Pengyu Ren, Thomas E. Milner and Christopher A. Jolly. Completion of this dissertation would not be possible without their support and advice.

I would like to extend my appreciations to my labmates and precious friends, especially, Dr. Ming Yao, Zuyun Zhao, Wenbing Ouyang, Dr. Yeyi Zhu and Bingfei Gu. Their warm-hearted help and suggestions have made the past four and a half years a joyful and wonderful memory to me. I am also thankful to Professor Freeland-Graves and her students, Drs. Reese Pepper and Jane Lee.

I would like to express my deepest love and appreciation to my dear parents Li Sun and Jinyong Liu for their years of sacrifices and unconditional love. To my wonderful and intelligent husband Tianyi for editing my dissertation with great patience, for always

supporting me in my academic pursuits and for love, care, and encouragement throughout the years. I can barely accomplish anything without you.

Last but not least, my heartfelt thanks go to Mr. and Mrs. Boudreaux and all my friends in the Life Group. Thank you for always being there and listening to me especially when I felt stressed in my research. I feel incredibly lucky to have you all in my life. Finally, I thank my God, the Almighty, who has been giving me all strength to complete this dissertation.

Quantitative Body Shape Analysis for Obesity Evaluation

Jingjing Sun, Ph.D.

The University of Texas at Austin, 2016

Supervisor: Bugao Xu

Obesity is a public health concern as it is associated with a number of diseases, such as diabetes mellitus type 2, cardiovascular disease, some forms of renal failure and certain types of cancers. Growing evidence suggests that it is not only the amount of fat, but also its distribution in the body that is important to predict metabolic risk factors and adverse changes in organs. In this respect, it is necessary to develop convenient and inexpensive measures to characterize human body fat distribution and to investigate the unknown linkage between intrinsic adiposity and external body shape.

This dissertation research aims to improve the obesity assessment by developing new quantitative measurements that comprehensively characterize body shape, and are highly relevant to intrinsic abdominal adiposity conditions. The proposed body shape descriptors were defined based on three-dimensional body images reconstructed from a custom-made stereovision body imaging system, which is particularly suitable for clinical use as an obesity monitoring equipment for its high portability and affordability.

In this study, we developed a fully-automated algorithm to process T1-weighted magnetic resonance imaging (MRI) slices for abdominal adiposity measurements. This algorithm dramatically reduces the processing time and workload compared with

traditional manual or semi-automatic methods for MRI processing, and greatly improves the repeatability and objectivity of fat assessments. A new obesity categorization method was then defined based on MRI adiposity data to depict characteristics of abdominal fat distribution, and the associations between the body shape descriptors and the MRI abdominal adiposity were explored. It was shown that the proposed body shape descriptors are able to capture the body shape differences between the subjects with dissimilar internal fat distribution (i.e., different categories), and to provide excellent prediction for the category of fat distribution through an optimized support-vector-machine classifier. The predictive models established in this dissertation demonstrate that the novel body shape descriptors were also effective for prediction of the volumes of abdominal visceral fat and subcutaneous fat accumulated in male and female adults.

This dissertation introduces an innovative approach to assess obesity and fat distribution based on newly defined shape descriptors, and provides new findings that reveal the associations of intrinsic fat distribution with external body shapes, which enable both qualitative and quantitative assessment of obesity from body shape measurements.

Table of Contents

List of Tables

List of Figures

Chapter 1 Introduction

1.1 MOTIVATIONS AND RESEARCH OBJECTIVES

Currently, 33.1% adults are overweight and 35.7% are obese in the United States [1]. Excessive body fat is associated with high risks of diabetes mellitus type 2, cardiovascular disease, chronic renal failure and certain types of cancers [2]–[4]. The prevalence of obesity necessitates a safe, accurate, reliable and convenient method for obesity evaluation. Instrumental methods such as magnetic resonance imaging (MRI) [5], computed tomography (CT) [6] and dual energy x-ray absorptiometry (DXA) [7] have shown the ability to directly measure fat volume or fat percentage of the human body. Yet, the high capital expense, operational cost and sophistication associated with these instruments limit their use in field settings. Furthermore, the utilization of DXA and CT may be restricted due to the risk of radiation exposure. Bioelectrical impedance analysis (BIA) [8], air displacement plethysmography (ADP) [9] and underwater weighing (UWW) [10] were developed to estimate body compositions and body fat percentage. The accuracy of these techniques is limited because they are based on pre-defined body compartment assumptions which may not meet in certain population.

Traditional anthropometric measurements, including body mass index (BMI), waist circumference (WC) and waist to hip ratio (WHR), have been widely used to evaluate the obesity for their simplicity and cost-effectiveness for many years [11]–[14]. However, accuracy and efficacy of these simple measurements are questionable. The Emerging Risk Factors Collaboration involving 220,000 individuals and >14, 000 cardiovascular events

in 17 countries [15], concluded that BMI, WC and WHR do not improve the prediction accuracy for cardiovascular disease when concurrent blood-test data are available, and BMI has the similar strength of association with coronary heart disease and ischemic stroke as WC and WHR. These findings contradicted many previous studies [2], [12], [16]–[20] and caused a worldwide controversy on the validity of the current anthropometric measurements for obesity research [21]–[23].

These discrepancies revealed the drawbacks of the traditional measurements. First, inherent errors in the manual measurements may weaken the intra- and inter-observers' reliability [19]. Lack of a universal protocol of tape measurements may result in wide heterogeneity in the data [24]. Second, the traditional measurements may not represent sufficient information of individuals' adiposity conditions. For example, it is well known that BMI ignores body composition and shape [25]. WC and WHR contain no information of anatomical location of the fat depots (i.e. visceral adiposity and subcutaneous adiposity). Previous studies suggested that visceral adiposity is a unique, pathogenic fat depot that is highly correlated to metabolic factors [26], while subcutaneous adiposity is associated with adiponectin levels and insulin resistance [27]. Hence, it is not only the amount of fat, but also its distribution and anatomic locations in the body that is related to disease risks. However, the traditional measurements are not able to provide such in-depth information. Third, although it is widely accepted that the body shape is related to metabolic risk factors, there is currently no efficient method that comprehensively and quantitatively characterizes human body shape. Therefore, the relationship between body shape and intrinsic adiposity remains to be explored.

In order to address the aforementioned drawbacks and challenges existing in the current obesity evaluation methods, the overall goal of this dissertation is to develop new obesity evaluation measurements (i.e. body shape descriptors) that can characterize body shape and are highly relevant to intrinsic abdominal adiposity. The innovative shape descriptors based on a custom-made stereovision body imaging (SBI) system are used to elucidate the unexplored linkage between external shape features and internal fat depots.

Objectives of my research are achieved through the following specific aims:

(1) Develop an image processing algorithm for unsupervised quantification of visceral and subcutaneous adipose tissue volumes from MRI.

(2) Design novel body shape descriptors to quantitatively characterize overall and central obesity using three-dimensional (3D) images.

(3) Explore a novel obesity categorization method using MRI adiposity data and develop new classifier to predict the categorizations using body shape descriptors and the conventional obesity measurements.

(4) Investigate the associations between external shape features and intrinsic fat depots and develop mathematical equations for abdominal subcutaneous and visceral adiposity prediction.

1.2 METHODS FOR ASSESSING OBESITY

1.2.1 Anthropometric measurements

Body mass index (BMI) measured by a subject's weight in kilograms divided by the square of height in meters, is one of the most commonly used anthropometric

measurement to assess overall obesity conditions. Based on the calculated BMI value in kg/m^2, each individual can be categorized into different classes: underweight (BMI < 18.5), normal ($18.5 \leq BMI \leq 24.99$), overweight ($25 \leq BMI \leq 29.99$) and obese (BMI > 30). The obese class can be further divided into three sub-classes: obese class I ($30 \leq BMI \leq 34.99$), obese class II ($35 \leq BMI \leq 39.99$) and obese class III (BMI > 40). BMI is convenient to use for preliminary screening in clinical and field settings.

Skinfold thickness [28], [29] is an older measure that uses a special caliper to measure the thickness of skin and fat at specific locations of the body, such as abdomen, triceps and thighs. This method is easy to perform; however, it is suffering from low reproducibility and not able to provide adequate accuracy for the subjects with high BMI.

Waist circumference (WC) [30] measures the central obesity which is defined as the excessive fat accumulated around waist and abdomen. WC shows higher correlation with obesity-related health risks compared with BMI [31]. WC is also highly correlated with levels of plasma lipids and lipoprotein in children [32]. WC is easy to measure, however, there is currently no standard protocol of the measuring location [33]. In addition, the WC measured by tape is notoriously subjective. Hip circumference (HC) and thigh circumference (TC) are the ways to measure gynoid fat which is the adiposity located around hips, thighs and bottom. Studies have shown that HC and TC are two inverse risk estimators associated with lower risk of type 2 diabetes and other health risks [27], [28].

Several measurements based on the ratio of the anthropometric measurements are also frequently used. Waist to hip ratio (WHR), waist to height ratio (WHtR) and body adiposity index [11] provide information of overall fat distribution. A number of studies

showed that they are effective estimators of cardiovascular diseases, metabolic risks and health disorders [36]–[38]. Sagittal diameters (SAD) measures the distance between the back and the upper abdomen with a special stool. SAD is considered as a measure of visceral fat and has been shown to be related to cardiovascular risk factors and metabolic variables [39]–[42].

The conventional measurements mentioned above are commonly used in clinical settings for routing obesity evaluation because they are inexpensive and relatively simple. However, limitations of those measurements affecting the accuracy of obesity diagnosis should not be underestimated. First, manual methods without universal protocol are known to be problematic. For example, a previous study reported 14 different definitions in three different manuals and reference guides for WC measurements [33]. Second, manual tape measurements are notoriously subjective to low intra- and inter-observer repeatability[19]. In addition, awkwardness resulting from the proximity between the observer and the patient may cause the patient's reluctance to be evaluated.

1.2.2 Densitometric measurements

Densitometry based measurements have been used to estimate individuals' body density for studying human body composition. A number of models were established for body composition on the level of atomic, molecular, cellular, tissue-organ and whole body. The most commonly used model is based on the molecular level which considers the major components of human body are water, protein, mineral and fat. Siri [43] proposed a simplified model that human body can be divided into two compartments: fat mass (FM)

and fat free mass (FFM) which includes protein, mineral and total body water. Initial assumption of Siri's model is that the density of the FM and the density of the FFM are constant values of 0.9 kg/L and 1.1 kg/L, respectively. Then body fat percentage (*%BF*) can be calculated as:

$$\%BF = (\frac{4.96}{D_b} - 4.50) \times 100\% \tag{1.1}$$

,where D_b is the body density measured by special techniques.

Underwater weighing (UWW) (i.e. hydrodensitomery) is one of the techniques [44] that measures total body volume using Archimede's principle. During the UWW procedure, a subject is completed submerged in water. Then the total body volume can be estimated by the weight difference of the subject before and after the submerging. The D_b can be calculated by:

$$D_b = \frac{M_a}{(M_a - M_w) / D_w - RV} \tag{1.2}$$

,where M_a and M_w are mass in air and mass in water, respectively. D_w is the density of water (pre-determined at specific temperature), RV is the residual volume (i.e. unfilled space in the lungs) [45]. Although UWW is simple and inexpensive, it is not suitable for children, elders or certain patients who cannot be submerged in water.

Air displacement plethysmography (ADP) [46] is a device estimating body density based on air displacement instead of water immersion. A popular commercialized version is the BodPod (Life Measurement Instrument, Concord, CA) [47]. In this procedure, a subject wearing bathing suits is asked to sit in a closed chamber. The volume of the subject

can be measured by the changed volume of air based on Bolye's law when a subject sits inside. Bolye's law states that under stable temperature, air volume would be increasing with the reduction of its pressure [48]. Although ADP is more comfortable to use than UWW, its usage is limited due to the high cost (more than $40,000 per unit).

The densitometric methods either using UWW or ADP are indirect estimation of the %BF, not direct measurements of the body compartments and therefore, the accuracy is limited. The accuracy also largely depends on the assumption of the two compartments model (Equation 1.1), which may need adjustments when use it on infants, children and the patients who has constantly changing proportions of FFM. For these subjects, a four compartment model consisting of the measurements of body mass, volume, total body water and bone mineral is considered as a more accurate model. However, specialized equipment is required for this four compartment model and its usage is highly restricted [49].

1.2.3 Body composition measurements

Bioelectric impedance analysis (BIA) is a simple, non-invasive and inexpensive tool to estimate body composition by measuring resistance of human body to alternating current [50]. BIA assumes that 73% of the FFM is water. The more muscle a person has, the more water his/her body can contain and the easier for electric current to pass through [51], while high resistance of the current means greater amount of body fat. Single-frequency BIA is frequently used for assessing total body water and thus estimating FFM to date. Multi-frequency BIA can provide higher accuracy of the FFM estimation, but it is

less appealing to large-scale study in that it is less portable and more expensive [52]. The accuracy of the BIA depends on individual's hydration level which may be affected by illness, dehydration and weight loss.

Dual energy X-ray absorptiometry (DXA) was originally developed to measure bone density and bone loss using an enhanced form of X-ray. When applying DXA to measure obesity, DXA directly measures X-ray photon energy attenuation passing through the three pre-defined types of body tissue: fat, non-fat lean tissue and non-fat bones. The typical energy levels of the photon utilized by DXA are 40 and 70 keV. The visualization and segmentation analysis of the body fat were realized by the different attenuation rates of these three tissue types from a single whole body scan [53]. Studies have shown that the radiation dosage to patients from a DXA whole body scan is relatively small compared with other sources of exposures [54]. For instance, the radiation exposure from DXA scan is equivalent to less than 10% of a chest radiography. DXA has been reported to be convenient and relatively safe to measure regional fat mass. DXA is also sensitive enough for assessing weighty loss [55]. Hence, DXA is an attractive technique for evaluating %BF and regional fat mass in clinical settings. Nevertheless, several studies have reported the limitations of the DXA. Snijder reported that DXA underestimated abdominal fat by 10%, compared with computed tomography [56]. Wong suggested that DXA may not be the optimal method for measuring body fatness for young female subjects since it may underestimated or overestimated by 28% [57]. Moreover, the measurement generated from DXA varies according to different manufacturers, scanners and software package [58]–[60].

Both computed tomography (CT) and magnetic resonance imaging (MRI) are advanced imaging modalities that allow rapid imaging of internal body structures and accurate assessment of body composition. CT and MRI enable direct visualization of adipose tissue, skeletal muscles, bones and other internal organs as well as differentiation between visceral adiposity and subcutaneous adiposity. Basically, CT measures photon energy attenuation passing through different types of body tissue, and thus the subject has to be exposed to ionizing radiation [61]. Therefore, CT is not suitable for whole body obesity study and only limited number of image slices can be obtained from a human subject.

Adiposity can be easily identified on MRI slices since fat tissue show higher signal intensity and appear brighter in T1-weighted images. The slow molecular motion of a fat nucleus causes a quick regaining of longitudinal magnetization, resulting in short longitudinal relaxation time and higher image intensity [62], [63]. Without radiation, MRI is thus a safer and more favorable method for adiposity measurement [64].

In conclusion, MRI and CT have been considered as gold standards for body composition assessment. Both CT and DXA involve the application of radiation, while MRI is a safer technique without radiation or any known long-term side effects. MRI and CT are less attractive to large-scale practical use due to the low portability and high expenses.

1.3 METHODS FOR 3D BODY IMAGING

The demands for accurate, fast and convenient body dimension measurements have given rise to rapid developments of three dimensional (3D) body imaging modalities in recent years. Circumferences, volumes and further estimated body composition were now can be calculated by 3D body imaging systems. These 3D imaging systems provide a more objective and efficient way to assess body dimension compared with manual tape measurements. To date, 3D body images can be acquired through laser scanning, structured light and stereovision techniques. Here, we briefly introduce the currently available 3D imaging techniques and systems.

1.3.1 Current 3D body imaging techniques

1.3.1.1 Laser scanning

Triangulation and time-of-flight (TOF) are the two major technologies used in laser scanning systems. The triangulation based laser scanner projects laser dot or beam on an object and uses a CCD camera to look for location of the laser. The location of the laser presenting in the camera's field of view (FOV) is dependent on the distance between the object and the laser projector. The laser dot, the camera and the laser projector together form a triangular based on which the depth information of the object can be determined. Single-point probes and slit camera with projection of a laser line instead of dot have been developed for body dimension research and other industrial applications. The measuring range of the triangulation based scanner is limited within a few meters but the accuracy of

it is relatively high. Therefore, the triangulation based laser scanner is suitable for human body scan.

FOV based system employs a laser range finder which finds the distance between the laser emitter and the target by calculating the round-trip time of a light pulse. With the known speed of light c and round-trip time t, the distance can be calculated by $c \times t /2$. Of note, the accuracy of the FOV based laser system is highly dependent on the precision of the time measurement. Rotating mirror was frequently used with the FOV laser to change the laser direction. The strength of the FOV based laser scanner is that it can measure the object far away from the emitter, therefore, it can be used to scan large buildings and historical constructions.

A number of laser scanners have been proposed for human dimension research and obesity evaluations. Cyberware Inc. (US) developed WB4 which is one of the first laser scanners that captures the whole human body image [65]. Although this company was dissolved in 2011, it was considered as the worldwide leader in the area of body scanner development for a long time. Besides, Xu, et al. developed a laser body scanner which employs a rotary laser unit and enables whole body scanning with a relatively fast speed [66]. This system has been validated for circumference and body volume measurements and body composition estimation [67].

1.3.1.2 Structured light

Structured light based scanner sheds certain types of light patterns on the surface of an object and the distortion of the light pattern observed by cameras was used to

reconstruct 3D image of the object [68], [69]. Three commonly used light patterns are sequential binary-coded pattern, gray-level coding pattern and sinusoidal fringe pattern.

The binary pattern uses a series of light patterns containing black and white stripes to encode each point on the surface of the target [70]. It is noteworthy that the horizontal resolution is determined by the finest stripes on the pattern and quite a few patterns are required to achieve a good resolution. Gray-level coding pattern was developed to reduce the required number of patterns and scanning time [71]. Instead of using binary color, the gray-level coding pattern applies various levels of gray intensity to provide unique coding of the projection patterns. In addition, sinusoidal fringe pattern is a phase-shift pattern with continuous colors, which is frequently used to scan colored and dense structured surfaces and moving objects [72]. For example, the NY-16 body scanner developed by TC^2 (US) uses sinusoidal strip patterns to capture and reconstruct human body with 16 sensors preset on four corners of an imaging cube. The TC^2 scanner has been used to measure the body circumferences at various locations for obesity research [73]. Moreover, Mephisto EX (4DDynamics, Belgium) employs HDTV cameras to provide a high resolution of 3D body image based on structured light theory [74].

1.3.1.3 Stereovision

The imaging system based on stereovision technology greatly improves portability and the affordability of the system and significantly reduces acquisition time. In most cases, the stereovision imaging system consists of multiple cameras and projectors. The cameras are used to capture images from different angles, which are similar to human binocular

vision. In order to increase the texture of the target, the projectors are used to cast speckle or other types of light patterns. By analyzing the images captured from different angles, the relative depth information can be achieved from information of disparities which decreases with the increasing distance between cameras and objects. In comparison with laser and structured light based body scanners, stereovision system is fast in terms of data acquisition -- as quickly as taking a picture. This instantaneous image acquisition procedure effectively prevents the errors and artifacts caused by slightly body movements which are commonly seen in children.

Challenges of the stereovision system exist in computational process after the image acquisition. The major algorithms involved in stereovision imaging systems are camera calibration and registration, stereo matching and surface reconstruction [75], [76]. The development and implementation of these algorithms highly depend on specific applications and requirements of resolution, processing time and smoothness of the reconstructed model. In the following section, we will introduce the technical details of a customized stereovision system developed in our lab for body shape analysis and obesity research.

1.3.2 Customized stereovision body imaging (SBI) system

1.3.2.1 System setup

A stereovision system has been developed in our lab using the off-the-shelf components including eight cameras and four projectors as shown in Figure 1.1 [77]. Each stereo unit of the SBI system consists of a pair of cameras and one projector which is used

to generate artificial texture onto the human body during the scan. The four stereo units can cover upper-front, lower-front, upper-back and lower-back of the body for a whole body imaging. This setting is highly portable and affordable compared with other existing whole-body scanners.

Specifically, the resolution of each CMOS camera (Videre Design, Menlo Park, California) is 1280 × 960. The focal length and baseline length are 12mm and 90mm, respectively. The ultrashort throw projectors of NEC 575VT LCD (NEC, Corp., Tokyo, Japan) were employed. For each projector, the image size is 1.5×1.15m at the projection distance of 2.3m. Thus, two projectors are enough to cover the majority of the human subjects. Texture patterns were sent to the projectors from a dual-port graphic card via a video graphics array (VGA) hub. IEEE 1394 Firewire was utilized to assist the communication between a host computer and the cameras.

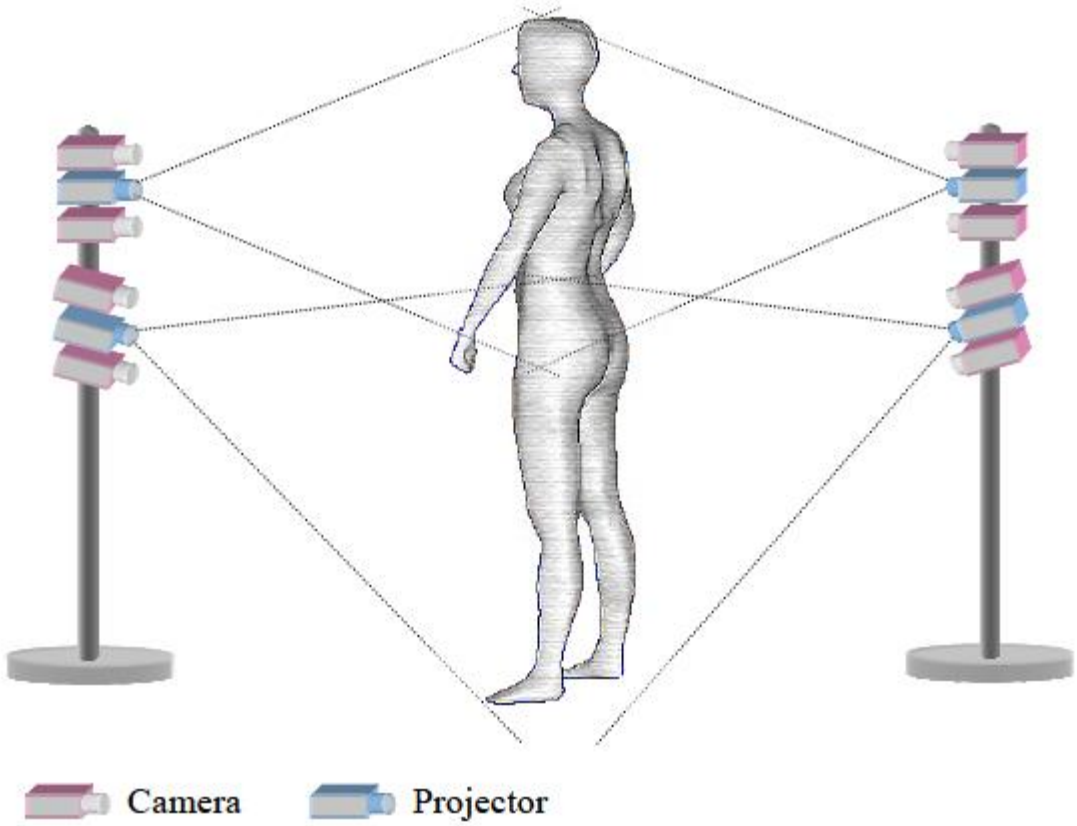

Figure 1.1 SBI system setup. Adapted from "Three-dimensional surface imaging system for assessing human obesity" by Bugao Xu et.al, 2009, *Optical Engineering, 48*, p. 107204-107204-11 [77].

1.3.2.2 Data processing algorithms

Major phases associated with the 3D scanning include image acquisition, system calibration, stereo matching and surface reconstruction. Next, key algorithms and procedures are introduced.

With the random texture pattern projected on an object, all four pairs of the cameras were captured simultaneously. During this 200ms image acquisition procedure, human subject needs to keep still. Due to the extremely short scanning time, this SBI system is appropriate to scan children, elders or specific patients who cannot stand still for a long time.

System calibration is required before the first time use or after transporting the SBI system to a different location. Firstly, intrinsic and extrinsic camera parameters were determined using a flexible camera calibration method proposed by Zhang [78]. The intrinsic parameters were used to correct the distortion caused by camera itself and the extrinsic parameters including rotation matrix and translation vectors were used to define the relative position of each camera pair. After that, the camera coordinate of each stereo unit was obtained and a 3D registration procedure was then performed to transform each camera coordinate to a common world coordinate system by using a rigid model with known 3D information.

Stereo matching procedure was employed to resolve the correspondence problem between different stereo units [79], [80] . There are two main problems to be solved by stereo matching: 1) Segment the foreground objects from the background and generating a disparity map. 2) Refine the disparity map from integer-pixel to sub-pixel accuracy which is essential for further obesity measurements. The results of the stereo matching are isolated 3-D points (around 1.2 million points) (Figure 1.2a). In order to make these points more manageable and interpretable, surface reconstruction is required [81]. Firstly, the original 3-D points are resampled, and the explicit neighborhood information of the resampled data

were used to generate a new dense mesh (Figure 1.2b). This dense mesh was further simplified to produce a control mesh (Figure 1.2c) which was then optimized by fitting its subdivision surface to the original data to create the final body model. An effective body surface reconstruction algorithm based on subdivision surface representation was employed to solve the gap between the front view and the rear view due to the invisible areas to the cameras. The final reconstructed 3D model is a good approximation to the original body data and smooth without noise, gaps or holes (Figure 1.2e).

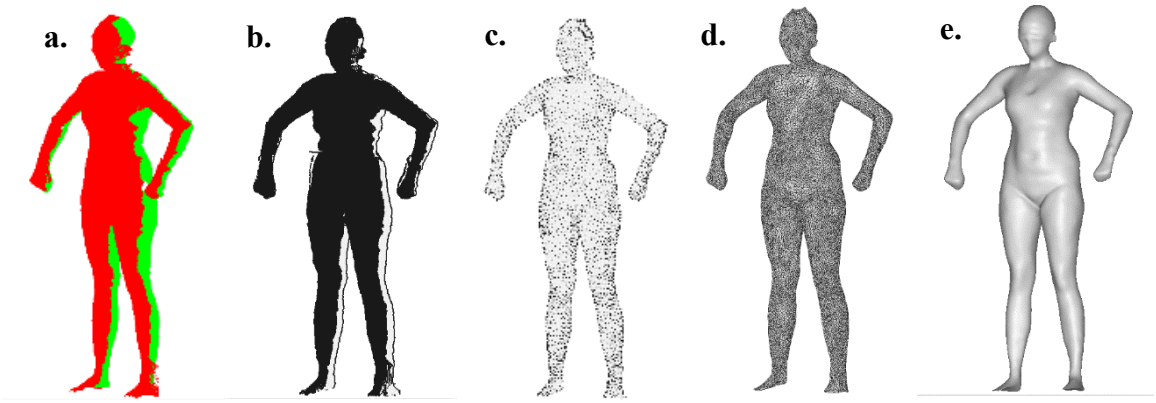

Figure 1.2 Example of surface reconstruction: (a) original 3-D data, red denotes front view and green shows rear view, (b) dense mesh, (c) simplified mesh, (d) final triangular mesh and (e) final shaded 3D model.

1.3.2.3 2D and 3D measurements

After reconstructing 3D body images, measurements can be obtained by using of an application programming interface (API): OpenGL which helps to render 2D and 3D vector graphics. Previous measurement algorithm proposed by our lab [82] employed the conception of depth buffer (i.e. z-buffer) since z is commonly used to denote the depth dimension in modern computer graphics. Such z-buffer provides a way to get the minimum and maximum depth for each pixel of a 3D model showing on a screen and the z-buffer is used to calculate the 2D and 3D body measurements. Specifically, a 3D body model was rendered twice in the anterior view. Then, the minimum and maximum depth of each pixel was calculated and two depth maps were generated for the front side and back side of the body, respectively. Based on the difference between the two depth maps, a thickness map covering the whole body was achieved. 3D information of each pixel on a desired contour can be easily obtained from the thickness map in order to calculate width, depth and circumference. Volume can be calculated by integrating the thickness of each pixel and the known pixel size calibrated at the beginning.

The SBI system can be applied to various fields besides obesity research, such as fashion design, clothes fitting and children development evaluation. Moreover, this system is able to calculate various types of measurements to accommodate to applications. Over a hundred parameters including circumferences, width, depth and cross-sectional area at neck, chest, upper- and under- bust, waist, abdomen, hip, thigh, mid-thigh, calf, ankle, wrist, bicep and elbow; whole and segmental volumes at arm, thigh, leg, trunk and hip; bust span, shoulder length, shoulder slope, pant outseam, crotch length, etc., can be

automatically measured from a 3D body image. Figure 1.3a and Figure 1.3b exemplify the reconstructed 3D image and several pre-defined landmark measurements on a female subject and a male subject, respectively. It should be noted that not all the measurements introduced here are relevant to obesity evaluation. Chapter 3 describes innovative body shape measurements developed in this dissertation to characterize body shape and fat distribution for obesity evaluations.

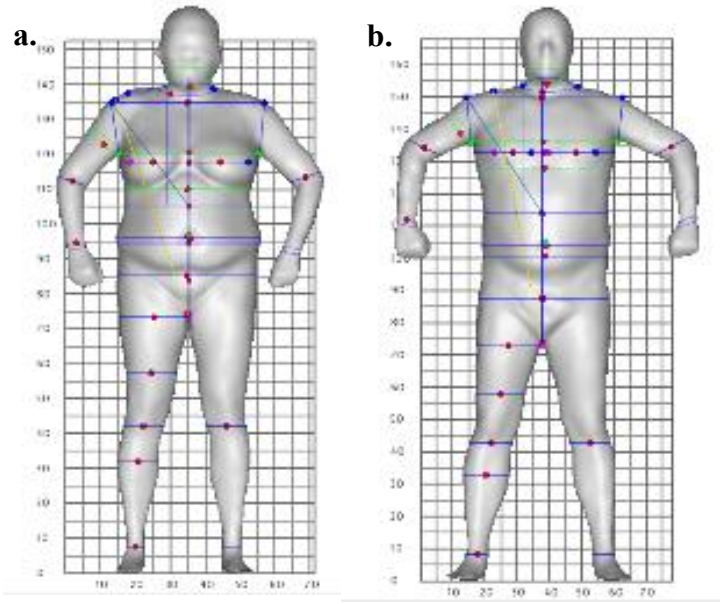

Figure 1.3 Examples of parameters measured by the SBI system with (a) female subject and (b) male subject.

1.4 DATASETS

1.4.1 Characteristics of subjects

The data used in this dissertation were obtained from a total of 121 subjects (66 men and 55 women) recruited via posted notice or word of mouth. Subjects with any serious illness, metallic fragments or implants were excluded from the study due to the risks involved with the MRI scan. Female subjects who were pregnant, or lactating were not recruited due to University regulations. Demographic and health history questionnaires were completed and anthropometric measurements, including weight, height, and body tape circumferences were also taken from all of the subjects. Subjects were aged from 19 to 61 years old, with BMIs ranging from 18.19 kg/m^2 to 40.35 kg/m^2, which classify the participants as normal to obese class III [83]. This study was approved by the Institutional Review Board of the University of Texas at Austin and informed consent from each subject was obtained.

1.4.2 Anthropometric data

Anthropometric measurements were made by trained nutrition experts following a standard protocol established by the National Institutes of Health (NIH) guidelines. Height was measured with a stadiometer (Health o Meter, South Shelton, CT) in centimeters to the nearest 0.1 centimeter. Subjects were asked to remove shoes and socks before the height measurement. Weight was measured by using an electronic scale (Tanita, Arlington, IL) in kilograms with the nearest 0.01 kilogram. BMI (body mass index) was calculated by the equation: weight (kg) / height (m^2). Circumferences at arm, waist, hip, and thigh were

measured by a MyoTape body tape measure (AccuFitness, Greenwood Village, CO) in centimeters. Waist hip ratio was calculated by: waist circumferences (cm) / hip circumferences (cm). Anthropometric measurements were mainly used in Chapter 4 to predict the categories of abdominal fat distribution.

1.4.3 Abdominal adiposity data via MRI

Abdominal scans via a 3.0T MRI scanner (GE Health Care, Milwaukee, WI) were performed on each of the subjects. During the scan, subjects were positioned at the center of the magnetic field. A 4-second, 3-plane localizer scan was conducted to visualize anatomical landmarks. Subjects were asked to place arms on the sides of their trunk, without hard pressing against the abdominal area. For each person, a total of 20 T1 - weighted axial slices covering the abdominal area were obtained with 140 ms repetition time, 2.1 ms echo time, 80º flip angle, 8 mm slice thickness, and 2 mm gap between each slice. Anatomical landmarks of the locations of the slices were saved during scanning. An acquisition matrix of 512×192, a reconstruction matrix of 512× 512 and a field of view varying from 400 mm× 400 mm to 480 mm× 480 mm, depending on the body size, were utilized. Figure 1.4 shows a total of five MR images located at different anatomical markers from a male. The MR images were employed for the development of an automatic MRI processing algorithm presented in Chapter 2 and served as the ground truth of abdominal adiposity in Chapter 4 and Chapter 5.

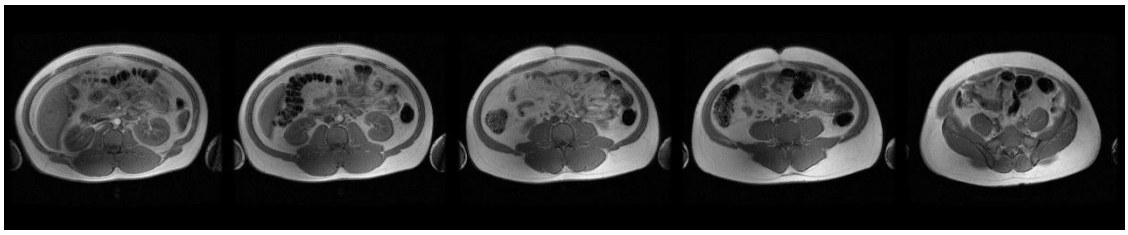

Figure 1.4 MR images showing abdominal adiposity obtained from a male subject. The images listed from left to right are located from the 1st lumbar vertebra (L1) to L5.

1.4.4 Body composition data via DXA

DXA was employed to measure body composition via a Lunar Prodigy system (GE Medical Systems, Madison, WI). Subjects were asked to lay on the scanner table for the X-ray scan for about 7 to 20minutes depending on the size of the subject. The subjects needed to remove any metal prior to the scan.

Total and regional fat mass, including android, gynoid, trunk, and leg fat mass were assessed and recorded. Specifically, the trunk region includes the area of neck, chest, abdomen and pelvis. In the Figure 1.5, the trunk region is demarked by the line at the chin, the two lines through the shoulder, and the two lines through the pelvis. Then, the leg region contains all of the area lower than the lower boundary of the trunk. The android region is defined as the area between the ribs and the pelvis, located within the trunk region. The upper boundary of the android region is 20% of the distance between the iliac crest and the neck, and the lower boundary is the top of the pelvis, as shown in Figure 1.5. The gynoid region embraces hips and upper thighs area, with the upper boundary located below the top

of the iliac crest at a distance of 1.5 times the android height. Thus, the total height of the gynoid region is two times the height of the android region. Details of the segmentation of DXA measurements can be found in a previous study [84].

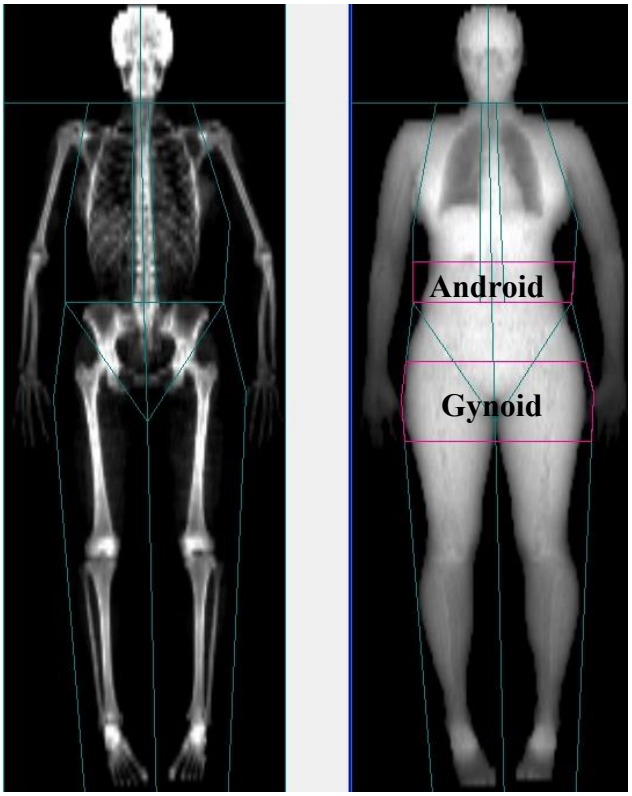

Figure 1.5 DXA image obtained from a female subject illustrating regional fat areas

1.4.5 3D body images via SBI

3D body imaging were conducted at the Human Dimension Laboratory at the University of Texas at Austin. All subjects were instructed to wear light-colored undergarments, a swimming cap and a blindfold during the scan for accurate scanning

results and eye protection. Subjects stood with arms placed away from the torso and legs separated about shoulder-width distance. During the 200 msec body scan, subjects were told to keep still. Ten scans for each subject were obtained and the best two scans were selected to measure the innovative SBI body shape descriptors (see Chapter 3). Average value between the two scans were calculated and recorded. The body shape descriptors were used to predict the distribution categories of abdominal adiposity in Chapter 4 and the exact volumes of VAT and SAT in Chapter 5.

1.5 SUMMARY

Excessive body fat is highly associated with increased risks of cardiovascular diseases, diabetes, some forms of renal failures, certain cancers and other metabolic related health issues. Growing evidence suggests that it is not only the amount of fat, but also its distribution in the body that is related to the disease risks. Thus, it is essential to assess adiposity and fat distribution with inexpensive and convenient methods that can be easily implemented in clinical settings. This dissertation research aims to develop new obesity measurements that are more relevant to intrinsic adiposity conditions and to investigate the unexplored linkage between internal adiposity and external body shape. The novel body shape descriptors proposed in this dissertation will provide more comprehensive and in-depth information of fat accumulation and distribution and may revolutionize obesity evaluation.

The remainder of this dissertation presents quantitative analysis of internal adiposity and external body shape with the datasets acquired from multiple medical devices

and imaging modalities including MRI, DXA and SBI. Chapter 2 introduces a fully-automated algorithm which was developed to quantify the abdominal adipose tissue from T1-weighted MRI slices with a high degree of accuracy and repeatability. The algorithm was evaluated with a dataset contains both male and female subjects with a wide range of BMIs and fat amounts. Chapter 3 describes the effective and innovative body shape descriptors that were developed based on reconstructed 3D body images in order to quantitatively characterize body shape and fat distribution. In Chapter 4, categories of abdominal obesity were formed based on natural clusters of the visceral fat volume and subcutaneous fat volumes. Then, we attempted to predict these abdominal obesity categories by using three sets of obesity measurements: traditional measurements, regional fat mass measured from DXA and the body shape descriptors. Classification accuracy obtained with an optimized support-vector-machine classifier are presented to determine which set of obesity measurements is able to provide the highest prediction accuracy. Chapter 5 investigates the association between intrinsic adiposity and body shape and further develops the mathematical equations for predicting the volumes of abdominal adiposity with the body shape descriptors. In Chapter 6, we conclude this dissertation with summation of our findings and discussion on how these findings can help us improve the evaluation of obesity and enhance people's understanding of the relationship between body shape and intrinsic adiposity.

Chapter 2 Automated Quantification of Abdominal Adiposity from MRI

Magnetic resonance imaging (MRI) is consider as a gold standard to measure abdominal adiposity. In MRI slices, the voxel intensity of fat tissue is distinct from that of non-fat tissue (i.e. muscle and bones) and background. In this chapter, we present a fully-automated algorithm to process T1-weighted axial MRI slices for quantification of abdominal visceral, subcutaneous and total adipose tissue (i.e. VAT, SAT and TAT), without human intervention or prior knowledge. This algorithm shows good performance against the reference method in both single umbilical slices and full MRI sequences. The VAT and SAT volumes assessed by the proposed algorithm were used as the ground truth of abdominal adiposity in Chapter 4 and Chapter 5. The related work in this Chapter has been published on American Journal of Human Biology [85]. Jingjing Sun developed and tested the algorithm, analyzed the data and drafted the manuscript. Dr. Bugao Xu supervised the project, finalized the manuscript and served as a corresponding author. Dr. Jeanne Freeland-Graves supervised the collection of MRI data, edited the manuscript and provided critical comments.

2.1 INTRODUCTION

Excessive abdominal adiposity, including both visceral adipose tissue (VAT) and subcutaneous adipose tissue (SAT), has adverse effects on health as it increases risks of diseases. Specifically, VAT is a major predictor for metabolic syndrome, diabetes mellitus

type 2, cardiovascular disease and certain types of cancers [86]–[88]. SAT is a better indicator of insulin resistance [27], [89]. Since SAT and VAT have different health implications, assessing VAT and SAT separately is more important than just measuring total adipose tissue (TAT). Total body fat can be assessed by indirect methods including air displacement plethysmography (ADP) [9], underwater weighing (UWW) [10], and bioelectrical impedance analysis (BIA) [8]. Although these methods are relatively accessible, they are unable to discriminate visceral and subcutaneous fat depots.

Magnetic resonance imaging (MRI) [5] and computed tomography (CT) [6] are the more advanced methods that can be used to accurately measure VAT and SAT. A newly developed dual-energy X-ray absorptiometry (DXA) [7] has been used to estimate VAT based on some abdominal geometric assumptions [90]. MRI and CT allow a direct differentiation of VAT from SAT, and are often considered as gold standards in adiposity quantification [86], [87]. T1-weighted MRI is a commonly used tool to measure adiposity, as fat tissue show higher signal intensity and appear brighter in T1-weighted images. The slow molecular motion of a fat nucleus causes a quick regaining of longitudinal magnetization, resulting in short longitudinal relaxation time and higher image intensity [62], [63]. Although CT can detect internal fat, the subject has to be exposed to ionizing radiation [6]. Thus, MRI is a safer and more favorable method for adiposity measurement [64].

MRI slices have been analyzed with manual, semi- and fully- automated methods to extract SAT and VAT regions. A typical two-step manual assessment requires trained experts to draw boundaries of the whole abdominal area and delineate areas of VAT and

SAT separately [91]. This manual process is very time-consuming and subjective. Semi-automated methods employ adjustable thresholds, boundary enhancement and other image processing tools to help observers identify adipose tissue [92], [93]. These software packages, such as sliceOmatic, Analyze and ImageJ, are less laborious and more objective than the manual segmentation method, but still require more than 10 minutes on average for a trained expert to process one single slice [94]. A whole abdominal scan typically consists of 15 to 50 slices, imposing a substantial image-processing task when processed by a semi-automated segmentation method. Both manual and semi-automated methods require users' interventions, which may cause inter- and intra-observer variations that undermine the data reliability [95]. In order to circumvent the above disadvantages, user-independent and fully-automated MR image processing methods have been investigated [95]–[99]. However, three major challenges still exist. Inhomogeneity of image intensity in T1-weighted MRI slices has not been thoroughly studied [95]. In addition, prior knowledge is required to train the automated algorithm, limiting usage to a small range of body types and fat amount [96]. Another challenge is the presence of validation cohorts with a wide range of BMIs, various body sizes and fat depots to confirm the robustness of the algorithms.

In this chapter, we aim to develop a novel MR image processing algorithm in order to provide a solution to abdominal adiposity assessment without human intervention or prior knowledge. The new algorithm integrates intensity correction, image clustering and image segmentation methods. This fully-automated algorithm eliminates observer's bias and increases reliability by avoiding human supervision. The algorithm performance was

evaluated on 85 subjects having a wide range of BMIs, and compared to a semi-automated method–sliceOmatic (Version 4.3).

2.2 METHODS

2.2.1 Datasets

We used the MRI dataset described in Chapter 1.4 to evaluate the proposed algorithm. The subset of 60 male and 25 female were selected according to the availability of the manual measurements by using the SliceOmatic software package. The characteristics of subjects is shown in Table 2.1.

Table 2.1 Characteristics of subjects

Sex	Subjects (n)	BMI (kg/m^2) Mean (range)	BMI Classification	Age (years) Mean (range)
Male	60	28.07 (19.96 - 40.35)	Normal to Obese Class III	35 (19-60)
Female	25	29.30 (20.92-40.1)	Normal to Obese Class III	36 (19-61)

BMI: body mass index.

2.2.2 Semi-automated segmentation

In order to obtain the reference adiposity data to validate the proposed automatic method, a semi-automated MRI processing method, sliceOmatic, was utilized, as it is

recognized as an easy-to-use method for fat assessment [94]. This method was referred to as the reference method in the study. Mathematical morphology functions in sliceOmatic were used to segment an MRI slice into a number of sub-regions by computing the watershed line of the image gradient (Figure 2.1a). Then the operators manually filled those separated regions with appropriate tags for visceral fat (green) and subcutaneous fat (red). The sub-regions can be merged into larger area for easier tagging when large area has consistent tissue type. However, the possibility of false labeling may arise. As shown in Figure 2.1b for example, both VAT and SAT are mistakenly tagged as SAT with red color. Therefore, caution and processing time are highly demanded during the semi-automated MRI processing.

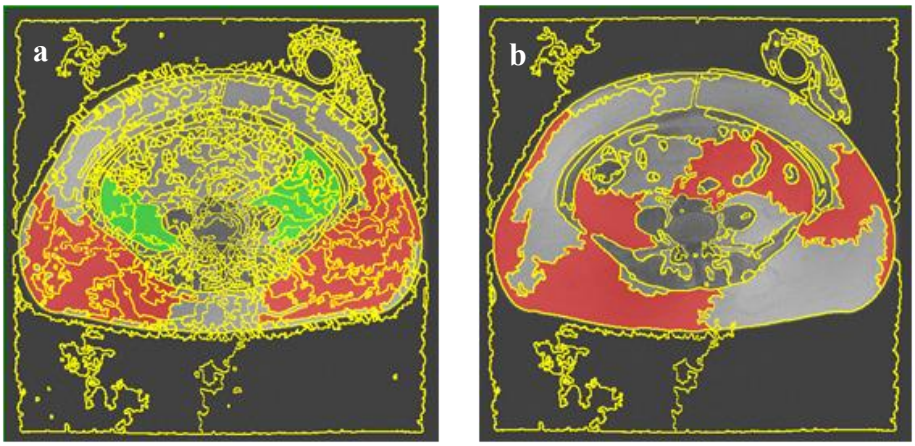

Figure 2.1 (a) (b) Manual tagging results with different sizes of region after watershed computation in SliceOMatic.

In the first stage of the study, the single umbilical slices of the 85 subjects were analyzed with sliceOmatic because of its subjective and time-consuming nature. Three

trained operators analyzed the 60 male subjects and two trained operators did the 25 female subjects. The SAT, VAT and TAT in this single slice evaluation from all the operators were averaged to reduce the subjectivity. In addition, the umbilical slice was used for the single slice evaluation because it is easy to be located and compared among the subjects with different body shapes and heights. In the second stage, 20 subjects (10 male and 10 female) were randomly selected for their MRI sequence analysis with the reference method. For each sequence, the twenty slices across a subject's abdomen area were processed by one trained operator. The volumetric adiposity data were obtained by summing the VAT and SAT measured from each slice. This volumetric evaluation was only performed on the 20 subjects due to the heavy workload for an operator to segment the slices when using sliceOmatic.

2.2.3 Fully-automated algorithm

2.2.3.1 Abdominal tissue mask computation

In order to separate abdominal tissue voxels from air background and unimportant limbs, a region growing method was employed. This process started from four corners of the original MRI slice where air background is always present. For each growing region iteration, mean value (μ_b) and standard deviation (σ_b) of the air background voxels were calculated and used as a standard to determine the category of each voxel in the new growing region. If the new voxel value was less than $\mu_b + 3\sigma_b$, the voxel was classified as background; otherwise, the voxel was determined as tissue. Image morphological

algorithms were employed to close the image and fill the holes. Then, the size of each tissue area in the image was measured. Only the largest tissue area representing the abdomen was retained. Smaller areas containing the limbs were removed. The original T1-weighed abdominal MRI slice with unwanted limbs on two sides from a male subject is shown in Figure 2.2a. Figure 2.2b shows a tissue mask and Figure 2.2c shows a processed image with the retained abdominal tissue after limbs were removed. This mask constrains the calculation area for the following image processing steps, accelerating computation and reducing MRI artifacts/noise outside the abdomen.

2.2.3.2 Intensity inhomogeneity correction

Spatial inhomogeneity of the MRI coil sensitivity and main magnetic field gives rise to the artifact of inhomogeneous signal intensities across MRI slices [100]. Therefore, intensity correction step is critical for MRI voxel intensity-based computation, especially for T1-weighted images. The model to describe the bias field causing such inhomogeneity can be summarized as: $I_b=I_cB+n$, where I_b is the observed inhomogeneous MR image, B is the bias field with intensity variation, I_c is the corrected or true image of interest, and n is the additive noise.

The original T1-weighed MR image (Figure 2.2a) has noticeable inhomogeneous intensity, especially within the SAT. Without correction, such variations within the same tissue compartment (i.e., fat or muscle) often mislead conventional segmentation process. In this algorithm, the correction of the bias field was implemented using a modified version of " local entropy minimization with a bicubic spline model " (LEMS) proposed by Salvado

[101]. First, the initial bias field B_0 was predicted by fitting a 2D polynomial function to I_b using voxels above the average intensity of I_b (threshold of $T_{avg(Ib)}$). The corresponding corrected image was then calculated by using $I_{c0} = I_b/B_0$. I_{c0} and B_0 were separated into small knots which were ordered by the B_0 values of each knot center. Entropy optimization started at the knot with the highest B_0 value with its eight neighboring knots denoted as Region1 (R1) because it may contain adipose tissue, which is of our interest. The center B_0 value was updated to ensure the lowest local entropy in I_{c0} within R1. The second optimization step within Region2 (R2) started at the knot with the second highest B_0 value. If the average intensity value of the corrected I_{c0} in R2 was similar to that in R1, then two regions (R1∪R2) were merged before the optimization. Otherwise, R2 was optimized independently. This adaptive piecewise optimizing process continued until all knots were processed, and the final image was the corrected image I_c. The modified LEMS model proposed in this study improves the homogeneity of the MR image in the same tissue compartments while preventing the over-correction in non-fat area (Figure 2.2d). Details about knot's definition and its size choosing criteria can be found in Ref. [101].

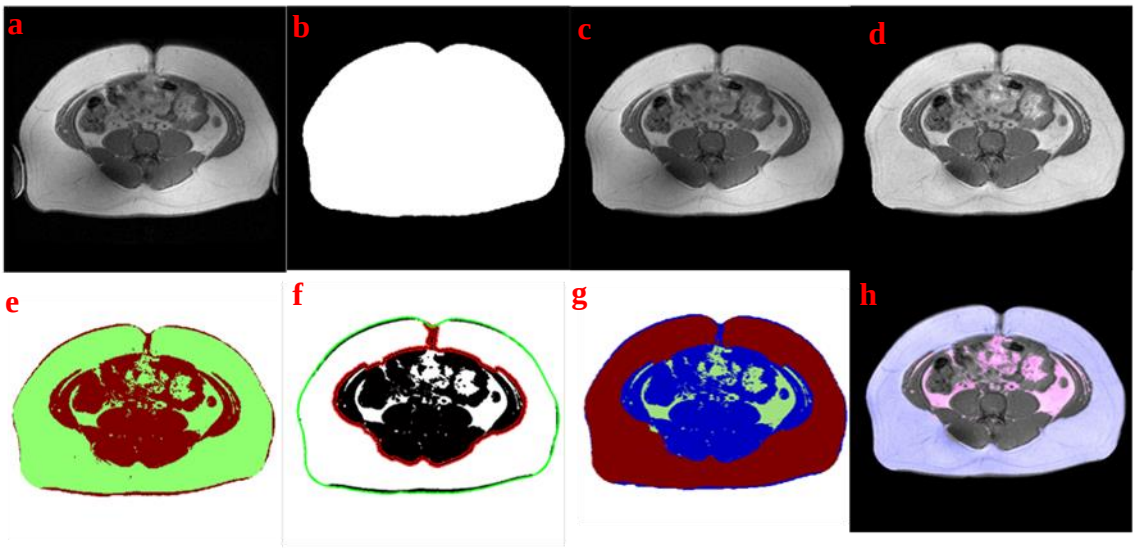

Figure 2.2 Examples of the fully-automated fat assessment processing. (a) Original MRI slice with limbs on two sides. (b) Abdominal tissue mask after region growing. (c) Clean image with limbs removed by (b). (d) Intensity corrected image. (e) Discrimination of fat and non-fat tissue using FCM clustering. (f) Segmentation of VAT and SAT using active contour, the initial and final contour are marked with green and red lines, respectively. (g) Segmentation result: green - visceral fat, red - subcutaneous fat and blue - non-fat tissue. (h) Final assessment result (Overlaying segmentation result on original MRI slice): pink - VAT and blue - SAT.

2.2.3.3 Image clustering

Image clustering algorithm needs to be employed to automatically classify MR image into fat and non-fat tissue after the intensity correction. The fuzzy *c*-means (FCM) algorithm with Euclidian norm was used in this study since it does not require prior information and is computationally efficient. The energy function to be minimized during the FCM iterations is defined as [102]: $J(y,c) = \sum_{i=1}^{N}\sum_{k=1}^{K}\left\|y_i - c_k\right\|^2$, where N is the total number of voxels of the MR image, K is the number of clusters (K=3 in this study—fat tissue, non-fat tissue and background), y_i is the voxel intensity and c_k is the center intensity of the k^{th} cluster. Iterative optimization of the above objective function was carried out with the update of fuzzy cluster membership of each voxel and the center of each cluster. Iteration stopped when the centers and the membership were stabilized, or the allowed iteration was reached. Figure 2.2e exemplifies the clustering result of one MR image after inhomogeneity correction. The green color indicates fat tissue while the red color shows muscle and other non-fat tissue.

2.2.3.4 Image segmentation

Image segmentation is a procedure to further distinguish VAT from SAT by locating the abdominal muscle wall (i.e. target contour). “Chan-Vese” active contour algorithm is a well-known image segmentation method which defines the contour by balancing a shrinking force and an expanding force of the contour defined by regional average intensities [103]. Because the algorithm is not based on image gradient like other traditional segmentation methods, it is insensitive to noisy voxels in an MRI slice. In order to prevent human

interference, the “Chan-Vese” algorithm was modified in this study. The abdominal contour obtained in the previous region-growing step was utilized as the initial contour (green line in Figure 2.2f). Iteration stopped automatically when the contour was stabilized or the maximum iteration number was achieved. As a result, the optimized contour encompasses the non-fat region (red line in Figure 2.2f). As shown in Figure 2.2g, fat voxels inside the final contour are classified as VAT (green) while other fat voxels are counted as SAT (red). Final computation result is shown in Figure 2.2h where the segmentation result is overlaid on the original corrected MR image. Pink denotes VAT and blue indicates SAT.

2.2.3.5 Sequence analysis

The MRI sequence (20 slices per subject) was analyzed slice by slice with the algorithm to quantify the abdominal adiposity based on volumetric data. Among the MRI sequence of a subject, the middle slice was chosen as a starting slice and its calculated bias field provided an initial value for the rest of the slices for the subject. Then, the active contour calculated in each slice was used as the initial contour in the adjacent slices. From one slice, VAT (cm^3) and SAT (cm^3) were calculated by multiplying the number of voxels by the voxel volume. TAT (cm^3) was the sum of the VAT and SAT volumes.

SAT and VAT calculated in each slice within one MRI sequence should be varying smoothly over slices. If the fat volumes quantified in the one slice are significantly different from that calculated in the adjacent slices, the intensity inhomogeneity may not be corrected well. Such insufficient correction mainly happened when there is a sudden change of MRI intensity primarily due to the inhomogeneity between the slices. In that

case, inhomogeneity correction need to be redone with a modified threshold $T_{avg(Ib)}$ (minus 10 or 20, based on our experience). This simple strategy based on adaptive threshold effectively solved the inter-slice intensity variation in our dataset.

After the twenty slices were processed, the 3D images indicating the total abdominal VAT and SAT volumes were constructed by stacking up the VAT and SAT from each slice according to the slice's position and thickness (see Figure 2.3), and the total volumetric VAT, SAT and TAT measurements were obtained by summing the fat volumes of each slice in the sequence. Figure 2.3a, Figure 2.3b and Figure 2.3c are the SAT, VAT and TAT volumes reconstructed from multiple slices in one MRI sequence.

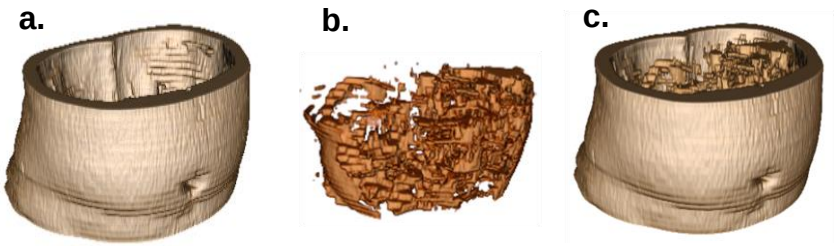

Figure 2.3 Visualization of volumetric abdominal adiposity reconstructed from all twenty MRI slices. (a) SAT, (b) VAT and (c) Combined SAT and VAT.

2.2.4 Algorithm evaluation

The SAT, VAT and TAT volumes measured by the automatic and the reference methods were statistically analyzed by using Pearson correlations and Bland-Altman plots to evaluate the accuracy of the automated algorithm. The umbilical slices from the 60 male and 25 female subjects were utilized for the single slice evaluation, while 20 randomly

selected subjects were used for the abdominal MRI sequence evaluation. The inter-observer reliability of the semi-automated (reference) method was assessed using the intra-class correlation (ICC, single score, two-way random) of the three independent operators' segmented adiposity volumes from umbilical slices of male subjects [104]. For comparison, the reliability of the automated algorithm also was tested by processing the same slice twice.

The VAT and SAT volumes assessed from one of multiple slices at different anatomical locations of a subject, i.e. umbilicus, 2nd lumbar vertebra (L2), L3, L4 and L5, were compared to the total abdominal adiposity of the slices covered from L2 to L5 to explore the relevancy of each slice. The fat distribution across the abdomen was also analyzed by examining the fat depots assessed at different anatomical locations. All these analyses were performed using Matlab (MathWorks Inc, Natic, MA) and SPSS Statistics (IBM SPSS, Chicago, IL). A P-value less than 0.05 was adopted for the significance level.

2.3 RESULTS

For the single slice (umbilical) evaluation, an operator needed approximately 5 minutes to analyze one umbilical MRI slice when using sliceOmatic (reference), and 20 to 103 seconds when using the automated algorithm (automatic) depending on the trans-axial size of a subject. For the MRI sequence evaluation in the second stage, the operator needed about 1.5 hour to analyze the 20 MRI slices in one sequence with the reference method, but only 10 to 20 minutes to process a sequence with the automatic method. Thus, the fully-automated algorithm has tremendously increased the efficiency of extracting adiposity data

from an MRI slice, which makes the MRI sequence evaluation of a large subject set more attainable.

A semi-automatically segmented result using sliceOmatic is shown in Figure 2.4a and compared to its corresponding result using the fully-automated algorithm in Figure 2.4b. It should be noted that the hand area one tope of the abdomen was automatically removed by the proposed algorithm in the Figure 2.4b.

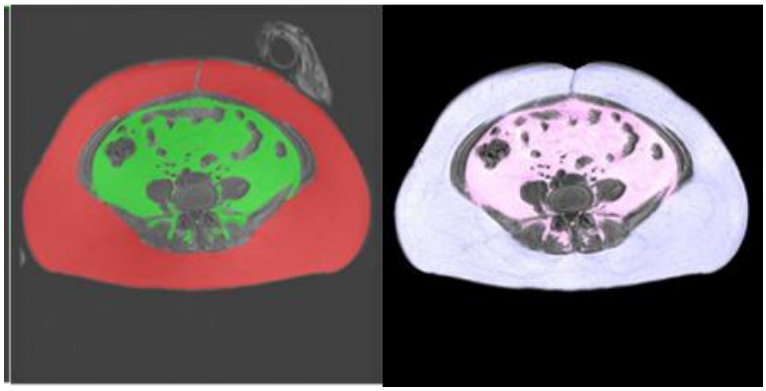

Figure 2.4 (a) segmentation result after semi-automated processing and (b) segmentation results after automated processing

2.3.1 Single slice evaluation

Figure 2.5 plots the VAT, SAT and TAT measurements from the umbilical slices made by the reference method (the x-axis) and the automatic method (the y-axis). The square of the Pearson correlation coefficient (R^2) between the two sets of measurements is displayed also on the left side of each plot in the figure. The strongest correlations occurred in SAT (R^2=0.998, slope=1.01) and TAT (R^2=0.997, slope=0.988) measurements between the two methods (Figure 2.5b and Figure 2.5c). A strong correlation (R^2=0.977, slope=1.09)

also existed in VAT measurements (Figure 2.5a). The Bland-Altman plots [105] of the three volume measurements from the automatic method in comparison with the reference method also shown on the right side of the Figure 2.5, in which the x-axis is the average of the fat volumes assessed from the reference method and the automatic method. The y-axis is the measurement difference between the two methods. Measurement differences between the two methods primarily lied within the 95% limits and no substantial difference was found between the two methods.

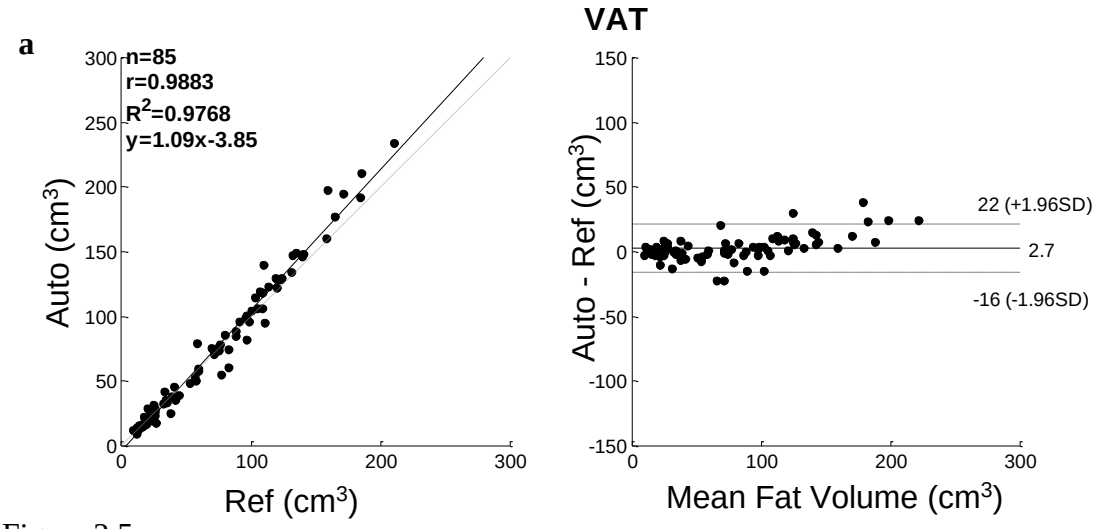

Figure 2.5

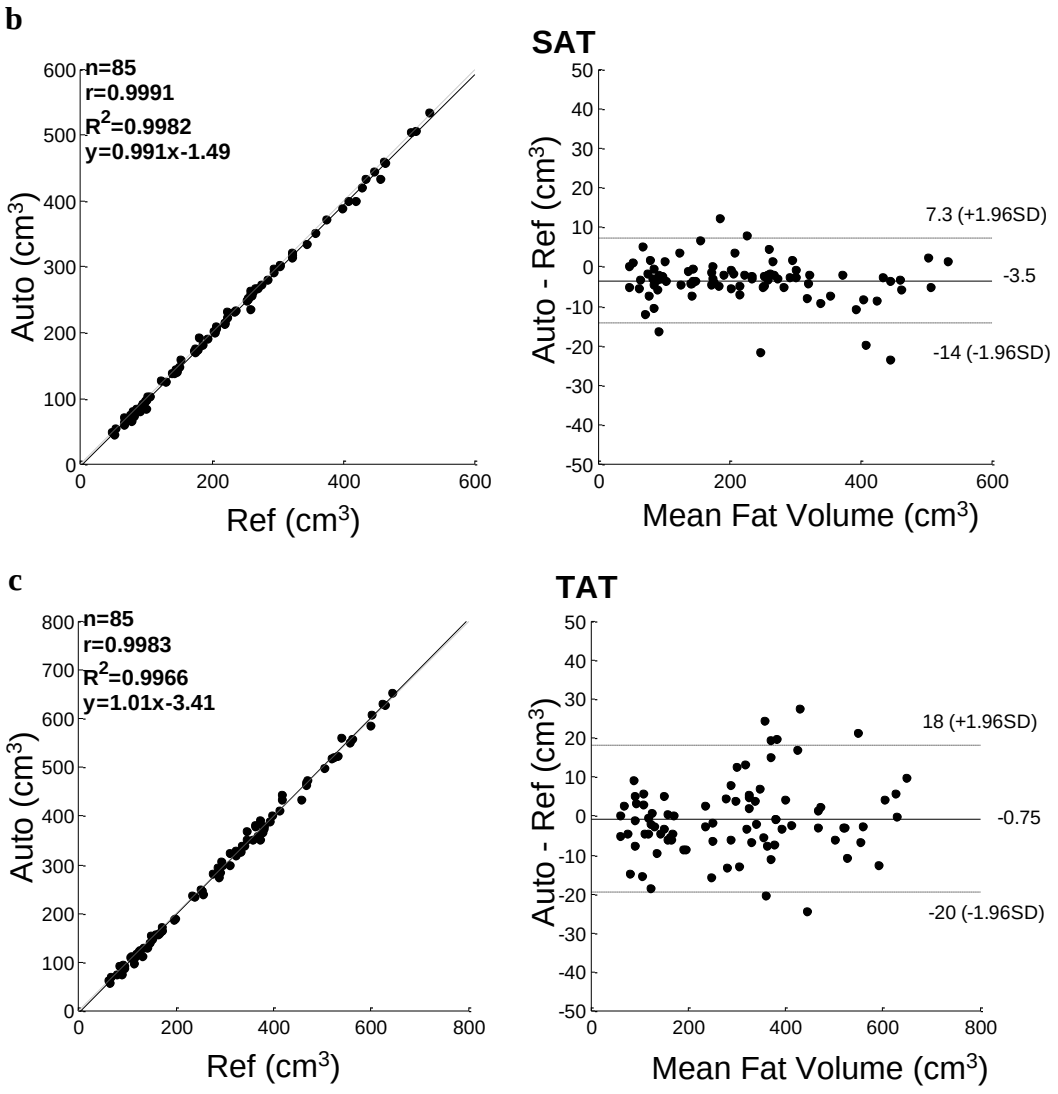

Figure 2.5 Linear correlation (left) and Bland-Altman (right) plots for the slice-wise evaluation based on 85 umbilical slices from 85 subjects. Differences between automated (Auto) and semi-automated (Ref) assessment of (a) VAT (b) SAT and (c) TAT are shown. Upper- and lower- limits represent 95% of differences. Mean difference is indicated as the solid bar in the middle of Bland-Altman plots.

In order to assess the accuracy of the single slice evaluation made by the automatic method, mean difference between the two methods, *Auto-Ref*, and their relative difference, (*Auto-Ref*)*/Ref*, were calculated and shown in Table 2.2. The results show that the VAT measured by the automatic method is slightly higher than those measured by the reference method, while the SAT exhibited an opposite trend.

Reliability for the semi-automated segmentation and the fully-automated algorithm were analyzed on the dataset of male subjects with an umbilical slice (Table 2.2). The ICC for the manual segmentation from the three independent observers using sliceOmatic were 0.9989, 0.9393 and 0.9900 for SAT, VAT and TAT, respectively. Since no user intervention is needed for automated processing, there will be no difference in results if more than one user were involved. In this study, one operator used the fully-automated algorithm to process the same slices twice. The ICC for SAT, VAT and TAT was all above 0.999. Thus, these results indicate that the reliability of the fully-automated algorithm for SAT, VAT and TAT assessment is higher than that of the semi-automated segmentation.

Table 2.2 Accuracy and inter-observer reliability

	Single-slice[a]		Sequence[b]		ICC	
	(Auto-Ref)[c] (cm^3)	(Auto-Ref)/Ref (%)	Auto-Ref (cm^3)	(Auto-Ref)/Ref (%)	Ref	Auto
VAT	2.72±9.63	2.57±14.20	38.10±127.04	-1.35±9.14	0.9393*	0.9999*
SAT	-3.47±5.38	-1.94±3.53	-130.50±50.42	-4.47±3.50	0.9989*	0.9999*
TAT	-0.75±9.64	-0.75±4.3	-92.20±135.74	-3.46±4.49	0.9900*	0.9999*

[a] Measurements based on the single umbilical slices from subjects (n=85).

[b] Measurements based on the MRI sequences (20 slices/sequence) from randomly selected subjects (n=20).

Accuracy data are given as mean ± standard deviation in cm^3 and percentage (%).

VAT: visceral adipose tissue; SAT: subcutaneous adipose tissue; TAT: total abdominal adipose tissue; Auto: the automatic method; Ref: the reference method; ICC: intra-class correlation; *P<0.001.

2.3.2 Sequence evaluation

For the MRI sequence evaluation based on 20 subjects (20 slices /subject), accuracy also was analyzed by the mean difference and the relative difference (Table 2.2). For volumetric VAT, the mean difference is 38.1±127.04 (cm^3) and the relative difference is -1.35±9.14 (%). For volumetric SAT, the mean difference is -130.5±50.42 (cm^3), and the relative difference is -4.47±3.50 (%) which are higher than that of VAT, for volumetric TAT, the mean difference is -92.20±135.74 (cm^3) and the relative difference is -3.46±4.49

(%). The R^2 between the two sets of measurements of VAT, SAT, and TAT are 0.995, 0.999 and 0.999 respectively.

Table 2.3 presents the fat volumes determined by the two methods for both men and women. As previously indicated [2], this study also revealed noticeable differences in fat distribution between men and women. Based on the measurements from umbilical slices, female subjects tended to accumulate more subcutaneous fat, but less visceral fat, than male subjects.

Table 2.3 Adipose tissue volumes (cm^3) from umbilical slices of male (n=60) and female (n=25) subjects

Sex	VAT		SAT		TAT	
	Ref	Auto	Ref	Auto	Ref	Auto
Male	74.8±53.5	77.0±58.9	196.7±122.3	192.6±122.3	271.9±158.7	272.5±161.6
Female	68.0±43.0	69.4±47.9	280.0±118.5	273.7±116.1	348.1±156.3	343.2±157.0

VAT, visceral adipose tissue; SAT, subcutaneous adipose tissue; TAT, total abdominal adipose tissue; Auto: volumes measured by the automatic method; Ref: volumes measured by the reference method; Data are given as mean ± standard deviation in cm^3.

2.3.3 Associations between abdominal adiposity and anthropometric measurements

We also explored the associations between the VAT, SAT and TAT measured from the single umbilical slice by the automatic method and the traditional anthropometric measurements, such as BMI, waist circumference (WC) and waist-hip-ratio (WHR) (see

Table 2.4). Among the three anthropometric parameters, WHR and BMI possessed, respectively, the highest and the lowest correlations with VAT (r, Pearson correlation coefficient). WC provided the highest correlation with SAT and TAT. The WHR was the only measurement that was significantly correlated with the ratio of VAT/SAT, which represents the relative amount of the two fat types.

Table 2.4 Relationship between traditional anthropometric measurements and fat volumes measured from umbilical slices, using the automatic method (n=60)

	Fat Volumes			
	VAT	SAT	TAT	VAT/SAT
BMI	r=0.59(P<0.001)	r=0.79(P<0.001)	r=0.81(P<0.001)	r=0.16(P>0.05)
WC	r=0.72(P<0.001)	r=0.94(P<0.001)	r=0.97(P<0.001)	r=0.25(P>0.05)
WHR	r=0.77(P<0.001)	r=0.77(P<0.001)	r=0.86(P<0.001)	r=0.38(P<0.005)

r: Pearson correlation coefficient; VAT: visceral adipose tissue; SAT: subcutaneous adipose tissue; TAT: total abdominal adipose tissue; BMI: body mass index; WC: waist circumference; WHR: waist to hip ratio.

2.3.4 Relationship between localized fat volumes and total abdominal adiposity

In order to determine which slice carried the highest correlation with the total abdominal adiposity, the VAT, SAT and TAT measured from one of the MRI slices at different anatomical locations, i.e., umbilicus, L2 to L5 vertebra, were compared with the total VAT, SAT and TAT measured from all slices between L2 and L5 for the 60 male subjects (Table 2.5). The data showed that the VAT was more likely to be concentrated

between L3 and L4 slices, while SAT existed primarily at the lower position of the abdomen, with the L5 slice containing the most SAT. The VAT and SAT measured from the L3 slice had the highest correlations with the total abdominal VAT (r=0.99) and SAT (r=0.99). Among all locations, the umbilical slice showed the lowest correlation (r=0.89) of the total abdominal VAT.

Table 2.5 Mean fat volumes and associations between fat on single slice and total abdominal adiposity (n=60)

Fat depots	Total	Umbilicus		L2		L3		L4		L5	
	Mean volume (cm^3)	Mean volume (cm^3)	r	Mean volume (cm^3)	r	Mean volume (cm^3)	r	Mean volume (cm^3)	r	Mean volume (cm^3)	r
VAT	1.29×10^3	77.95	0.89	88.13	0.97	99.31	0.99	91.36	0.98	65.42	0.92
SAT	2.49×10^3	191.74	0.99	113.74	0.98	149.40	0.99	190.06	0.99	198.02	0.99
TAT	3.78×10^3	269.69	0.97	201.87	0.97	248.71	0.99	281.42	0.99	263.44	0.97

L: lumbar vertebra; Total: fat depots measured on slices from L2- L5;

r: Pearson correlation coefficients measured between fat volume assessed from a single slice and total fat volume from L2- L5.

All measurements of adipose tissue were assessed by the automatic method.

2.4 DISCUSSION

A reliable method for fat quantification is important due to the high prevalence of obesity. We have demonstrated a fully-automated algorithm which is able to assess the abdominal adipose tissue on T1-weighted MRI slices, with a high degree of accuracy and reliability. The proposed algorithm was validated in a dataset of both male and female subjects, with a wide range of BMIs and fat depots.

Major challenges that exist in the automation of T1-weighted MRI segmentation of the abdominal area include inhomogeneity correction in slices, fat/non-fat classifications, delineation of abdominal wall, and varying body size, shape and internal fat distribution. In our dataset, the inhomogeneity was more common in obese subjects and may have caused errors in the clustering and classification procedures. In the presented algorithm, a modified LEMS model was utilized to correct the shading effect to ensure the homogeneity in the same tissue type. Figure 2.6a is an original MRI slice after the region growing procedure with the voxels outside of the abdominal area removed. Variations in signal intensity of the subcutaneous fat resulted in an inaccurate clustering computation in Figure 2.6b. The LEMS model proposed by Salvado was used originally to correct spinal MRI [101]. When the LEMS approach was applied to the abdominal MRI with a large amount of fat issue, the dark areas containing muscle and bones were frequently over-corrected. This may impact the following clustering procedure. The modified LEMS model proposed in this study is able to prevent the over-correction while keeping homogeneity within the

same type of tissue (Figure 2.6c). This ensures accurate segmentation of fat from non-fat tissue (Figure 2.6d).

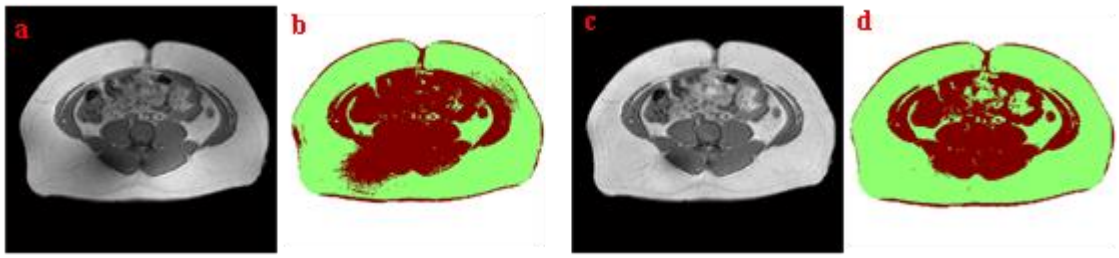

Figure 2.6 (a) MRI slice after region growing, (b) clustered result based on (a), (c) Intensity corrected image, and (d) clustered result based on (c)

Intermuscular fat and vertebral bone marrow fat were not separated from abdominal fat in this study since such fat have been proved to be either positively correlated with visceral fat volume or associated with increased risk of developing obesity-related health issues [106], [107].

Three trained operators in this study enhanced the accuracy of the semi-automated measurements. The lower operators agreement was similar to what has been reported elsewhere [95]. In contrast, the reliability of the fully-automated algorithm was excellent because human interventions in MRI processing were eliminated.

The accuracy of the fully-automated algorithm was evaluated with both single-slice and MRI sequence data. First, the single umbilical slice was analyzed to assess the accuracy of the algorithm for the 85 subjects that had a wide range of BMI and body shapes. Then,

the MRI sequences were analyzed to validate the algorithm with multiple MRI slices that covered the entire abdominal area with diverse organ and fat contents.

Overall, the fat amount assessed using the fully-automated algorithm is in a high agreement with that obtained from sliceOmatic. The VAT volumes measured automatically were slightly higher than the reference values, possibly because it is hard to identify tiny and spread adipose tissue, such as intramuscular fat and bone marrow, in the sliceOmatic. On the other hand, it is easier to select bulky SAT area as a whole, even if there are tiny non-fat tissue present in the sliceOmatic. This is attributed to the higher SAT measurements of the sliceOmatic. A systematic trend was observed nevertheless in the Bland-Altman plot of the VAT measurement. Data points were tightly clustered on the left side of the plot and spread out on the right side. This trend indicates that the deviation between the two methods might be increased in subjects with larger VAT volumes. A similar but less obvious trend was observed in the Bland-Altman plot of TAT measurement. The difference between the two TAT measurements was elevated in the middle of the plot. In the future, more subjects should be tested in order to reduce the sampling bias that might have caused these systematic trends. It is noted also that the equality lines in the three Bland-Altman plots were all within the 95% confidence intervals. This implies that the systematic differences between the automatic method and the reference method were not significant [108].

Compared with the results in the previous studies, our fat assessment results showed either equal or higher accuracy. For instance, Thörmer et al evaluated a fully-automated method in 20 morbidly obese subjects, and reported the Pearson correlation coefficients

were 0.966, 0.960 and 0.978 for SAT, VAT and TAT, respectively [95]. Kullberg et al presented an automated approach which underestimated the VAT by 4.7% [109]. Bryan et al reported a slice-wise analysis similar to our automated algorithm, with R^2 being 0.997 for VAT and 0.987 for SAT [110]. Finally, Positano et al explored an automated approach in which the Pearson correlation coefficients were 0.992 and 0.960 for SAT and VAT, respectively [98]. Yet, we could not make direct comparisons with the above studies due to differences in imaging protocols, segmentation approaches and numbers of slices.

The present research study also found that the VAT and SAT depots were not equally associated with the traditional adiposity predictors such as BMI, WC and WHR. Table 2.6 exemplifies this finding with two subjects who had similar WCs. The left image is from an individual who had higher BMI and was classified as overweight (BMI>25). The image on the right is from a subject with a lower and normal BMI, but a higher WHR. The right subject's VAT is twice that of the left subject, while the SAT is slightly smaller. Thus, BMI and WC do not indicate the true abdominal VAT volume as compared with WHR, and are less relevant to internal fat conditions.

In the single slice evaluation on slices at different anatomical locations, we found the umbilical slice is not the most representative of the total abdominal adiposity, which is consistent with the previous studies presented by Shen et al [111], [112]. As opposed to a single slice, the MRI sequence provides a more accurate assessment of the abdominal adiposity because it contains variations in fat distribution across slices [99], [113].

Table 2.6 Anthropometric and adipose measurements comparison between two male subjects

	Subject 1	Subject 2
BMI (kg/m^2)	28.67	23.49
WC (cm)	99	100
WHR	0.93	1.00
VAT (cm^3)*	32.90	128.44
SAT (cm^3)*	201.59	171.20
Umbilical slice	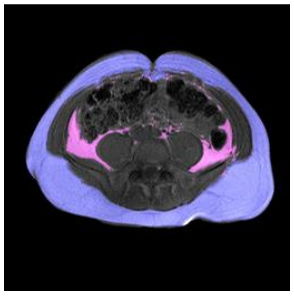	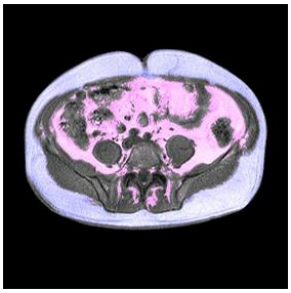

* Measurements based on single umbilical slice by using the automatic method;

BMI: body mass index; WC: waist circumference; WHR: waist to hip ratio; VAT: visceral adipose tissue; SAT: subcutaneous adipose tissue; TAT: total abdominal adipose tissue.

Due to the limitation of the T1-weighted MRI, the partial volume effect was not considered and this may have caused an inaccurate estimation of fat tissue. To deal with

this partial volume effect, advanced imaging modalities such as water-saturated images [97], Dixon MRI sequences [114] and IDEAL (Iterative Decomposition with Echo Asymmetry and Least squares estimation) technique [115] could be useful. Image processing algorithms based on these advanced MRI techniques have been also proposed for abdominal adiposity assessment. For example, Borga et al reported an automated muscle-fat quantification software with the utilization of the IDEAL technique [116]. Schaudinn et al explored the use of a semi-automated program for VAT segmentation on Dixon MRI sequences [117]. Despite the advantages of the Dixon MRI, T1-weighted MRI still remains popular because of its simpler operations and less scanning time, which is critical for certain applications [118]. The proposed algorithm has been validated only on the T1-weighted MRI slices acquired from one institution. An area for future investigation is to adapt the algorithm for different imaging protocols, such as T2-weighted images, chemical (frequency) selective images, Dixon sequences and even CT scans, as the condition allows.

2.5 SUMMARY

In this chapter, we presented a fully-automated MR image processing algorithm that can be used to identify and measure VAT, SAT and TAT volumes from a single MRI slice or a multiple-slice sequence. The new algorithm was validated with the MRI slices of 85 subjects who had a wide range of BMIs, body shapes, sizes and ages. The improved accuracy and reliability of the VAT, SAT and TAT data indicated that the fully-automated algorithm is more robust and effective than manual or semi-automated methods.

Chapter 3 Novel Body Shape Descriptors from 3D Body Images

Growing evidence suggests that body shape is important to predict metabolic risk factors, however, traditional measurements, such as waist circumference, hip circumference and body mass index, may not represent individuals' body shape and adiposity conditions. In this Chapter, innovative body shape descriptors are developed for quantitative characterization of human body shape and fat distribution. All descriptors were automatically measured from 3D body images using OpenGL functions presented in the Chapter 1.3. These descriptors providing in-depth and comprehensive information of body shape can be applied to evaluate obesity.

3.1 INTRODUCTION

Traditional obesity evaluation methods such as measurements body mass index (BMI), waist circumference (WC), hip circumference (HC) and waist-hip-ratio (WHR) may not be truly relevant to intrinsic adiposity conditions. Figure 3.1 shows 3D images of two women who have very similar BMIs, WCs and WHRs, but significantly different body shapes and adiposity data including %BF from Dual-energy X-ray Absorptiometry (DXA), visceral and subcutaneous adipose tissue (VAT and SAT) from Magnetic Resonance Imaging (MRI). In this respect, it is essential to develop new parameters that can depict body shape features which are more relevant to intrinsic adiposity conditions. With the custom-made three-dimensional (3D) stereovision body imaging (SBI) system introduced in Chapter 1.3, innovative body shape descriptors are developed in this chapter. Based on

the different body shape characteristics that are captured, the body shape descriptors can be divided into three sub-groups: landmark measurements, regional volume measurements, and panoramic indices.

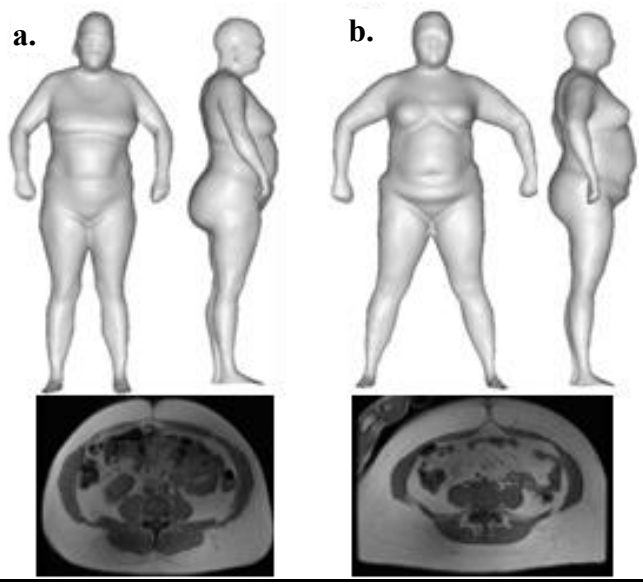

Subject	BMI	WHR	WC (cm)	BF%	VAT (mm^2)	SAT (mm^2)
A	33	0.91	105	36	73	280
B	34	0.88	103	44	102	333

Figure 3.1 Subjects with similar BMI, WHR and WC, but significantly different body shapes and adiposity levels.

3.2 LANDMARK MEASUREMENTS

Nine landmark measurements were defined as body circumference, width and depth taken at pre-defined landmarks including waist, hip and upper thigh. These three landmarks were selected because they are located at central body where should be more relevant to the

abdominal adiposity. Specifically, the waist circumference (WaistC) was conventionally defined as the smallest girth on torso between under bust line to crotch. On the same contour, waist width (WaistW) and waist depth (WaistD) were calculated. Hip circumference (HipC) is the largest girth between the waist line and crotch point. Hip width (HipW) and hip depth (HipD) were then measured on the hip contour. Thigh circumference (ThighC) was measured at the proximal location on the right thigh, since previous studies have suggested that the proximal thigh circumference shows a higher association with the abdominal adiposity than that measured at distal and middle thigh sites [119]. Thigh width (ThighW) and thigh depth (ThighD) were measured at the determined upper thigh contour. These three landmarks of waist, hip and thigh are shown in Figure 3.2a with black lines. It should be noted that abdominal measurements are not included here because currently there is no unified definition of abdomen contour. However, innovative parameters related to the abdomen are developed and will be discussed in the following sessions.

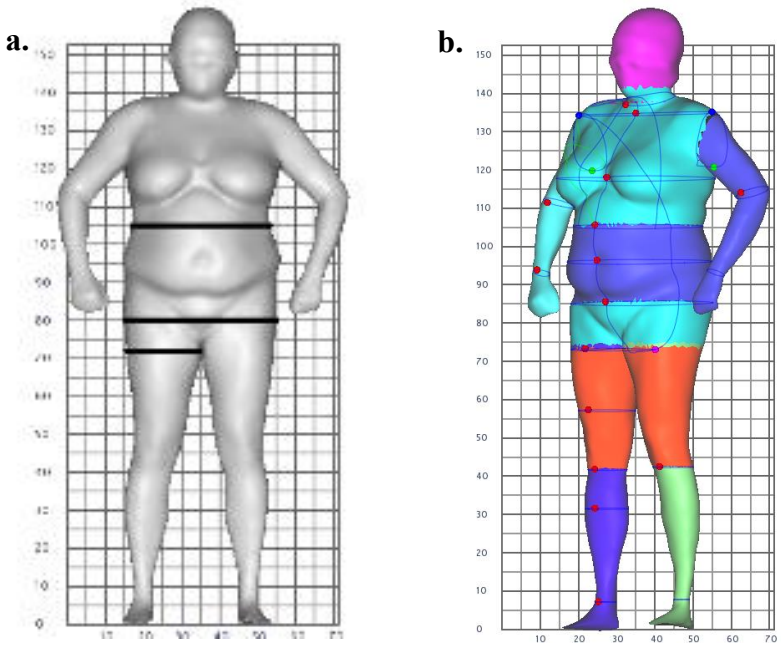

Figure 3.2 (a) An example of a reconstructed 3D body image with three selected landmarks at waist, hip and upper thigh and (b) An example showing regional volume measurements

3.3 REGIONAL VOLUME MEASUREMENTS

Five regional body volume measurements describing the body fat distribution are defined as:

1. TorsoV (Torso volume): regional trunk volume from neck line to crotch.
2. WaistV (Waist to hip volume): regional volume from waist line to hip line (purple section on central body area in Figure 3.2b).
3. HipV (Hip volume): regional volume from hip line to crotch (light blue section on central body area in Figure 3.2b).

4. WCV (Waist to crotch volume): regional volume from waist line to crotch; equals to the sum of HipV and WaistV.
5. ThighV (Thigh volume): regional volume of two thighs (orange section in Figure 3.2b).

3.4 PANORAMIC INDICES

Panoramic indices comprehensively characterizing the full body shape can be summarized into four categories based on measuring locations and implications:

1) Central Obesity Measurements: Central width (CW), central depth (CD) and central protrusion (CP) are three measurements defined on the axial plane of the body with the largest girth between waist line and hip line (blue line in Figure 3.3a). On this axial plane, CW is the distance between left and right side of the body on the same plane, and the depth represents the distance between front and back points of the body, as shown in the Figure 3.3b. CP = CD/CW, reflects how much the abdominal cross section protrudes to the front of the horizontal placement

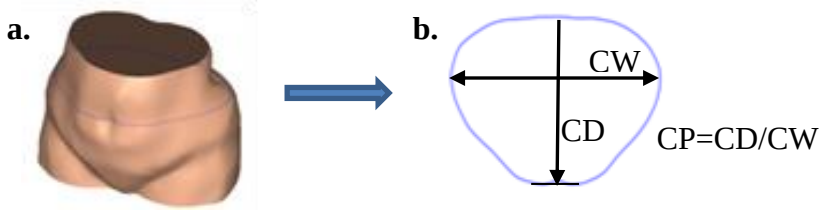

Figure 3.3 Examples of central obesity measurements: (a) Central segmental 3D image and (b) Central width, depth and protrusion measurements

2) Volume Ratio Measurements: Waist volume ratio (WVR) = WaistV /Total body volume. Thigh volume ratio (TVR) =ThighV /Total body volume. WVR and TVR indicate android and gynoid body shapes, respectively.

3) Central Girth (CG) Profile: 20 girths, named CG0, CG1, …, CG19, were measured from waist line to crotch with equal space between each measurement. These measurements established a profile of the central body as shown in Figure 3.4a. The 20 girth measurements were compared to VAT and SAT volumes obtained from MRI, in order to explore the relevancy of each girth (Figure 3.4b). For both men and women, SAT was more related to the girth measured around the central body than VAT. The highest correlation to SAT was found by CG6 which is similar to definition of the circumference of the high hip or abdomen. In regards to VAT, girths measured around the waist provided higher association to VAT than other girths in the profile. Specifically, CG0 (i.e. waist circumference) showed the highest correlation to VAT. Therefore, according to the correlation analysis, CG0 and CG6, the two girth measurements showing the highest correlations for both men and women will be retained as potential predictor variables of the predictions of VAT and SAT prospectively.

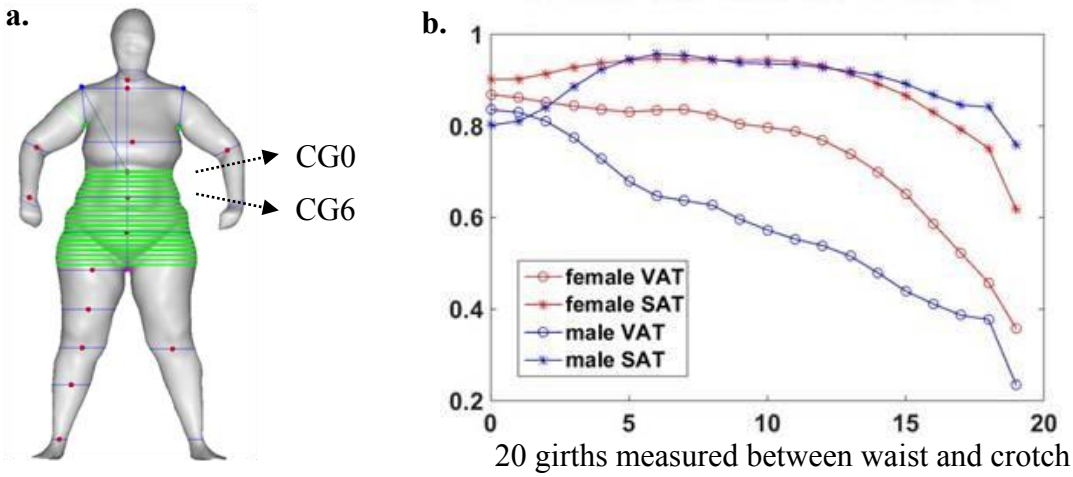

Figure 3.4 (a) An example of central profile established by 20 girth measurements (green lines) and (b) Linear correlations between abdominal fat volumes and the girth profile

4) Body shape index: A pear-shaped (Figure 3.5a) or apple-shaped (Figure 3.5b) body can be viewed better from the side silhouette. The vertical line passing the center of the underbust is used as the reference (R in Figure 3.5). Apple shape index (ASI) and pear shape index (PSI) are defined as: ASI = Da / Dr, and PSI = Dh / Dr, where Dr is half of the under bust depth, Da is the front abdominal (most front protruding) depth, and Dh is the back hip (most back protruding) depth. Thus, the ASI and PSI are quantitative measures of fat distribution and body shape. Specifically, a subject with a higher ASI value is more prone to have apple shaped body since more fat was accumulated around abdomen. A higher PSI value means

the subject has more fat tissue around lower body and therefore the subject has a pear shape body. The ratio of ASI/PSI, is defined as central shape index (CSI) to reflect the difference between the ASI and PSI.

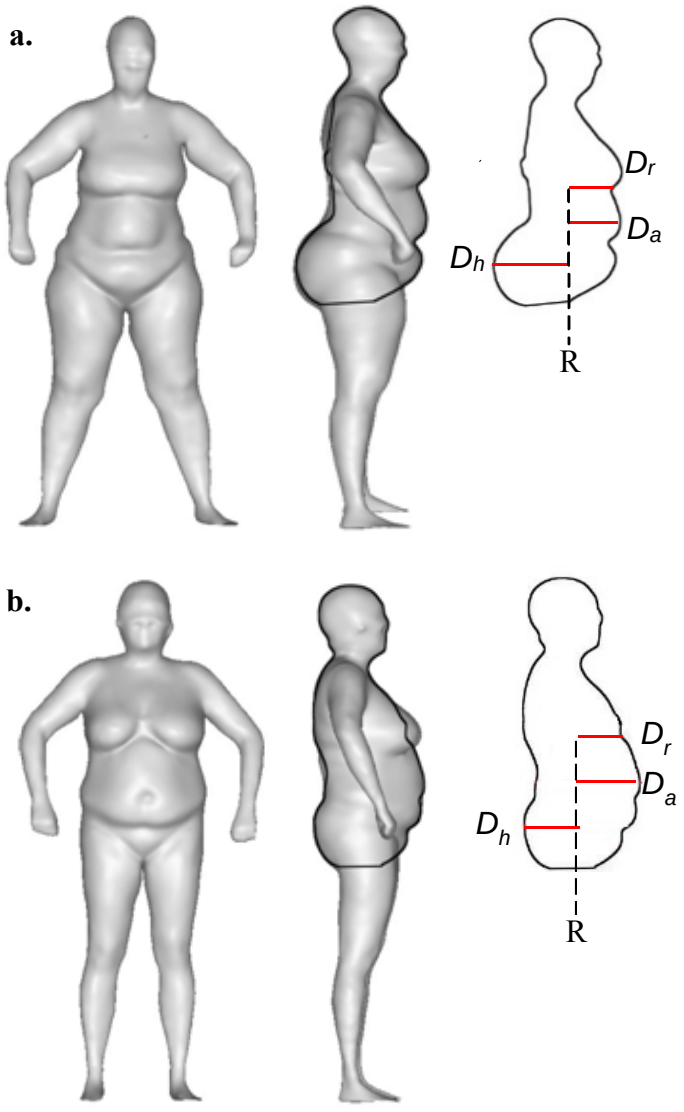

Figure 3.5 (a) Pear-shaped body and (b) Apple-shaped body.

3.5 SUMMARY

In Chapter 3, we proposed a set of novel body shape descriptors assessed from 3D body images that quantitatively characterizing the body shape of human subjects from external perspective. In following chapters, we applied these body shape descriptors to investigate the relations between body shape and internal adiposity. In Chapter 4 and 5, further qualitative analysis of abdominal fat distribution and quantitatively prediction of the visceral and subcutaneous fat volumes are performed.

Chapter 4 Categorization of Abdominal Fat Distribution

The first purpose of this study was to develop a new obesity categorization method based on the abdominal adiposity quantified from MRI with a fully-automated algorithm developed in Chapter 2. Then, we examined whether the new body shape descriptors developed in Chapter 3 were more effective in detecting individuals with specific pattern of abdominal fat distribution than the conventional obesity measurements.

4.1 INTRODUCTION

Currently, the prevalence of obesity remains high in the United States, and more than two-thirds of adults are either overweight or obese defined by body mass index (BMI) [83]. Obesity has become a public health concern because obesity is an important risk factor for various chronical diseases [3], [23], [120] and is highly associated with mortality rates [121], [122]. Also, a recent study of medical care costs showed that more than 160 billion dollars were spent on treating obesity related diseases every year in the United States [123]. Therefore, it is essential to accurately evaluate and categorize obesity status in clinical settings for effective prevention and treatment of the obesity related disorders.

At present, the obesity status can be categorized with a number of measures and approaches. The most commonly used one is the BMI which is calculated by dividing an individual's weight in kilograms by square of height in meters. According to the World Health Organization (WHO), individuals' obesity status can be classified into four categories: underweight (BMI< 18.5), normal ($18.5 \leq \text{BMI} \leq 24.99$), overweight ($25 \leq \text{BMI} \leq 29.99$) and obese (BMI > 30). The obese category can be further divided into three

classes: obese class I ($30 \leq BMI \leq 34.99$), obese class II ($35 \leq BMI \leq 39.99$) and obese class III (BMI >40) [124]. BMI possesses advantages compared with pure weight or weight percentage measurements because it carries some information about body size. BMI is convenient to use and correlated to body fat, morbidity and mortality rates [125]. Moreover, the cutoff values for overweight and obese classes are helpful to identify the patients with higher risks of obesity related chronic diseases [126]. However, BMI is limited for it does not differentiate fat mass and non-fat mass (i.e. muscles and bones). Besides, it cannot state the distribution of the fat mass (i.e. android or gynoid fat). Due to these limitations of BMI, the National health and Nutrition Examination Survey [127] has reported paradoxical findings that 24% normal adults showed metabolically abnormity, while 51% overweight and 32% obese subjects were actually metabolically healthy. In addition, the BMI cutoff values should be adjusted for the population in different ethnic groups [128].

Another body shape related categorization method is waist circumference (WC). In the United States, the subjects were classified as obese if their WC is larger than 102 cm for men or 88 cm for women [129], [130]. WC has been recognized as a useful tool to assess central obesity which has negative impacts on health [13], [131]. Numbers of studies showed that WC is more effective than BMI in terms of predicting obesity-related comorbidity and health risks [14], [132], [133]. However, current WC cutoff values were determined based on their correlation with BMI categories instead of the associations with metabolic risk factors, cardiovascular disease (CVD) risk or other significant information.

In addition, intra- and inter- variations coming from manual tape measurements of WC may cause confounding obesity assessment results [24], [33].

Body fat percentage (BF%) measured via dual energy x-ray absorptiometry (DXA) offers a new obesity categorization method [134]–[136]. There is currently no standard protocol to classify obesity status with BF%, but most researchers have used BF% > 25% in men, and BF > 30% in women, as the cutoff points. DXA provides separate measurements of fat mass, bone mass and muscle mass; therefore, BF% is a more accurate and direct way for measuring adipose tissue amounts than BMI and WC. Nevertheless, BF% ignores several important factors that affect obesity evaluation. First, the overall BF% cannot identify the anatomical location of the fat mass. Also, it is not able to directly discriminate the subcutaneous fat and the visceral fat which has higher impact to health. Although previous studies have proposed models to estimate the visceral adiposity using DXA[90], the accuracy and validity of those models need to be further examined. These limitations of the overall BF% may cause the lower accuracy than BMI and WC when applying BF% to detect metabolic disorders [137].

Abdominal obesity indicating the excess fat depots around abdominal area has shown a very strong correlation with certain types of obesity related diseases [138]. Based on the anatomic location, two types of abdominal adipose tissue are found. The first one is visceral adipose tissue (VAT) which is the body fat stored within the abdominal cavity and around internal organs such as liver, pancreas and intestines. The other type is subcutaneous adipose tissue (SAT) which is accumulated just beneath the skin. With the advanced medical imaging system, intrinsic adiposity can be measured by the magnetic

resonance imaging (MRI) and computed tomography (CT). Several categorization methods were proposed based on visceral fat area (VFA) value which is often assessed from single CT or MRI slice [139]. VFA higher than 103.8 cm^2 on a CT slice cross L4-L5 is highly associated with increased risk of obesity-related disorders, according to Korean researchers [140]. Yumi et.al suggested to use a more complex VFA cutoff system for people in different sex and age groups [139]. Although excessive VAT showed associations with obesity related disorders, the relationship between visceral fat and subcutaneous fat, which cannot be reflected by VFA value, should not be underestimated [141]. Besides, current studies based on the VFA calculated from a single MRI or CT slice may restricted the classification accuracy to a specific slice location due to the variation of the fat distributed within abdominal area (see Chapter 2).

Currently, there is no categorization method representing the precise abdominal fat distribution conditions based on the volumes of adipose tissue across the whole abdominal area. Thus, the first objective of this chapter is to explore the natural grouping of the abdominal adiposity in order to build a new categorization method reflecting the intrinsic abdominal fat distribution. A fuzzy clustering process was used to partition VAT and SAT data into several meaningful subsets. As a result, the samples within the same group should have similar fat distribution pattern, while such similarity between different groups is low. Second, with the utilization of the novel body shape descriptors developed in Chapter 3, we explored if the individuals in the same fat distribution category own the similar characteristics of body shape. Then, we attempted to predict the fat distribution categories by using three different sets of measurements: traditional anthropometric measurements,

DXA based regional fat mass and the body shape descriptors. Cross-validation classification accuracy with an optimized support-vector-machine (SVM) classifier was reported to determine the most effective set of obesity measurements.

4.2 METHODS

4.2.1 Datasets

MRI dataset, DXA dataset, anthropometry dataset and 3D SBI dataset described in Chapter 1.4 were used in this study. A total of 120 subjects (66 men and 54 women) were recruited in this study. Subjects were aged from 19 to 61 years old, with a wide BMI range from 18.61 kg/m^2 to 40.30 kg/m^2, which could be classified as normal to obese class III BMI groups. This study was approved by the Institutional Review Board of the University of Texas at Austin and the informed consent from each subject was obtained.

The fully-automated MRI sequence processing algorithm developed in Chapter 2 was employed to calculate the VAT and SAT volumes of the entire abdominal area without human intervention. VAT and SAT volumes from the 2^{nd} Lumbar vertebra (L2) to L5 (approximately 11 to 16 slices for each subject) were recorded as the ground truth of the abdominal adiposity for the categorization study.

4.2.2 Clustering of abdominal adiposity

Prior to clustering analysis, a modified version of zscore [142] was used to standardize the volume measurements because the range of VAT is significantly different from that of SAT.

$$Z_i = \frac{x_i - median(x)}{MAD(x)} \tag{5.1}$$

here, x is the adiposity volume (i.e. VAT and SAT) measured from the MR images. MAD is the median absolute deviation of the x.

Clustering algorithm was then employed to divide all subjects into different fat distribution categories with distinct abdominal VAT and SAT volumes. The fuzzy *c*-means (FCM) algorithm with Euclidian norm was used. The energy function to be minimized during the FCM iterations is defined as [143]:

$$\min \sum_{k=1}^{N} \sum_{i=1}^{c} \left\| y_k - c_i \right\|^2 \tag{5.2}$$

where N is the total number of data points, c is the number of clusters, y_k is the abdominal adiposity volume (i.e. VAT and SAT) and c_i is the center of the i^{th} cluster. Iterative optimization of the above objective function was carried out with the update of the fuzzy cluster membership of each data point, i.e. subjects and the center of each cluster. Iteration stopped when the centers and the membership were stabilized, or the allowed iteration limit was reached. Finally, the FCM algorithm generated a degree value of belonging to each cluster for every data point. The total degree value of each data point is

equal to 1. In order to simplify the process, the cluster exhibiting the highest degree value was chosen for each data point as the corresponding category label.

In order to find out the optimal cluster numbers, we attempted to partition the data into 2, 3, 4, 5, and 6 clusters. Then, silhouettes graphics [144] and average silhouettes[145] value were employed to examine the clustering quality and determine the optimal cluster numbers. For the data point i, the silhouette value Si can be calculated by:

$$S_i = \frac{(b_i - a_i)}{\max(a_i, b_i)} \tag{4.3}$$

where, a_i is the average distance of the point *i* from other points in the same cluster, b_i is the minimum average distance of the point *i* from the points in different clusters (minimized over clusters). The silhouette value of each data point in the range of [-1, 1] is a measure of how similar that the point is to other points in the same cluster, when compared with other points in different clusters. *Si* close to 1 means this point is very distant from its neighboring clusters; while the *Si* close to -1 indicates the point is not distinct in one cluster or another. The distribution of the *Si* of all data points can be directly displayed by the silhouette graphics. The average silhouettes of the entire dataset is the mean of the S_i over all data points, which demonstrates how appropriately all the points have been clustered [146].

4.2.3 Relationship between fat distribution categories and body shape characteristics

After the category labels of the fat distribution were determined by the fuzzy clustering algorithm, we further explored if the individuals in the same fat distribution category share the similar body shape characteristics. Meanwhile, we also examined if the body shape descriptors are able to capture the body shape differences for the subjects with dissimilar internal fat distribution patterns. One-way ANOVA [147] was utilized to determine if the body shape descriptors are able to capture the body shape differences for the subjects in different categories of fat distribution. Bar charts were plotted for visual examination of the shape body differences between the categories.

4.2.4 SVM classification scheme

An optimized SVM classifier with an embedded feature selection scheme was employed to explore which set of the obesity measurements offers the highest classification accuracy. The three sets of the obesity measurements are:

I. Traditional anthropometric and demographic measurements:

   Sex, ethnicity, age, BMI, weight, height, WC, HC and WHR.

II. Fat mass assessed from DXA scan:

   Total fat mass (Total FM), android fat mass (Android FM), gynoid fat mass (Gynoid FM), trunk fat mass (Trunk FM) and leg fat mass (Leg FM).

III. SBI body shape descriptors:

WaistC (waist circumference), WaistW (waist width), WaistD (waist depth), HipC (hip circumference), HipW (hip width), HipD (hip depth), ThighC (thigh circumference), ThighW (thigh width), ThighD (thigh depth).

TorsoV (torso volume), WCV (waist to crotch volume), WaistV (waist volume), HipV (hip volume) and ThighV (thigh volume).

CW (central width), CD (central depth), CP (central protrusion), WVR (waist volume ratio), TVR (thigh volume ratio), CG6 (6^{th} central girth), ASI (apple shape index), PSI (pear shape index) and CSI (central shape index).

Details of these obesity measurements can be found in Chapter 1 and Chapter 3.

4.2.4.1 Pre-processing

Scaling before using the SVM is very important for preventing biased classification. All measurements were independently normalized into the range of [0, 1]. Therefore, the obesity measurements with larger values would not overwhelm the measurements with smaller values.

4.2.4.2 Multi-classes SVM classifier

A multiclass SVM classifier based on a radial-basis-function (RBF) kernel was used to classify the subjects into the four categories of fat distribution. The basic idea of a non-linear binary SVM classifier is to find an optimal hyperplane that maximizes the margin between two classes in a multi-dimensional data space. Such theory of the maximized soft margin provides a good out-of-sample generalization ability [148]. An one-

against-one scheme was used to manage the multi-class classification problem in the present study [149]. As a results, 6 (=4×3/2) binary classifiers were constructed to differentiate the four fat distribution categories.

Kernel function in SVM is defined as: $K(x_i, x_j) \equiv \phi(x_i^T)\phi(x_j)$, where x_i and x_j are the two vectors in feature subsets. Function ϕ maps the x_i and x_j into a higher dimensional space [150], [151]. With the use of kernel functions, such mapping function does not need to be computed explicitly.(RBF kernel [152] was chosen in this study because it is able to manage the dataset that may not be separable in linear space while preserving high computational efficiency compared to other non-linear kernels, such as sigmoid kernel.

$$RBF : K(x, y) = \exp(-\gamma \|x - y\|^2), r > 0 \tag{4.4}$$

where γ is bandwidth of RBF kernel, which would greatly affect the performance of the classifier.

There are two adjustable parameters in the RBF- SVM classifier: the penalty factor C and the kernel parameter γ. The classification accuracy is largely dependent on the selection of these two parameters [153]. Therefore, a "grid searching" procedure proposed by Lin [154] was employed in this study to determine the optimal selection of the two parameters. The values of (C, γ) pair exponentially grew during the cross-validation process and the final optimized parameters would be the pair of (C, γ) generating the highest classification accuracy. The searching range was preset as: $C = 2^{-10}, 2^{-8}, \ldots, 2^{10}$; $\gamma = 2^{-10}, 2^{-8}, \ldots, 2^{10}$. Thus, 121 pairs of C and γ were attempted for RBF-SVM classifier. LIBSVM [154] function was used to perform the classification study.

In order to prevent over-fitting problem, a five-fold cross-validation procedure was used [155]. During the five-fold cross-validation, the dataset was randomly separated into five subsets (i.e. folds). Each time, the SVM classifier was firstly trained with four subsets and tested by the last subset. Classification accuracy was calculated as: (number of correctly predicted samples / number of total testing samples) ×100%. This procedure was repeated five times to generate an average classification accuracy (i.e. CV accuracy).

4.2.4.3 Feature selection

The objective of feature selection is to reduce the dimensionality of the features (i.e. the three sets of obesity measurements) for eliminating the redundant information within the feature subsets and meanwhile enhancing the generalization ability of the classifier [156], [157]. A four-stage based feature selection scheme was used to produce the optimal subset of features.

Stage 1: Filtering features

One-way ANOVA test was performed to identify which obesity measurement has significant differences ($p<0.01$) between the four fat distribution categories. All significant measurements were retained for the next stage.

Stage 2: Ranking features

A min-redundancy, max-relevance (mRMR) scheme firstly proposed by Peng [158], [159] was utilized to rank the features retained from the *Stage 1*. Ranking the features can improve and facilitate the following feature selection procedure with higher accuracy and less computational demands. The mRMR has been verified to provide good

performance on different types of classifiers including the multiclass SVM classifier used in this study [159].

The mRMR scheme was developed based on mutual information (MI) which is defined as a measure of the mutual dependence between any two variables in probability theory.

$$I(x, y) = \iint p(x, y) \log(\frac{p(x, y)}{p(x), p(y)}) dxdy \tag{4.5}$$

where, *p(x,y)* is the joint probability density function of two variables *x* and *y*, while *p(x)* and *p(y)* are the marginal probability density functions of *x* and *y*, respectively. In our study, *x* denotes the obesity measurements and *y* is the category labels of fat distribution.

Based on the definition of MI, the maximum relevance (i.e. dependency) can be obtained by optimizing the following equation:

$$D = \frac{1}{|S|} \sum_{x_i \in S} I(x_i; c) \tag{4.6}$$

Similarly, the minimized redundancy between features can be achieved through the equation:

$$R = \frac{1}{|S|^2} \sum_{x_i, x_j} I(x_i; x_j) \tag{4.7}$$

where x_i and x_j are the *ith and jth* feature in the feature subset S. c is the target class labels.

The above two equations can be simply combined to get the final mutual information difference equation: $\max \Phi(D, R), \Phi = D - R$.

The inputs of the mRMR scheme is all of the features retained after *Stage 1* and the target class labels (i.e. fat distribution categories). The output is a candidate list of features which can be used to facilitate the searching procedure in the next stage.

Stage 3 Searching for the optimal subset of features

In order to find the optimal subset of features providing the highest classification accuracy, a sequential forward searching procedure was used [160]. The forward searching procedure starts with an empty set, then, firstly takes the feature ranked the first place from S*tage 2* and computes the average classification accuracy to get the initial *CV accuracy*. Next, the procedure selects a new feature according to the feature ranking result and computes the new *CV accuracy* -- if it is increased, then adds the new feature to the feature subset. This forward searching repeats until the classification accuracy cannot be increased anymore. In this study, the final output is the optimal set of features that offers the highest CV accuracy.

4.3 RESULTS

4.3.1 Clustering of central obesity

Figure 4.1 displays the silhouette graphics and the average silhouette values for each attempted cluster number C (C=2,3,4,5,6). The highest average silhouette value (0.6672) reflecting the best clustering quality was achieved when C equals 4. Also, when C equals 4, least numbers of data points had the silhouette value less than 0, suggesting least numbers of data points were mistakenly clustered. The second highest average

silhouette value was achieved at C = 3, but visibly higher clustering errors are noted on the corresponding silhouette graphic. Therefore, the optimal number of clusters is four.

Four clusters representing four different patterns of fat distribution are shown in Figure 4.2. Red color (C1) indicates the subjects with normal VAT and SAT volumes and purple color (C4) shows the subjects with equally elevated VAT and SAT volumes. Unbalanced growth of abdominal fat was showed with green color (C2) and blue color (C3), which represent significantly higher VAT growth and significantly higher SAT growth, respectively. It should be noted that for the data points on boundaries of clusters, trivial degree differences between two or three clusters were obtained. The small difference of degrees means that these data might belong to more than one cluster. However, those data points were not eliminated for further classification study since it is important for a robust classifier to manage the data on the boundaries of clusters.

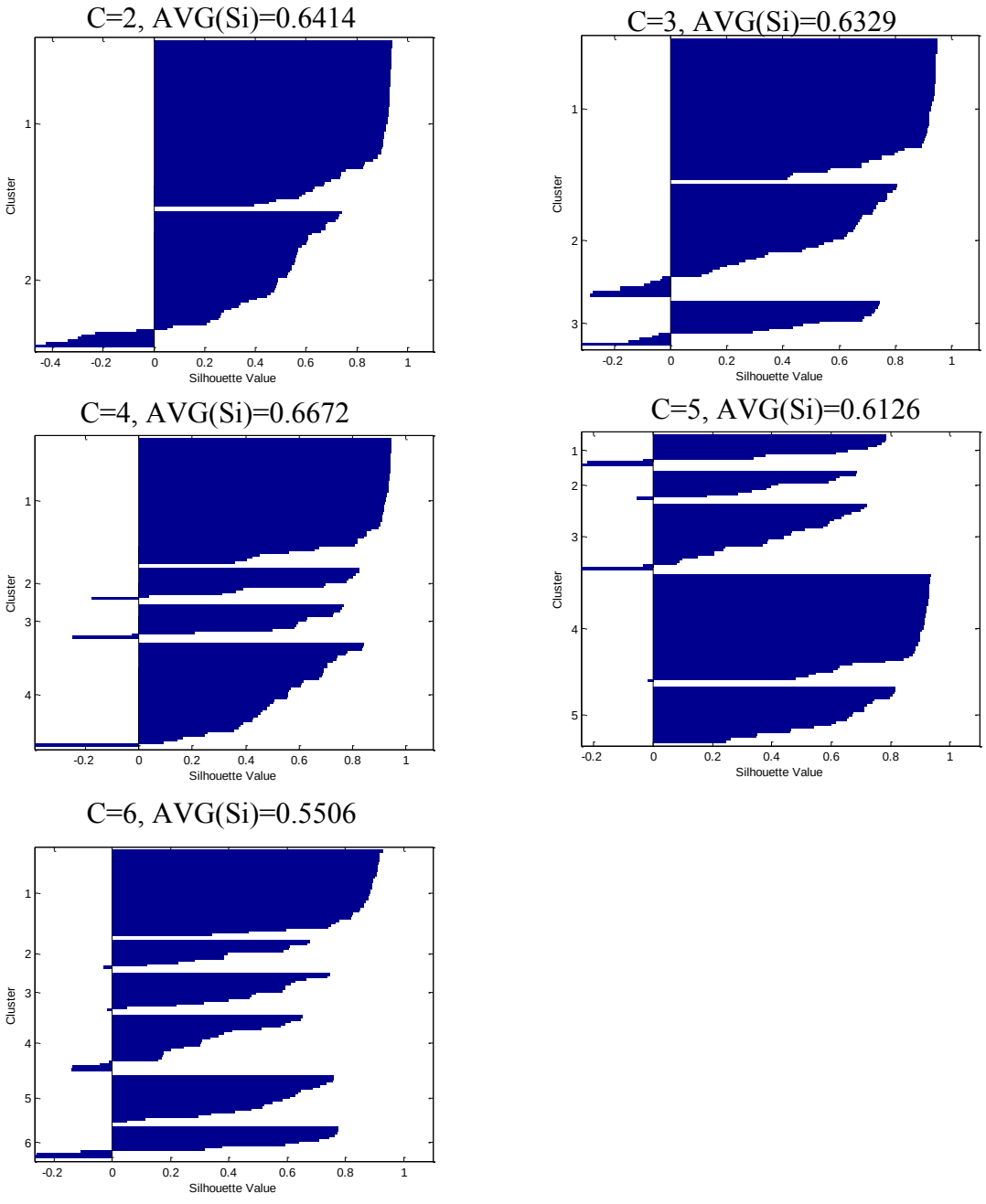

Figure 4.1 Silhouette graphics and average silhouette values with different cluster numbers

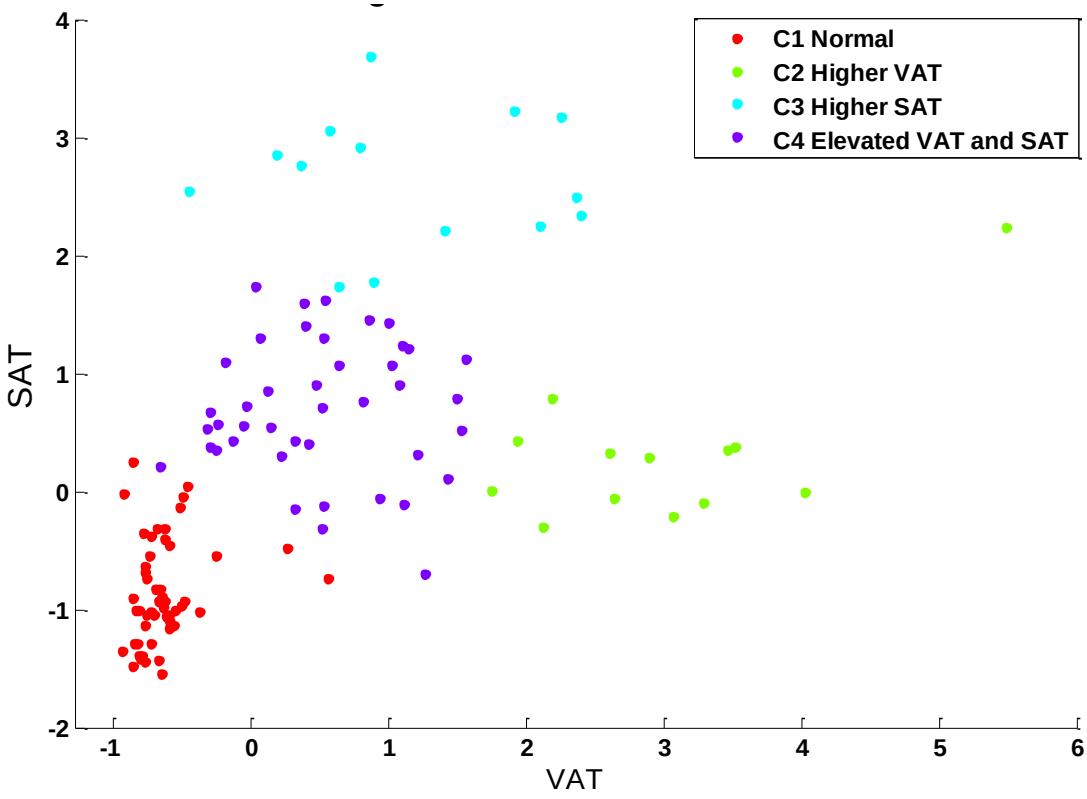

Figure 4.2 Final clustering results with the optimal cluster numbers (C=4) reflecting four categories of abdominal fat distribution. SAT (y-axis) and VAT (x-axis) values were standardized.

We firstly examined the sex information of the subjects with different fat distribution patterns, and found out that there are 22 women and 29 men subjects in C1. In C2, all of the 13 subjects are men. 6 women and 8 men were grouped into C3. In C4, there are 10 male subjects and 26 female subjects. It is important to note that there are no female subjects grouped into C2 which is the cluster of unbalanced higher growth of visceral fat.

This finding is in agreement with previous studies that white men tends to accumulate more visceral fat around abdomen that compared to white women [161].

A one-way ANOVA test indicates that SAT volume, VAT volume, and the ratio of VAT/SAT are significantly different between four catteries of fat distribution. Further, a Games-Howell [162] post-hoc analysis was performed for pair-wise comparison between the categories. This specific post-hoc method was chosen because the data set has unbalanced sample size and unequal variance among categories based on Levene's statistics test [163]. For VAT volume, except C3 and C4, all other pairs of categories are significantly different. For SAT volume, comparison between all possible pairs of groups are significantly different. For VAT/SAT, C2 was significantly different from the other three categories. The boxplot of the three measurements are shown in Figure 4.3

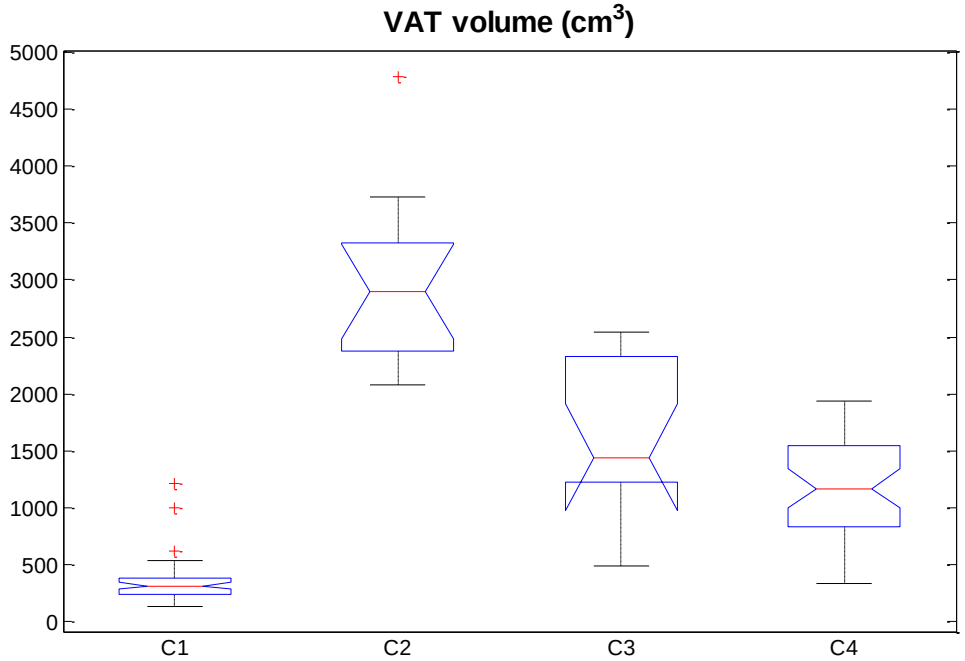

Figure 4.3

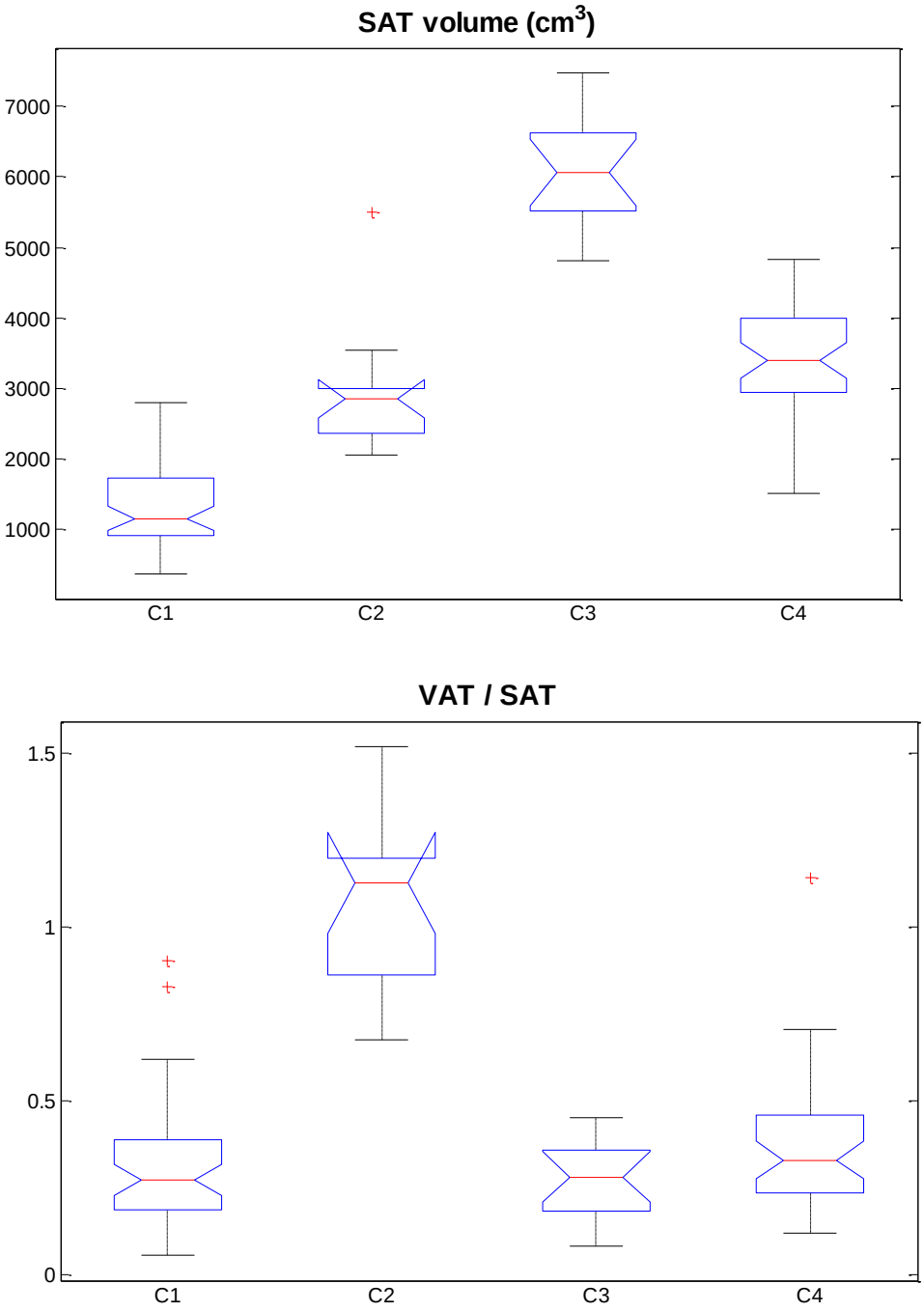

Figure 4.3 Box plots of VAT volume, SAT volume and VAT/SAT ratio of the four fat distribution categories.

4.3.2 Relationship between body shape and fat distribution categories

One-way ANOVA analysis was performed to identify which body shape descriptors were able to indicate statistical differences between the four fat distribution categories. It turns out that all of the body shape descriptors expect ASI showed significant differences ($p<0.01$) between the four categories.

Bar charts are selectively shown in Figure 4.4 to illustrate if the individuals in the same fat distribution category also possess the similar body shape. The subjects with lower level abdominal adiposity in C1 show higher TVR value than the subjects in other categories, which suggests a large portion of the body fat tissue is located around thighs. However, the absolute thigh volumes (Figure 4.4 a) of those subjects are not as high as the subjects in C3 and C4. Moreover, the subjects with equally elevated VAT and SAT in C4 have slightly higher WVR value and lower TVR value than the subjects in C1, which indicates that those subjects with more internal adiposity are having more fat tissue around waist and less fat tissue around thighs compared to normal subjects. For the subjects in C3 with higher SAT growth, they show significantly higher thigh volumes (ThighV) as well as higher WVR than other subjects, suggesting that these subjects with more SAT may have higher accumulation of fat tissue around thighs and waist than other subjects.

C2 is the category we are most interested in because C2 indicates a potentially harmful pattern of fat distribution – the higher VAT growth which is highly associated with the risk of various types of diseases. Two noteworthy trends are found in the Figure 4.4d and e. Subjects in C2 have significantly higher value of CSI and TVR, which means their body shapes have prominently front protrusion around abdomen and very small portion of

their fat is located around the hips and thighs. Figure 4.5 shows examples of 3D body images belonging to each fat distribution category for visualization of the body shape characteristics in the corresponding categories.

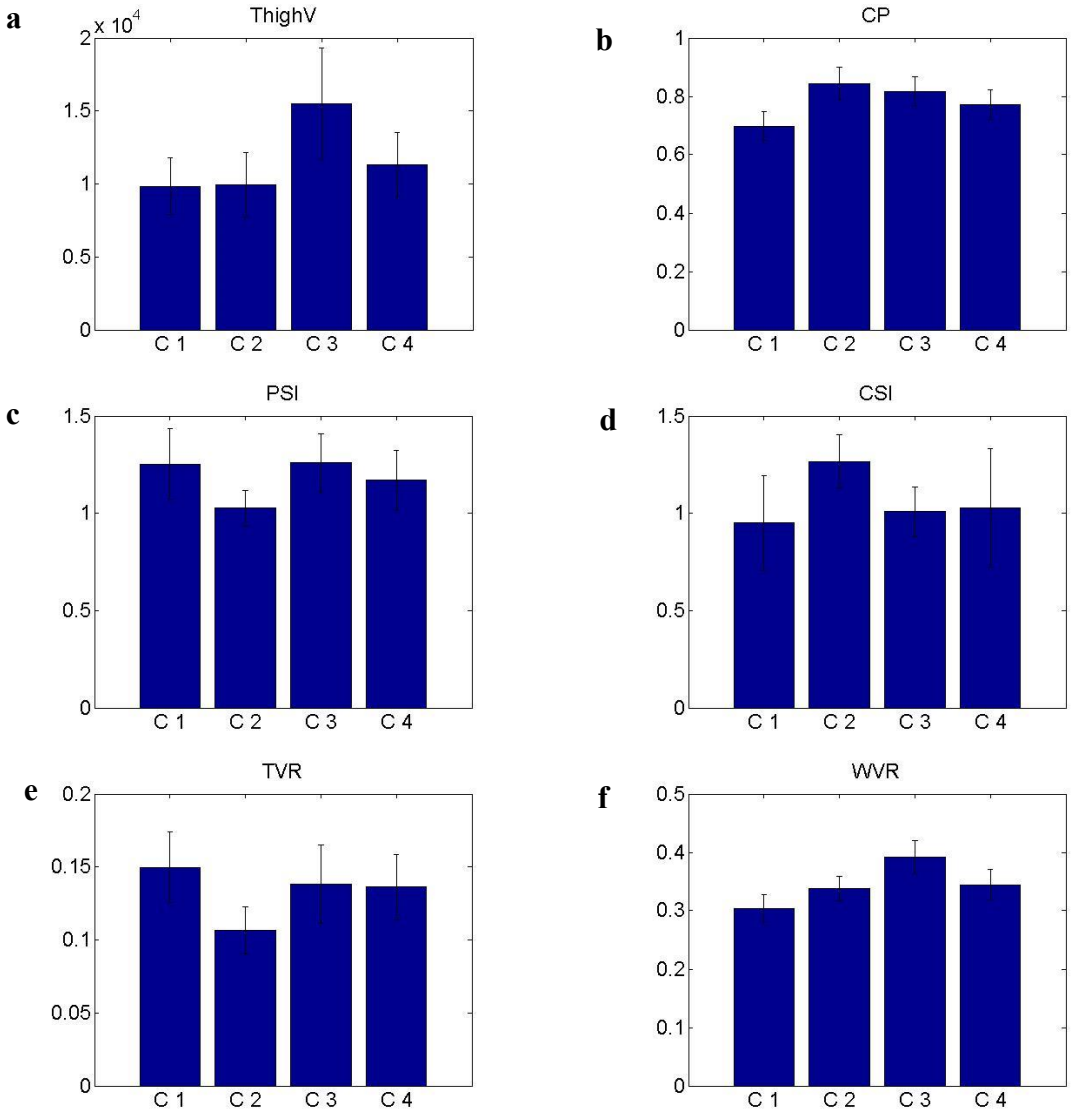

Figure 4.4 Bar charts of the value of the body shape descriptors in four fat distribution categories. (a) ThighV, (b) CP, (c) PSI (d) CSI (e) TVR and (f) WVR

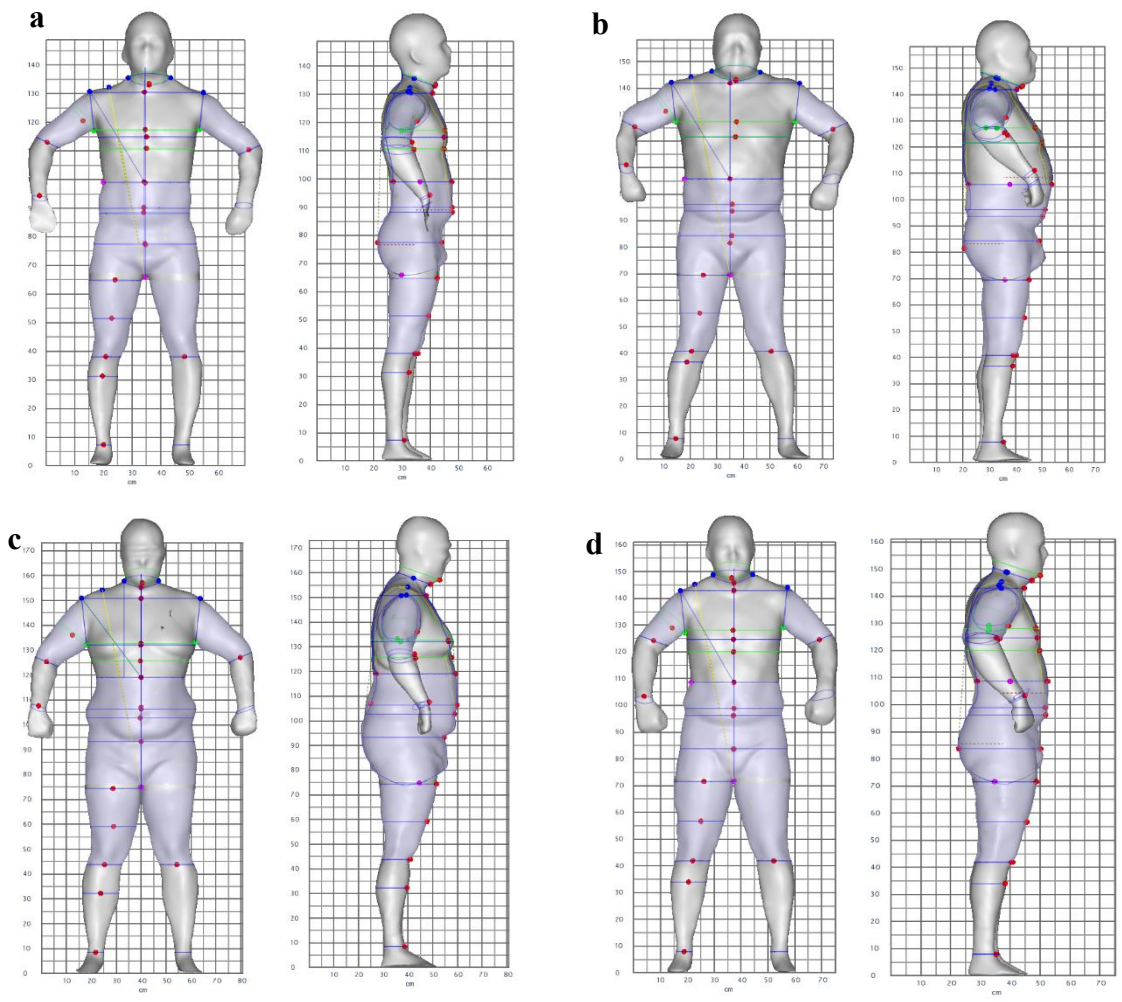

Figure 4.5 Examples of male subjects in four categories of abdominal adiposity. (a) C1, (b) C2, (c) C3 and (d) C4.

4.3.3 Classification and comparison

4.3.3.1 Managing unbalanced class size

In this study, sample numbers in different fat distribution categories (i.e. classes) are unequal: class 1 - normal subject: *51 samples*, class 2 - significantly higher growth of VAT, *13 samples*, class 3 - significantly higher growth of SAT, *14 samples* and class 4 - equal elevated VAT and SAT, *42 samples*. Obviously, two majority classes (C1 and C4) have more samples than the two minority classes (C2 and C4). As mentioned above, the SVM classifier searches for the best hyperplane that can maximize the margin between classes for a lower expected risk for future unknown samples [164]. However, SVM classifier may lose its effectiveness and generalization ability when a highly unbalanced dataset is present.

Undersampling and oversampling techniques are very popular methods that randomly reduce or add the samples to specific classes in order to generate a more balanced dataset [165]. These two techniques are easy to implement but it may cause the inherent loss of valuable information or addition of noise. Therefore, in this study, we chose a different technique to manage the unbalanced sample size by assigning different weights (w_i) to different classes [166]–[168]. Basically, this technique gives different penalty parameters to the classes with different sizes. The value of the weight should be inversely proportional to the sample size. In this this study, for the four fat distribution categories: class1/class2/class3/class4, the sample size ratio between them is around 4/1/1/4. Therefore the weight w_i assigned to the four classes should be: w_1=1, w_2=4, w_3=4 and w_4=1. It should

be noted that a common penalty parameter C was optimized with the grid searching procedure mentioned in 4.2.3.2, so the final penalty parameter for each class can be calculated by $C_i = C \times w_i$..

4.3.3.2 Classification results

First, the three sets of obesity measurements (i.e. traditional measurements, DXA FM and 3D body shape descriptors) were scaled into [0, 1] and analyzed using ANOVA analysis. Ethnicity (in traditional set) and ASI (in 3D body shape descriptors set) do not show significant difference between the four categories ($p > 0.05$). Therefore, the two measurements were excluded from further feature selection. All other measurements were used as inputs of the RBF SVM classifier with the embedded mRMR feature ranking and forward feature selection procedure. The feature selection and classification results are:

1. Traditional measurements

   Waist C, sex and BMI were selected as the optimal feature set and produced the CV accuracy at 85%.

2. DXA measurements

   Android FM, Gynoid FM and Trunk FM were chosen as the best feature set with a CV accuracy at 87.5%

3. 3D Body shape descriptors

   Eight features, CD, HipW, WaistW, HipV, WaistD, TorsoV, CW and CG6 were selected, and the corresponding CV classification accuracy was 90%.

As a result, the 3D body shape descriptors provide the most accurate prediction of category labels of the abdominal fat distribution. The forward searching method used in this study incrementally selects the optimal features in order to obtain the highest accuracy without adding too much redundant information.

In order to examine the body shape descriptors that were not automatically selected by the feature selection scheme, we arbitrarily eliminated some selected descriptors or replaced them by other descriptors. The tested feature sets and their corresponding CV accuracy are:

1) CD, WaistD, TorsoV, CG6; CV accuracy: 89.16%
2) WasitD, CG6, WC , WaistV, CentralW, HipD, HipV; CV accuracy: 87.5%
3) PSI, WVR, TVR, CW; CV accuracy: 84.17%

It turns out that the above four tested sets of features either provide similar high accuracy like the optimal feature sets do, or gives a decent prediction result. It is suggested that the novel body shape descriptors are able to predict the categories of fat distribution from different perspectives and the performance of the prediction is not strongly dependent on the choice of the specific sets of descriptors.

4.4 DISCUSSION

Abdominal obesity defined as excessive adipose tissue accumulated around abdominal area has been linked to a number of metabolic abnormalities such as hyper insulinemia, glucose intolerance, insulin resistance, elevated triglyceride levels and increased risk of hypertension, diabetes and cardiovascular diseases [169]–[174].

However, currently there is no available categorization method designed for internal abdominal obesity and its distribution. In this study, we developed a new categorization method using fuzzy clustering algorithm in order to explore the intrinsic grouping of the abdominal fat distribution. The ground truth of the abdominal adiposity was assessed from the MRI sequences acquired from 120 subjects with a wide range of BMIs and age. As a result, four natural clusters of abdominal adiposity were determined. The two major clusters are C1 (normal amount of adipose tissue) and C4 (elevated abdominal adiposity with balanced growth of visceral fat and subcutaneous fat). The two minor clusters are C2 (significantly higher growth of visceral fat) and C3 (significantly higher growth of subcutaneous fat).

With the utilization of the novel 3D body shape descriptors, we then investigated the relation between fat distribution pattern and body shape characteristics. It is found that the subjects with higher internal VAT growth also have more prominent abdominal protrusion than hip protrusion. In contrast, the subjects with an equal VAT&SAT growth or a higher SAT growth possess more fat accumulated around hip and thighs. Furthermore, the higher thigh volume ratio is found in the subjects with lower VAT growth, which is consistent with the previous reports that lower extremity fat is favorably associated with glucose metabolism [175]. These findings reveal the linkage between the intrinsic abdominal adiposity and the external body shape study by using the body shape descriptors and the adiposity volume statistically. The present study, for the first time, quantitatively proves that subjects with apple-shaped body is less healthy than others with pear-shaped body with in-depth 3D measures.

In this study, we also compared the effectiveness of different obesity measurements in predicting the known fat distribution categories through an optimized SVM classification scheme. A four stage feature selection method was utilized to search for the optimal subsets of the measurements that can provide the highest classification accuracy with least redundant information. The reported unbiased cross validation accuracy indicates that the body shape descriptors are able to provide a higher prediction accuracy compared to other conventional measurements and DXA indices. This finding is promising and shows that the 3D body shape descriptors are more accurate way to diagnose obesity and have the potential to substitute the traditional diagnostic methods. It should be noted that the body shape descriptors were obtained from a low cost, highly portable 3D stereovision system that completes image acquisition and quantitative measurements within a few seconds, while the traditional tape measurements are more labor intensive, time-consuming, and inconvenient. For DXA, high cost and radiation make it a less favorable tool for routine obesity assessment.

One limitation of this study is the lack of direct measures of metabolic risk factors, such as blood pressure, level of high- and low-density-lipoprotein cholesterol, glucose tolerance and level of triglyceridaemia. The future work needs to consider the exploration of the relations between the body shape and the status of metabolism with more direct lab test results, such as the Comprehensive Metabolic Panel (CMP) [176], [177]. Another limitation is the sample size used in the study for natural clustering of abdominal adiposity. More subjects should be recruited in the future to improve the statistical power of the study and to eliminate any potential sampling bias.

In conclusion, the development and usage of the quantitative measurements of body shape signify advancement of the 3D body imaging technique in medical applications. Clinically, the 3D SBI system can be used as indicators of intrinsic fat distribution of abdominal adiposity that highly impacts the morbidity and mortality of several obesity-related diseases.

4.5 SUMMARY

In Chapter 4, we applied the novel 3D body shape descriptors developed in Chapter 3 to predict the categories of the abdominal fat distribution. Utilization of the automated MRI processing algorithm developed in Chapter 2 enabled the clustering analysis of the abdominal adiposity. The findings in this chapter statistically proved the linkage between internal adiposity and external body shape.

Chapter 5 Associations between Abdominal Adiposity and Body Shape

Excessive adipose tissue is associated with high risks of developing diabetes mellitus type 2, cardiovascular disease and metabolic syndrome. Magnetic resonance imaging (MRI) is a gold standard to measure intrinsic adiposity, yet its usage is limited by high cost and intensive labor required for analyzing MR images. In this chapter, we attempt to utilize the innovative body shape descriptors designed based on a stereovision body imaging (SBI) system to predict intrinsic abdominal adiposity, (i.e. visceral (VAT) and subcutaneous (SAT) adipose tissue). The accuracy of the predictive models developed in this study demonstrates the possibility to use the safe, low-cost and portable SBI as a substitute for expensive instrumentations such as MRI and CT for routine obesity assessment.

5.1 INTRODUCTION

Magnetic resonance imaging (MRI) technique often is used as a gold standard for abdominal adiposity quantification, nevertheless, its usage is highly limited due to the high cost and low accessibility. Therefore, it is critical to establish mathematical models to predict the intrinsic VAT and SAT volumes through other more attainable and inexpensive equipment. Simple anthropometric measurements, such as waist circumference (WC), waist to hip ratio (WHR), sagittal abdominal diameter (SAD) and body mass index (BMI) have been investigated to predict the abdominal adiposity assessed from a single abdominal MRI slice [119], [132], [178], [179]. However, the accuracy of the prediction equations is limited by three major challenges. First, SAT and VAT measured from a single MRI or

computed tomography (CT) slice may not sufficiently represent the total abdominal adiposity condition, if there is high body composition variability among slices [113]. Second, manual anthropometric measurements and supervised MR image processing are time consuming and subject to human errors [33], [180]. Third, the currently available anthropometric measurements may not be able to reflect the intrinsic fat distribution condition, thus these are inadequate to accurately predict the adiposity [22], [23], [181].

This study seeks to address the above challenges by utilizing a 3-dimensional (3D) stereovision body imaging (SBI) system and the MRI sequences of the whole abdominal area, from the 2nd Lumbar vertebra (L2) to L5. A fully-automated MRI sequence processing algorithm developed in Chapter 2 was employed to assess VAT and SAT volumes from the MRI sequences without human intervention. Novel shape descriptors characterizing fat distribution and body shape from exterior perspectives (see Chapter 3) were compared with VAT and SAT volumes to determine the associations between external shape features and intrinsic fat depots. In addition, the novel shape descriptors were used to develop mathematical equations for direct predictions of abdominal subcutaneous and visceral adiposity.

5.2 METHODS

5.2.1 Datasets

MRI dataset and 3D SBI dataset described in Chapter 1.4 were used in this study. The study is based on a total of 121 subjects (66 men and 55 women) aged from 19 to 61 years old, with a wide BMI range from 18.19 kg/m^2 to 40.35 kg/m^2, which could be

classified as normal to obese class III BMI groups [83]. The fully-automated MRI processing algorithm developed in Chapter 2 was employed to calculate VAT and SAT volumes of the entire abdominal area without human supervision. VAT and SAT volumes from L2 to L5 (approximately 11 to 16 slices for each subject) are considered as the reference standard for prediction of abdominal adiposity.

5.2.2 Design of abdominal adiposity prediction equations and statistical analysis

66 men and 55 women participants were assigned randomly into the training group (70% of sample) and the validation group (30% of sample). As a result, 46 men and 38 women were used to develop the prediction equations and the remaining 20 men and 17 women were used to assess the validity of the developed equations. Since men and women are likely to exhibit different fat distributions [2], the predictive equations were designed according to sex.

Linear Pearson correlation coefficients (R) were utilized to test relationships of abdominal VAT and SAT versus age, BMI and SBI body shape descriptors. Three categories of the body shape descriptors include:

1) 12 landmark measurements: WaistC (waist circumference), WaistW (waist width), WaistD (waist depth), HipC (hip circumference), HipW (hip width), HipD (hip depth), ThighC (thigh circumference), ThighW (thigh width) and ThighD (thigh depth).

2) Five regional volume measurements: TorsoV (torso volume), WCV(waist to crotch volume), WaistV (waist volume), HipV (hip volume) and ThighV (two thighs volume).

3) Eight panoramic indices: CW (central width), CD (central depth), CP (central protrusion), WVR (waist volume ratio), TVR (thighs volume ratio), CG6 (6^{th} central girth), ASI (apple shape index) and PSI (pear shape index).

Detailed explanations of the body shape descriptors measured from 3D body images can be found in Chapter 3. Central shape index (CSI) is not used in the study since it is highly correlated to ASI and PSI.

The above parameters exhibited high correlation ($R>0.3$, $p<0.05$) with SAT or VAT measurements were retained as the potential predictors for developing the prediction equations through multiple linear regression analyses. In the regression analyses, VAT and SAT were the dependent variables and the retained traditional and body shape descriptors are independent variables. Multicollinearity between the independent variables was prevented by examining the variance inflation factor (VIF). Any regression model showing a VIF>10 was removed. The prediction model exhibiting the highest R^2 based on the training data set was selected as the final prediction equations for abdominal adiposity. R, R^2 and standard error estimation (SSE, cm^3) were calculated.

Validation data sets that were different from the samples used to develop the equations, were employed to test the validity and generalization ability of the prediction equations. R^2, mean error (observed value - predicted value, ME, cm^3) and 95% confidence intervals (CI) were calculated. All statistical analyses were performed using Matlab

(MathWorksInc, Natic, MA) and SPSS Statistics (IBM SPSS, Chicago, IL). The alpha level of 0.05 was adopted to determine statistical significance.

5.3 RESULTS

5.3.1 Characteristics of training and validation datasets

Characteristics of 112 subjects are shown in Table 5.1. T-tests showed no significant differences ($p>0.05$) of parameters of age, weight, BMI, WC, VAT and SAT, between the subjects in the training group (46 men and 38 women) and in the validation group (20 men and 17 women).

Table 5.1 Characteristics of training and validation data set

	Men			**Women**		
	46 Training Mean±SD (Range)	20 Validation Mean±SD (Range)	P-value	38 Training Mean±SD (Range)	17 Validation Mean±SD (Range)	P-value
Age (years)	34±11.3 (19-60)	36±12.4 (22-60)	0.59	35±9.1 (19-61)	35±11.7 (19-55)	0.83
Weight (kg)	86.7±16.5 (59.5-128.1)	86.7±20.7 (65.0-129.5)	0.99	77.0±17.5 (47.3-126.8)	74.6±14.6 (53.5-109.2)	0.61
BMI (kg/m^2)	28.5±6.0 (20.34-40.35)	27.8±4.8 (20.3-40.3)	0.64	29.1±5.8 (18.2-40.1)	27.2±5.4 (19.0-35.8)	0.25
Waist C (cm)	93.4±12.8 (72.0-116.2)	94.9±15.9 (73.7-133.9)	0.69	88.7±15.3 (63.1-113.9)	86.0±12.9 (70.0-105.4)	0.53
VAT (cm^3)	1258.2±1021.0 (187.7-3723.0)	1347.4±1256.2 (222.4-4782.9)	0.76	822.1±554.0 (134.9-2517.4)	816.6±606.4 (137.8-2517.4)	0.97
SAT (cm^3)	2536.2±1647.9 (502.1-6770.6)	2561.4±1955.3 (586.1-7473.4)	0.96	3214.9±1683.6 (376.0-6413.4)	2763.5±1409.9 (454.7-5015.3)	0.34

SD: standard deviation; BMI: body mass index; WaistC: waist circumference measured by SBI; VAT: visceral abdominal adipose tissue; SAT: subcutaneous abdominal adipose tissue; Levene's test confirmed equal variance between the training data set and the validation data set in all parameters.

5.3.2 Correlation between abdominal adiposity and predictor variables

Table 5.2 shows Pearson correlation coefficients (R) between abdominal adiposity (i.e., VAT and SAT volumes) and the potential predictor variables (age, BMI and body shape descriptors). BMI was significantly correlated to both VAT and SAT, while age was only significantly related to VAT. All body shape descriptors were significantly related to VAT in men, except thigh measurements (i.e. Thigh C, Thigh D and ThighV). In women, only Thigh D and ASI did not show significant correlations with VAT. The highest correlations to VAT were found at the waist landmark measurements (i.e. waist circumference and waist depth, for men and women, respectively).

All of the body shape descriptors were significantly related to SAT in men, except PSI and TVR. In women, the body shape index (i.e., ASI and PSI) were not significantly associated with SAT. In both sexes, the highest correlation coefficient was found at CG6 (i.e. the 6^{th} girth in central girth profile).

Moreover, novel body shape descriptors, such as CG6, CW, CD and CP showed very high correlations with both VAT and SAT. ASI was only correlated with abdominal adiposity in men. PSI is the only parameter showing negative correlations with VAT in both sexes. Potential predictor variables that were significantly correlated to abdominal adiposity were applied in the regression analyses to develop the prediction equations for men VAT, men SAT, women VAT and women SAT.

Table 5.2 Pearson correlation coefficients (R) of VAT and SAT versus age, BMI and SBI parameters.

	Men		Women	
Parameters	VAT	SAT	VAT	SAT
Age	0.594	--	0.462	--
BMI	0.658	0.881	0.783	0.910
Landmark measurements				
WaistC (CG0)	0.835	0.802	0.868	0.902
WaistW	0.783	0.794	0.829	0.890
WaistD	0.844	0.797	0.866	0.890
HipC	0.499	0.913	0.700	0.893
HipW	0.466	0.906	0.655	0.844
HipD	0.578	0.895	0.760	0.908
ThighC	--	0.548	0.308*	0.640
ThighW	0.299*	0.723	0.482	0.690
ThighD	--	0.756	--	0.567
Regional volume measurements				
TorsoV	0.665	0.916	0.798	0.927
WCV	0.568	0.954	0.762	0.921
WaistV	0.539	0.946	0.749	0.891

Table 5.2 (continued)

HipV	0.552	0.792	0.713	0.886
ThighV	--	0.521	0.312*	0.642
Panoramic indices				
CG6	0.647	0.956	0.835	0.947
CW	0.563	0.952	0.772	0.924
CD	0.760	0.902	0.869	0.892
CP	0.760	0.494	0.821	0.713
ASI	0.466	0.320	--	--
PSI	-0.392	--	-0.303*	--
WVR	0.434	0.891	0.667	0.776
TVR	-0.562	--	-0.588	-0.296*

VAT: visceral abdominal adipose tissue volume; SAT: subcutaneous abdominal adipose; BMI: body mass index; C: circumference; W: width; D: depth; CG: central girth; CW: central width, CD: central depth; CP: central protrusion ratio; ASI: apple shape index; PSI: pear shape index; WVR: waist volume ratio and TVR: thigh volume ratio. All correlations are significant at 0.01 level except *significant at 0.05 level. Non-significant values are not shown.

5.3.3 Final prediction equations and validation results

VAT prediction for men:

A stepwise multiple linear regression analysis with no controls generated the simplest prediction equation. Using WaistD, ASI and age as the independent parameters, 74.2% of the variance in men was explained:

$$VAT\ (cm^3) = -5163.506 + 113.866\ WaistD + 2024.210\ ASI + 29.191\ Age$$

Standardized Beta values of the selected parameters were: WaistD: 0.504, Age: 0.323, ASI: 0.227. The standard error of the estimate (SEE) was 518 cm^3 (Table 5.3).

VAT prediction for women:

Firstly, stepwise regression with no controls selected WaistC and age as the simplest model which explained 78.9% of the VAT variance. Adding TorsoV and TVR increased the variance to 80.4%. Thus, the final prediction equation is:

$$VAT\ (cm^3) = -1082.839 + 1.962\ WaistC + 8.451Age + 0.012TorsoV - 3736.809TVR$$

Standardized Beta values of the selected parameters are: WaistC: 0.541, age: 0.139, TorsoV: 0.231 and TVR: -0.145. This prediction equation generated a SEE at 259 cm^3 (Table 5.3).

SAT prediction for men:

For men, the optimal and simplest prediction equation is derived from no controlled stepwise regression:

$$SAT(cm^3) = -6707.8 + 12.4CG6 - 4100.1\ CP$$

This simple equation exhibited a high R^2 (93.3%), adding more variables only generated a marginal influence on the variance. Standardized Beta values for the two selected parameters are: CG6: 1.041 and CP: -0.161 and the SEE is 437 cm^3 (Table 5.3).

SAT prediction for women:

For women, the optimal prediction equation was obtained by using CG6, CP and HipV through multiple regression:

$$SAT\ (cm3) = -5211.3 + 10.525CG6 - 4240.7CP + 0.97HipV$$

This equation explained a high variance (93.0%) of SAT volume in women. The same parameters were selected to predict the SAT for men, with the exception of the *HipV*, this implies that hip volume has more influence on SAT prediction in women. Standardized Beta values for the selected parameters are *CG6*: 0.966, *CP*: -0.198 and *HipV*: 0.177, and the SEE is 463 cm^3 (Table 5.3).

The generalization ability of the four developed prediction equations was tested using the validation data set. R^2-validation, ME and 95% CI were calculated as cross-validation methods (Table 5.3). Similar R^2s were obtained in the validation groups: VAT (men): 79.9%, VAT (women): 80.1%, SAT (men): 90.4% and SAT (women): 89.0%. Differences between predicted values and observed value were calculated using ME and are shown in Table 5.3. 95% CI of ME encompassed zero, indicating that the predicted abdominal adiposity (both VAT and SAT) were not substantially different from the observed adiposity value at the significant level of 0.05.

It is noted that BMI was not selected as an independent variable in all equations, and age was selected only for VAT prediction in both sexes, while age and BMI were not selected for SAT prediction.

Table 5.3 Training and validation results of prediction equations

		Parameter selected	R	R^2	SEE (cm^3)	ME (CI)	R^2 Validation
VAT	Men	*WaistD/ Age /ASI*	0.861	0.742	537	16 (-253, 285)	0.806
	Women	*WaistC/Age /TorsoV/TVR*	0.897	0.804	259	65 (-76, 208)	0.801
SAT	Men	*CG6/CP*	0.966	0.933	437	85 (-180, 351)	0.904
	Women	*CG6/CP /HipV*	0.965	0.930	477	-146 (-418, 126)	0.890

VAT: visceral abdominal adipose tissue volume; SAT: subcutaneous abdominal; WaistD: waist depth; ASI: apple shape index; PSI: pear shape index; WaistC: waist circumference; TorsoV: torso volume; TVR: ratio of two thighs volume to whole body volume; CG: central girth; CP: central protrusion ratio; HipV: hip volume; SEE: standard error estimation; CI: confidence intervals and ME: mean error.

5.3.4 Regression analysis on combined dataset

In order to explore if the body shape descriptors are able to predict abdominal adiposity without sex information, we performed the multiple stepwise regression analysis on the dataset with a combination of both female and male subjects (n=121). 70% of sample (n=84) were randomly selected as training data and the remaining samples (n=37) were used as a validation data set.

The optimal prediction equation for VAT:

VAT (cm^3) = -3116.799 + 57.071 WaistC - 19.222 HipC + 514.039 ASI +13.956 Age.

The R^2s calculated by the training data and the validation data are 75.1% and 74.0%, respectively.

The optimal prediction equation for SAT:

SAT (cm^3) = -9522.096 + 8.864 CG6 +106.85 ThighD - 16.537 Age + 5634.656 WVR.

The R^2s calculated by the training data and the validation data are 93.8% and 85.9%, respectively.

5.4 DISCUSSION

This study developed the mathematical equations for predicting the volumes of abdominal adiposity by using age and novel body shape descriptors developed from 3D body images. The ground truth of VAT and SAT volumes across the entire abdomen were assessed automatically from MRI sequences. In the present research, the MRI data and the 3D body images were processed using unsupervised schemes in order to prevent human error and subjectivity. The final prediction equations explained 74.2% of the variance of

VAT in men and 80.4% in women. These are lower than those obtained for SAT prediction (93.3% in men and 93.0% in women, respectively). The developed equations also were tested with the validation data set as a method of cross-validation.

The 3D SBI system enables a fast and accurate measurement of numerous body measurements within a few seconds (see Chapter 1.3). This is much more efficient and convenient than that obtained manually by tape. Previous studies have confirmed the accuracy of the body dimensions measured by the SBI system. For example, Yu and Xu reported that the SBI system can realistically reconstruct whole body shape with a high accuracy and repeatability [82]. Xu et al. has shown that the SBI can accurately measure girth, width, depth and volume of human body [77]. Moreover, Lee et al. demonstrated that the SBI system was effective in predicting abdominal adiposity obtained from a single MRI slice [182]. The reported R^2 were 71.7% and 90.4% for VAT and SAT, respectively. However, this preliminary study has only employed few SBI parameters of simple body dimension. Besides, the VAT and SAT volumes were manually assessed from a single umbilical slice which may not represent the actual fat accumulation in the whole abdominal area. Therefore, in the current study, the utilization of the novel body shape descriptors and volumetric abdominal adiposity data based on multiple abdominal MRI slices are able to overcome the above limitations and, thus, improve the prediction accuracy.

In our SBI system, the WaistC is conventionally defined as the smallest girth on torso since it does not require manual palpation and shows consistent association with metabolic syndrome [183], [184]. Similar to previous studies [24], we found that the WaistC correlates more with VAT than SAT. Girth measurements at a few different sites of the

body and their relationship with adiposity have been reported previously [24], [33], yet, the present study is the first to analyze a full profile of the central body from waist line to crotch, utilizing the advances of the stereovision system. We found that the CG6, which is about 10 cm below the waist, shows the highest correlation with SAT in both sexes. Based on the location, CG6 can be considered as the abdominal circumference. Partial correlations between CG6 and SAT, after adjustment for age, are 0.962 in men and 0.955 in women. These high correlations presumably were due to the utilization of the automated processing in this study, this may have significantly decreased the intra- and inter-variance associated with the manual tape measurements.

The novel body shape descriptors utilized in this study were developed based on plentiful volumetric, circumferential and other body dimension data to characterize the body shape and quantify fat distribution from external perspective. It is shown that the ASI and PSI can effectively quantify whether a subject is apple- or pear-shaped. Specifically, a subject with a high ASI indicates an obvious abdominal bulge which means the subject is more apple-shaped. Additionally, a high PSI suggests that the individual has more fat accumulated around the hip. ASI and PSI contributed considerably in predicting VAT in men presumably because men tend to have more visceral fat depots than women (Table 5.1) [185]. Another important shape descriptor is CP which describes the extent of the abdominal cross-section protruding to the front. CP was positively correlated to both SAT and VAT as shown in the Table 5.2. After adjustment for abdominal girth (CG6), CP became negatively correlated with SAT (R = -0.366 in men and R = -0.279 in women), while still positively correlated with VAT (R = 0.607 in men and R = 0.425 in women). These findings suggest

that CP is a powerful indicator of abdominal adiposity independent of the size of abdomen. Furthermore, the body shape descriptors based on the regional volume measurements are also significant indicators of intrinsic VAT volumes. Especially, the negative correlation between VAT and TVR is in agreement with the theory that abundant quantities of lower body adipose tissue serve as a fat reservoir that reduces fat accumulation at visceral depots [186].

A number of mathematical models have been introduced for predicting abdominal adiposity via simple demographic and anthropometric parameters [119], [138], [187]–[189]. Overall, the results from our prediction models showed equal or higher accuracy as compared to the results from previous models. For example, Goel et al [187], used age, sex, anthropometric measurements (BMI, waist circumference and hip circumference) and a single MRI slice at L3-4 intervertebral level to predict VAT and SAT. The R^2 was 67.1% in SAT and 52.1% in VAT, these are lower than the R^2s determined by the models in the present research (74.2% of VAT in men, 80.4% of VAT in women, 93.3% of SAT in men and 93.0% of SAT in women).

Samouda et al. observed some associations between the proximal thigh girth and VAT (R = 0.211 in women and 0.238 in men) on a single CT slice at the level of L3-L4 [119]. In the present study, we observed a slightly higher R value between these two variables in women and lower R value in men (R=0.175 in men and 0.308 in women). However, thigh circumference was not selected as a predictor variable because other variables displayed more significant associations with volumetric VAT. Therefore, the thigh circumference may not be a robust estimator in different population. In addition, the thigh

girth reflects only limited cross-sectional information at a single level. TVR, a novel shape descriptor proposed in this study, determined the condition of thigh tissue accumulation with precise volumetric information.

The previous prediction models mentioned above only used the abdominal fat volumes on a single MRI or CT slice, often assessed at the level of L3-L4 or umbilicus. Therefore, the prediction results were restricted to a specific slice location due to the variation of fat distribution in the abdominal area [99], [113]. Presumably, the major reason for the popularity of these single-slice based studies was the lack of reliable and convenient methods to analyze MRI slices. Traditionally, the MRI processing methods have been time-consuming and required intense manual efforts [94]. In the current study, a fully-automated algorithm was employed to assess the abdominal adipose tissue on T1-weighted MRI sequences involving the whole abdomen. Based on our experience, a semi-automated process using a commercial software (sliceOmatic® Tomovision, Inc.) required 1.5 hours for a trained operator to analyze a MRI sequence (20 slices) of each subject. In comparison, this fully-automated algorithm only took 10 to 20 minutes to process one sequence on a computer with 2.6 GHz CPU. Thus, this fully-automated algorithm dramatically reduces processing time and workload, while providing accurate fat quantifications. As opposed to a single slice, the utilization of volumetric MRI data from L2 to L5 in this study provided a more accurate solution for assessment of abdominal adiposity.

In addition, age was significantly associated with VAT in both sexes and was selected as a predictor variable. Our results were in agreement with previous findings that age or menstrual stage (in women) influenced body composition and fat distribution [190].

Although BMI is a frequently used parameter to predict obesity [119], [187], [191], it was not chosen in our predictive equations, as addition of BMI did not improve the prediction accuracy. Our results imply that BMI may not be truly relevant to abdominal adiposity since it is not able to discern fat mass and lean (muscle) mass [181]. Waist to hip ratio (WHR) was excluded in the prediction models because it did not show higher correlation with abdominal adiposity than WaistC and HipC. Furthermore, it caused multicollinearity between other predictor variables related to WHR. Saggital diameters, skinfolds and other manual methods were not utilized in this study in order to prevent subjectivity and maintain simplicity of measurements.

According to a *t*-test conducted in this study, significant differences ($p<0.05$) between men and women existed for VAT, WaistC (CG0), WaistW, HipC, HipW, ThighC, TorsoV, ThighV, HipV, TVR and PSI. Thus, the relationships between abdominal adiposity and body shape should be analyzed separately for different sexes, despite the fact that splitting the data results in a smaller sample size and reduces statistical power. Nevertheless, in order to test the predictive ability of the body shape descriptors when gender information is unknown, we also developed the prediction equations for a combined dataset containing both male and female subjects. The obtained R^2 are 75.1% and 93.8% for VAT and SAT, respectively. Hence, the body shape descriptors provided similar effectiveness for predicting abdominal adiposity in a dataset with a combination of both men and women.

A limitation of this study is the small sample size which limited the statistical power of the regression analysis. In the future, more subjects will be added to reduce any potential

sampling bias and to enhance the statistical power of the research. Another future work is to investigate the validity of the developed prediction models for patients with obesity-related diseases such as metabolic syndrome, diabetes mellitus type 2 and insulin resistance.

5.5 SUMMARY

In this chapter, we investigated the relationship between intrinsic adiposity and external body shape using abdominal MRI scans and 3D stereovision system. The shape descriptors developed based on 3D body images provided an innovative way to characterize body shape and helped reveal the unknown relations between body shape and intrinsic adiposity. Prediction models based on age and the novel shape descriptors improved the accuracy for estimating abdominal VAT and SAT volumes. Thus, the SBI system is a cost-effective and reliable mean to quantify body shape and estimate intrinsic adiposity conditions.

Chapter 6 Conclusion and Future Studies

6.1 CONCLUSION

The overall goal of this dissertation was to develop new quantitative measures to assess obesity based on 3D body images and thereby to investigate the relationship between abdominal adiposity and body shape. At present, the most commonly used obesity evaluation methods rely on manual tape measurements which may cause intra- and inter-observers' variations and may not be relevant to intrinsic adiposity conditions. Therefore, it is essential to develop new measures that can accurately assess the adiposity status by using inexpensive, harmless and convenient equipment that can be easily implemented in clinical settings.

Magnetic resonance imaging (MRI) is considered "gold standard" for measuring the adiposity. T1-weighted MRI sequences covering the entire abdominal were acquired in this study in order to obtain the ground truth of abdominal adiposity. Currently, there is no generally accepted software package or algorithm to compute the visceral and subcutaneous adipose tissue (VAT and SAT) from T1-weighted MRI slices with intensity inhomogeneity within and between slices. Therefore, the first objective of this dissertation is developing a fully-automated algorithm to quantify the volumes of VAT and SAT from the 2nd lumbar vertebra (L2) to L5 without human intervention (Chapter 2). This algorithm significantly reduced processing time and workload compared to traditional manual and semi-automated methods, meanwhile, provided accurate and objective fat quantification results.

Body shape is considered as an important indicator of obesity and health conditions. However, there is no available method to date to comprehensively characterize human body shape. Furthermore, majority studies of obesity and body image only focused on philological and psychosocial issues [192]–[194]. For that reason, the second objective of this dissertation is developing quantitative, meaningful and comprehensive body shape descriptors to characterize individual's body shape and fat distribution from external perspective (Chapter 3). These innovative body shape descriptors were developed based on 3D body images reconstructed from a customized stereovision body imaging (SBI) system that can render 3D body image with high resolution and fast speed. This SBI system consists of four pairs of stereo units fabricated by off-the-shelf cameras and projectors. Due to the high portability and affordability, the SBI system can be easily utilized in clinical settings as an obesity diagnostic and monitoring equipment.

Subsequently, the relationship between adiposity and body shape was analyzed using the fat amounts measured from MRI sequences and the body shape descriptors developed from the 3D SBI system (Chapter 4 and Chapter 5). In Chapter 4, a new obesity categorization method that depicts the fat distribution characteristics in abdomen was defined. It was then showed that the proposed body shape descriptors were able to capture the body shape differences between the subjects with dissimilar internal fat distribution patterns. Moreover, the body shape descriptors provided a higher accuracy in predicting the category of fat distribution compared to traditional anthropometric measurements and dual-energy x-ray absorptiometry (DXA) measurements. In Chapter 5, the associations between the intrinsic adiposity and the external body shape were investigated. In addition,

the accuracy of the prediction models developed in this dissertation demonstrate that the novel body shape descriptors were effective for the prediction of abdominal visceral fat and subcutaneous fat accumulated in both male and female adults.

The results in this dissertation are promising in that they show, for the first time, the statistical linkage between objectively quantified characteristics of external body shape and intrinsic adiposity and fat distribution. Our findings indicate that the 3D SBI is able to provide more accurate, consistent and comprehensive measurements that are closely related to intrinsic adiposity and may revolutionize the obesity evaluation.

6.2 FUTURE STUDIES

There are a number of additional areas for further study that have been highlighted by the studies undertaken in this dissertation. Firstly, it is widely accepted that the visceral adiposity is a unique, pathogenic fat depot that is strongly associated with adverse metabolic related health disorders and risk factors. However, the impact of subcutaneous adiposity remains controversial [195]. For example, Preis et al., [89] and Park et al. [196] found that both SAT and VAT are correlated to insulin resistance while Frederisken et al., [27] reported that it is SAT not VAT associated with insulin resistance. Moreover, Hayashi et al. [197], suggested that VAT not SAT is associated with increasing insulin resistance in future. The discrepancy is presumably due to the two distinct SAT compartments that are divided by Scarpa's fascia: superficial subcutaneous adipose tissue (SSAT) and deep subcutaneous adipose tissue (DSAT). Previous studies have shown that the DSAT is strongly related to insulin resistance due to its anatomical location that is close to visceral

depots [198], [199]. These findings necessitate a further discrimination study of SSAT and DSAT with MRI or other imaging modalities. Therefore, one can develop additional functions based on the proposed MRI processing algorithm in this dissertation for further automatic discrimination of the SSAT from DSAT. Future studies are needed to further determine the relationship between body shape and the two identified compartments of SAT.

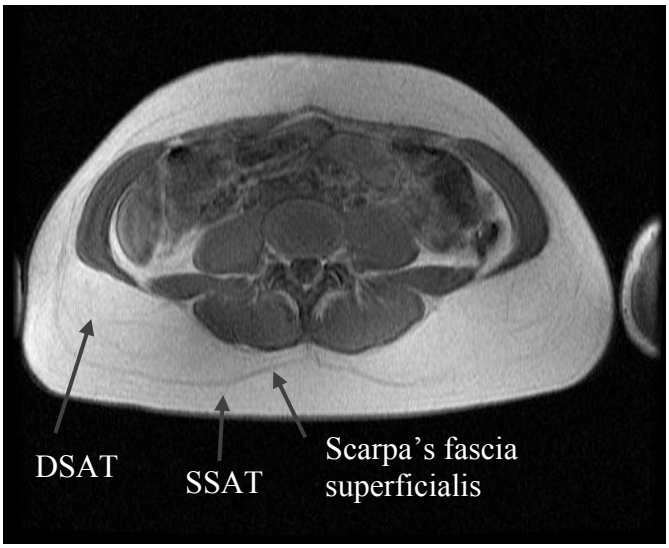

Figure 6.1 Illustration of superficial subcutaneous adipose tissue (SSAT) and deep subcutaneous adipose tissue (DSAT)

Second, direct clinical tests such as the comprehensive metabolic panel (CMP) are useful screening tools for evaluation of individual's metabolic status and diagnosis of a number of health conditions such as diabetes, liver disease and kidney disease. In this dissertation, such clinical tests were not available. In the future, the research can be

expanded to investigate the relationship between body shapes and the status of metabolism utilizing the clinical tests mentioned above.

Furthermore, previous studies have shown that race/ethnicity influences the intrinsic body fat accumulation [200]. For example, African Americans have lower visceral obesity than their white and Hispanic counterparts [201]. Asian women tends to accumulate more visceral fat than Caucasian women with similar BMI values [202]. In comparison to white women, white men tends to accumulate more visceral fat around abdomen [161]. It is not yet fully studied how the body shape and its relationship with adiposity are influenced by race/ethnicity. By using the proposed body shape descriptors and the developed MRI processing algorithm, one can further analyze the difference of the relationship between body shape and adiposity according to different racial groups.

In addition, the developed body shape descriptors and the customized stereovision system have the potential to be applied in enormous fields beside obesity evaluation. For example, the reconstructed 3D body images and body shape descriptors can be used to qualitatively and quantitatively evaluate the personal training outcomes. Visualization of the changes in body shape may provide inspirations and encouragements to the patients under fitness training. Also, the developed body shape descriptors can be adapted to measure the growth of infants and children. Due to the instantaneous image acquisition, the customized SBI system is appropriate to scan infants and children who cannot stand still for a long time.

Bibliography

[1] Flegal KM, Carroll MD, Ogden CL, and Curtin LR, "Prevalence and trends in obesity among us adults, 1999-2008," *JAMA*, vol. 303, no. 3, pp. 235–241, Jan. 2010.

[2] N. Katsiki, G. Ntaios, and K. Vemmos, "Stroke, obesity and gender: A review of the literature," *Maturitas*, vol. 69, no. 3, pp. 239–243, Jul. 2011.

[3] C. K. Abrass, "Overview: obesity: what does it have to do with kidney disease?," *J. Am. Soc. Nephrol.*, vol. 15, no. 11, pp. 2768–2772, Nov. 2004.

[4] R. Weiss, J. Dziura, T. S. Burgert, W. V. Tamborlane, S. E. Taksali, C. W. Yeckel, K. Allen, M. Lopes, M. Savoye, J. Morrison, R. S. Sherwin, and S. Caprio, "Obesity and the metabolic syndrome in children and adolescents," *N. Engl. J. Med.*, vol. 350, no. 23, pp. 2362–2374, 2004.

[5] E. L. Thomas, N. Saeed, J. V. Hajnal, A. Brynes, A. P. Goldstone, G. Frost, and J. D. Bell, "Magnetic resonance imaging of total body fat," *J. Appl. Physiol. Bethesda Md 1985*, vol. 85, no. 5, pp. 1778–1785, Nov. 1998.

[6] K. Tokunaga, Y. Matsuzawa, K. Ishikawa, and S. Tarui, "A novel technique for the determination of body fat by computed tomography," *Int. J. Obes.*, vol. 7, no. 5, pp. 437–445, 1983.

[7] J. Haarbo, A. Gotfredsen, C. Hassager, and C. Christiansen, "Validation of body composition by dual energy X-ray absorptiometry (DEXA)," *Clin. Physiol.*, vol. 11, no. 4, pp. 331–341, 1991.

[8] R. J. Kuczmarski, "Bioelectrical impedance analysis measurements as part of a national nutrition survey," *Am. J. Clin. Nutr.*, vol. 64, no. 3 Suppl, p. 453S–458S, Sep. 1996.

[9] D. A. Fields, M. I. Goran, and M. A. McCrory, "Body-composition assessment via air-displacement plethysmography in adults and children: a review," *Am. J. Clin. Nutr.*, vol. 75, no. 3, pp. 453–467, Mar. 2002.

[10] J. Wang, S. B. Heymsfield, M. Aulet, J. C. Thornton, and R. N. Pierson, "Body fat from body density: underwater weighing vs. dual-photon absorptiometry," *Am. J. Physiol. - Endocrinol. Metab.*, vol. 256, no. 6, pp. E829–E834, Jun. 1989.

[11] R. N. Bergman, D. Stefanovski, T. A. Buchanan, A. E. Sumner, J. C. Reynolds, N. G. Sebring, A. H. Xiang, and R. M. Watanabe, "A better index of body adiposity," *Obesity*, vol. 19, no. 5, pp. 1083–1089, Mar. 2011.

[12] T. V. Barreira, A. E. Staiano, D. M. Harrington, S. B. Heymsfield, S. R. Smith, C. Bouchard, and P. T. Katzmarzyk, "Anthropometric correlates of total body fat, abdominal adiposity, and cardiovascular disease risk factors in a biracial sample of men and women," *Mayo Clin. Proc.*, vol. 87, no. 5, pp. 452–460, May 2012.

[13] D. Ackermann, J. Jones, J. Barona, M. C. Calle, J. E. Kim, B. LaPia, J. S. Volek, M. McIntosh, C. Kalynych, W. Najm, R. H. Lerman, and M. L. Fernandez, "Waist circumference is positively correlated with markers of inflammation and negatively

with adiponectin in women with metabolic syndrome," *Nutr. Res. N. Y. N*, vol. 31, no. 3, pp. 197–204, Mar. 2011.
[14] Y. Chen, D. Rennie, Y. F. Cormier, and J. Dosman, "Waist circumference is associated with pulmonary function in normal-weight, overweight, and obese subjects," *Am. J. Clin. Nutr.*, vol. 85, no. 1, pp. 35–39, 2007.
[15] The Emerging Risk Factors Collaboration, "Separate and combined associations of body-mass index and abdominal adiposity with cardiovascular disease: collaborative analysis of 58 prospective studies," *The Lancet*, vol. 377, no. 9771, pp. 1085–1095.
[16] R. D. Brook, R. L. Bard, M. Rubenfire, P. M. Ridker, and S. Rajagopalan, "Usefulness of visceral obesity (waist/hip ratio) in predicting vascular endothelial function in healthy overweight adults," *Am. J. Cardiol.*, vol. 88, no. 11, pp. 1264–1269, Dec. 2001.
[17] S. B. Dijk, T. Takken, E. C. Prinsen, and H. Wittink, "Different anthropometric adiposity measures and their association with cardiovascular disease risk factors: a meta-analysis," *Neth. Heart J.*, vol. 20, no. 5, pp. 208–218, Jan. 2012.
[18] H. Ito, K. Nakasuga, A. Ohshima, T. Maruyama, Y. Kaji, M. Harada, M. Fukunaga, S. Jingu, and M. Sakamoto, "Detection of cardiovascular risk factors by indices of obesity obtained from anthropometry and dual-energy X-ray absorptiometry in Japanese individuals," *Int. J. Obes.*, vol. 27, no. 2, pp. 232–237, 2003.
[19] P. Sebo, S. Beer-Borst, D. M. Haller, and P. A. Bovier, "Reliability of doctors' anthropometric measurements to detect obesity," *Prev. Med.*, vol. 47, no. 4, pp. 389–393, Oct. 2008.
[20] J.-P. Despres, "Body fat distribution and risk of cardiovascular disease: an update," *Circulation*, vol. 126, no. 10, pp. 1301–1313, Sep. 2012.
[21] R. R. Huxley and D. R. Jacobs, "Size still matters…but not in the way we once thought," *The Lancet*, vol. 377, no. 9771, pp. 1051–1052, Mar. 2011.
[22] R. C. Rabin, "Patterns: for heart risk, no telltale body shape," *The New York Times*, 16-Mar-2011.
[23] F. Abbasi, C. Blasey, and G. M. Reaven, "Cardiometabolic risk factors and obesity: does it matter whether BMI or waist circumference is the index of obesity?," *Am. J. Clin. Nutr.*, vol. 98, no. 3, pp. 637–640, Sep. 2013.
[24] A. Bosy-Westphal, C. A. Booke, T. Blocker, E. Kossel, K. Goele, W. Later, B. Hitze, M. Heller, C. C. Gluer, and M. J. Muller, "Measurement site for waist circumference affects its accuracy as an index of visceral and abdominal subcutaneous fat in a Caucasian population," *J. Nutr.*, vol. 140, no. 5, pp. 954–961, Mar. 2010.
[25] Y.-M. Chen, S. C. Ho, S. S. H. Lam, and S. S. G. Chan, "Validity of body mass index and waist circumference in the classification of obesity as compared to percent body fat in Chinese middle-aged women," *Int. J. Obes. 2005*, vol. 30, no. 6, pp. 918–925, Jun. 2006.
[26] C. S. Fox, J. M. Massaro, U. Hoffmann, K. M. Pou, P. Maurovich-Horvat, C.-Y. Liu, R. S. Vasan, J. M. Murabito, J. B. Meigs, L. A. Cupples, R. B. D'Agostino, and C. J. O'Donnell, "Abdominal visceral and subcutaneous adipose tissue

compartments association with metabolic risk factors in the framingham heart study," *Circulation*, vol. 116, no. 1, pp. 39–48, Jul. 2007.
[27] L. Frederiksen, T. L. Nielsen, K. Wraae, C. Hagen, J. Frystyk, A. Flyvbjerg, K. Brixen, and M. Andersen, "Subcutaneous rather than visceral adipose tissue is associated with adiponectin levels and insulin resistance in young men," *J. Clin. Endocrinol. Metab.*, vol. 94, no. 10, pp. 4010–4015, Oct. 2009.
[28] J. V. G. A. Durnin and J. Womersley, "Body fat assessed from total body density and its estimation from skinfold thickness: measurements on 481 men and women aged from 16 to 72 Years," *Br. J. Nutr.*, vol. 32, no. 1, pp. 77–97, Jul. 1974.
[29] M. J. Albrink and J. W. Meigs, "Interrelationship between skinfold thickness, serum lipids and blood sugar in normal men," *Am. J. Clin. Nutr.*, vol. 15, no. 5, pp. 255–261, Nov. 1964.
[30] L. G. H. Goh, S. S. Dhaliwal, T. A. Welborn, A. H. Lee, and P. R. Della, "Anthropometric measurements of general and central obesity and the prediction of cardiovascular disease risk in women: a cross-sectional study," *BMJ Open*, vol. 4, no. 2, p. e004138, Feb. 2014.
[31] S. C. Savva, M. Tornaritis, M. E. Savva, Y. Kourides, A. Panagi, N. Silikiotou, C. Georgiou, and A. Kafatos, "Waist circumference and waist-to-height ratio are better predictors of cardiovascular disease risk factors in children than body mass index," *Int. J. Obes.*, vol. 24, no. 11, pp. 1453–1458, 2000.
[32] D. S. Freedman, M. K. Serdula, S. R. Srinivasan, and G. S. Berenson, "Relation of circumferences and skinfold thicknesses to lipid and insulin concentrations in children and adolescents: the Bogalusa Heart Study," *Am. J. Clin. Nutr.*, vol. 69, no. 2, pp. 308–317, Feb. 1999.
[33] J. Wang, J. C. Thornton, S. Bari, B. Williamson, D. Gallagher, S. B. Heymsfield, M. Horlick, D. Kotler, B. Laferrère, L. Mayer, F. X. Pi-Sunyer, and R. N. Pierson Jr, "Comparisons of waist circumferences measured at 4 sites," *Am. J. Clin. Nutr.*, vol. 77, no. 2, pp. 379–384, Feb. 2003.
[34] M. B. Snijder, J. M. Dekker, M. Visser, L. M. Bouter, C. D. Stehouwer, P. J. Kostense, J. S. Yudkin, R. J. Heine, G. Nijpels, and J. C. Seidell, "Associations of hip and thigh circumferences independent of waist circumference with the incidence of type 2 diabetes: the Hoorn Study," *Am. J. Clin. Nutr.*, vol. 77, no. 5, pp. 1192–1197, May 2003.
[35] L. Lissner, C. Björkelund, B. L. Heitmann, J. C. Seidell, and C. Bengtsson, "Larger hip circumference independently predicts health and longevity in a Swedish female cohort," *Obes. Res.*, vol. 9, no. 10, pp. 644–646, Oct. 2001.
[36] M. Ashwell, P. Gunn, and S. Gibson, "Waist-to-height ratio is a better screening tool than waist circumference and BMI for adult cardiometabolic risk factors: systematic review and meta-analysis," *Obes. Rev.*, vol. 13, no. 3, pp. 275–286, Mar. 2012.
[37] S. D. Hsieh, H. Yoshinaga, and T. Muto, "Waist-to-height ratio, a simple and practical index for assessing central fat distribution and metabolic risk in Japanese men and women," *Int. J. Obes.*, vol. 27, no. 5, pp. 610–616, 2003.

[38] L. de Koning, A. T. Merchant, J. Pogue, and S. S. Anand, “Waist circumference and waist-to-hip ratio as predictors of cardiovascular events: meta-regression analysis of prospective studies,” *Eur. Heart J.*, vol. 28, no. 7, pp. 850–856, Apr. 2007.
[39] E. Turcato, O. Bosello, V. Di Francesco, T. B. Harris, E. Zoico, L. Bissoli, E. Fracassi, and M. Zamboni, “Waist circumference and abdominal sagittal diameter as surrogates of body fat distribution in the elderly: their relation with cardiovascular risk factors,” *Int. J. Obes. Relat. Metab. Disord.*, vol. 24, no. 8, p. 1005, Aug. 2000.
[40] C. D. Sjöström, A. C. Håkangård, L. Lissner, and L. Sjöström, “Body compartment and subcutaneous adipose tissue distribution--risk factor patterns in obese subjects,” *Obes. Res.*, vol. 3, no. 1, pp. 9–22, Jan. 1995.
[41] P. Rissanen, P. Hämäläinen, E. Vanninen, M. Tenhunen-Eskelinen, and M. Uusitupa, “Relationship of metabolic variables to abdominal adiposity measured by different anthropometric measurements and dual-energy X-ray absorptiometry in obese middle-aged women,” *Int. J. Obes. Relat. Metab. Disord. J. Int. Assoc. Study Obes.*, vol. 21, no. 5, pp. 367–371, May 1997.
[42] J. C. Seidell, R. Andres, J. D. Sorkin, and D. C. Muller, “The sagittal waist diameter and mortality in men: the Baltimore Longitudinal Study on Aging,” *Int. J. Obes. Relat. Metab. Disord. J. Int. Assoc. Study Obes.*, vol. 18, no. 1, pp. 61–67, Jan. 1994.
[43] W. E. Siri, “Body composition from fluid spaces and density: analysis of methods,” California. Univ., Berkeley. Radiation Lab., UCRL-3349, Mar. 1956.
[44] J. Brožek, F. Grande, J. T. Anderson, and A. Keys, “Densitometric analysis of body composition: revision of some quantitative assumptions*,” *Ann. N. Y. Acad. Sci.*, vol. 110, no. 1, pp. 113–140, Sep. 1963.
[45] J. Wilmore, “The use of actual, predicted and constant residual volume in the assessment of the body composition by underwater weighing,” *Med Sci Sports*, vol. 1, pp. 87–90, 1969.
[46] M. Ma, G. Td, B. Em, and M. Pa, “Evaluation of a new air displacement plethysmograph for measuring human body composition,” *Med. Sci. Sports Exerc.*, vol. 27, no. 12, pp. 1686–1691, Dec. 1995.
[47] G. F. Maddalozzo, B. J. Cardinal, and C. M. Snow, “Concurrent validity of the BOD POD and dual energy x-ray absorptiometry techniques for assessing body composition in young women,” *J. Am. Diet. Assoc.*, vol. 102, no. 11, pp. 1677–1679, Nov. 2002.
[48] D. A. Fields, G. R. Hunter, and M. I. Goran, “Validation of the BOD POD with hydrostatic weighing: influence of body clothing,” *Int. J. Obes.*, vol. 24, no. 2, pp. 200–205, 2000.
[49] S. Y. Lee and D. Gallagher, “Assessment methods in human body composition,” *Curr. Opin. Clin. Nutr. Metab. Care*, vol. 11, no. 5, pp. 566–572, Sep. 2008.
[50] R. F. Kushner and D. A. Schoeller, “Estimation of total body water by bioelectrical impedance analysis,” *Am. J. Clin. Nutr.*, vol. 44, no. 3, pp. 417–424, Sep. 1986.
[51] U. G. Kyle, I. Bosaeus, A. D. De Lorenzo, P. Deurenberg, M. Elia, J. M. Gómez, B. L. Heitmann, L. Kent-Smith, J.-C. Melchior, M. Pirlich, H. Scharfetter, A. M. W. J.

Schols, and C. Pichard, “Bioelectrical impedance analysis—part I: review of principles and methods,” *Clin. Nutr.*, vol. 23, no. 5, pp. 1226–1243, Oct. 2004.
[52] E. Völgyi, F. A. Tylavsky, A. Lyytikäinen, H. Suominen, M. Alén, and S. Cheng, “Assessing body composition with DXA and bioimpedance: effects of obesity, physical activity, and age,” *Obes. Silver Spring Md*, vol. 16, no. 3, pp. 700–705, Mar. 2008.
[53] M. P. Rothney, R. J. Brychta, E. V. Schaefer, K. Y. Chen, and M. C. Skarulis, “Body composition measured by dual-energy x-ray absorptiometry half-body scans in obese adults,” *Obes. Silver Spring Md*, vol. 17, no. 6, pp. 1281–1286, Jun. 2009.
[54] C. V. Albanese, E. Diessel, and H. K. Genant, “Clinical applications of body composition measurements using DXA,” *J. Clin. Densitom. Off. J. Int. Soc. Clin. Densitom.*, vol. 6, no. 2, pp. 75–85, 2003.
[55] A. M. Weyers, S. A. Mazzetti, D. M. Love, A. L. Gómez, W. J. Kraemer, and J. S. Volek, “Comparison of methods for assessing body composition changes during weight loss,” *Med. Sci. Sports Exerc.*, vol. 34, no. 3, pp. 497–502, Mar. 2002.
[56] M. b. Snijder, M. Visser, J. m. Dekker, J. c. Seidell, T. Fuerst, F. Tylavsky, J. Cauley, T. Lang, M. Nevitt, and T. b. Harris, “The prediction of visceral fat by dual-energy X-ray absorptiometry in the elderly: a comparison with computed tomography and anthropometry,” *Int. J. Obes. Relat. Metab. Disord.*, vol. 26, no. 7, p. 984, Jul. 2002.
[57] W. W. Wong, A. C. Hergenroeder, J. E. Stuff, N. F. Butte, E. O. Smith, and K. J. Ellis, “Evaluating body fat in girls and female adolescents: advantages and disadvantages of dual-energy X-ray absorptiometry,” *Am. J. Clin. Nutr.*, vol. 76, no. 2, pp. 384–389, Aug. 2002.
[58] D. A. Schoeller, F. A. Tylavsky, D. J. Baer, W. C. Chumlea, C. P. Earthman, T. Fuerst, T. B. Harris, S. B. Heymsfield, M. Horlick, and T. G. Lohman, “QDR 4500A dual-energy X-ray absorptiometer underestimates fat mass in comparison with criterion methods in adults,” *Am. J. Clin. Nutr.*, 2005.
[59] F. Tylavsky, T. Lohman, B. A. Blunt, D. A. Schoeller, T. Fuerst, J. A. Cauley, M. C. Nevitt, M. Visser, and T. B. Harris, “QDR 4500A DXA overestimates fat-free mass compared with criterion methods,” *J. Appl. Physiol.*, vol. 94, no. 3, pp. 959–965, 2003.
[60] M. Visser, T. Fuerst, T. Lang, L. Salamone, and T. B. Harris, “Validity of fan-beam dual-energy X-ray absorptiometry for measuring fat-free mass and leg muscle mass. Health, Aging, and Body Composition Study--Dual-Energy X-ray Absorptiometry and Body Composition Working Group,” *J. Appl. Physiol. Bethesda Md 1985*, vol. 87, no. 4, pp. 1513–1520, Oct. 1999.
[61] C. B, S. L, A. M, K. J, K. H, and L. R, “A multicompartment body composition technique based on computerized tomography.,” *Int. J. Obes. Relat. Metab. Disord. J. Int. Assoc. Study Obes.*, vol. 18, no. 4, pp. 219–234, Apr. 1994.
[62] J. L. Lancaster, A. A. Ghiatas, A. Alyassin, R. F. Kilcoyne, E. Bonora, and R. A. Defronzo, “Measurement of abdominal fat with T1-weighted MR images,” *J. Magn. Reson. Imaging*, vol. 1, no. 3, pp. 363–369, 1991.

[63] N. Abate, D. Burns, R. M. Peshock, A. Garg, and S. M. Grundy, “Estimation of adipose tissue mass by magnetic resonance imaging: validation against dissection in human cadavers.,” *J. Lipid Res.*, vol. 35, no. 8, pp. 1490–1496, Aug. 1994.
[64] D. R. Martin and R. C. Semelka, “Health effects of ionising radiation from diagnostic CT,” *The Lancet*, vol. 367, no. 9524, pp. 1712–1714, Jun. 2006.
[65] H. M. Daanen and G. J. van de Water, “Whole body scanners,” *Displays*, vol. 19, no. 3, pp. 111–120, Nov. 1998.
[66] M. R. Pepper, J. H. Freeland-Graves, W. Yu, P. R. Stanforth, J. M. Cahill, M. Mahometa, and B. Xu, “Validation of a 3-dimensional laser body scanner for assessment of waist and hip circumference,” *J. Am. Coll. Nutr.*, vol. 29, no. 3, pp. 179–188, Jun. 2010.
[67] M. R. Pepper, J. H. Freeland-Graves, W. Yu, P. R. Stanforth, and B. Xu, “Evaluation of a rotary laser body scanner for body volume and fat assessment,” *J. Test. Eval.*, vol. 39, no. 1, pp. 1–6, Jul. 2010.
[68] C. Chen and A. Kak, “Modeling and calibration of a structured light scanner for 3-D robot vision,” in *1987 IEEE International Conference on Robotics and Automation. Proceedings*, 1987, vol. 4, pp. 807–815.
[69] C. Rocchini, P. Cignoni, C. Montani, P. Pingi, and R. Scopigno, “A low cost 3D scanner based on structured light,” *Comput. Graph. Forum*, vol. 20, no. 3, pp. 299–308, Sep. 2001.
[70] I. Ishii, K. Yamamoto, K. Doi, and T. Tsuji, “High-speed 3D image acquisition using coded structured light projection,” in *IEEE/RSJ International Conference on Intelligent Robots and Systems, 2007. IROS 2007*, 2007, pp. 925–930.
[71] O. Hall-Holt and S. Rusinkiewicz, “Stripe boundary codes for real-time structured-light range scanning of moving objects,” in *Eighth IEEE International Conference on Computer Vision, 2001. ICCV 2001. Proceedings*, 2001, vol. 2, pp. 359–366 vols.2.
[72] T. Pribanić, S. Mrvoš, and J. Salvi, “Efficient multiple phase shift patterns for dense 3D acquisition in structured light scanning,” *Image Vis. Comput.*, vol. 28, no. 8, pp. 1255–1266, Aug. 2010.
[73] J. C. Wells, P. Treleaven, and T. J. Cole, “BMI compared with 3-dimensional body shape: the UK National Sizing Survey,” *Am. J. Clin. Nutr.*, vol. 85, no. 2, pp. 419–425, Feb. 2007.
[74] H. A. M. Daanen and F. B. Ter Haar, “3D whole body scanners revisited,” *Displays*, vol. 34, no. 4, pp. 270–275, Oct. 2013.
[75] N. Lazaros, G. C. Sirakoulis, and A. Gasteratos, “Review of stereo vision algorithms: from software to hardware,” *Int. J. Optomechatronics*, vol. 2, no. 4, pp. 435–462, Nov. 2008.
[76] R. Szeliski, R. Zabih, D. Scharstein, O. Veksler, V. Kolmogorov, A. Agarwala, M. Tappen, and C. Rother, “A comparative study of energy minimization methods for markov random fields with smoothness-based priors,” *IEEE Trans. Pattern Anal. Mach. Intell.*, vol. 30, no. 6, pp. 1068–1080, Jun. 2008.

[77] B. Xu, M. R. Pepper, J. H. Freeland-Graves, W. Yu, and M. Yao, "Three-dimensional surface imaging system for assessing human obesity," *Opt. Eng.*, vol. 48, no. 10, pp. 107204-107204–11, 2009.
[78] Zhang, Zhengyou, "Flexible camera calibration by viewing a plane from unknown orientations," in *The Proceedings of the Seventh IEEE International Conference on Computer Vision, 1999*, 1999, vol. 1, pp. 666–673 vols.1.
[79] D. Scharstein and R. Szeliski, "A taxonomy and evaluation of dense two-frame stereo correspondence algorithms," *Int. J. Comput. Vis.*, vol. 47, no. 1–3, pp. 7–42, Apr. 2002.
[80] M. Z. Brown, D. Burschka, and G. D. Hager, "Advances in computational stereo," *IEEE Trans. Pattern Anal. Mach. Intell.*, vol. 25, no. 8, pp. 993–1008, Aug. 2003.
[81] W. Yu and B. Xu, "Surface reconstruction from two-view body scanner data," *Text. Res. J.*, vol. 78, no. 5, pp. 457–466, May 2008.
[82] W. Yu and B. Xu, "A portable stereo vision system for whole body surface imaging," *Image Vis. Comput.*, vol. 28, no. 4, pp. 605–613, Apr. 2010.
[83] Ogden CL, Carroll MD, Kit BK, and Flegal KM, "Prevalence of childhood and adult obesity in the united states, 2011-2012," *JAMA*, vol. 311, no. 8, pp. 806–814, Feb. 2014.
[84] M. A. Stults-Kolehmainen, P. R. Stanforth, J. B. Bartholomew, T. Lu, C. J. Abolt, and R. Sinha, "DXA estimates of fat in abdominal, trunk and hip regions varies by ethnicity in men," *Nutr. Diabetes*, vol. 3, no. 3, p. e64, Mar. 2013.
[85] J. Sun, B. Xu, and J. Freeland-Graves, "Automated quantification of abdominal adiposity by magnetic resonance imaging," *Am. J. Hum. Biol.*, p. n/a-n/a, Apr. 2016.
[86] S. Klein, "The case of visceral fat: argument for the defense," *J. Clin. Invest.*, vol. 113, no. 11, pp. 1530–1532, Jun. 2004.
[87] M. M. Ibrahim, "Subcutaneous and visceral adipose tissue: structural and functional differences," *Obes. Rev.*, vol. 11, no. 1, pp. 11–18, Jan. 2010.
[88] S. Baglioni, G. Cantini, G. Poli, M. Francalanci, R. Squecco, A. Di Franco, E. Borgogni, S. Frontera, G. Nesi, F. Liotta, M. Lucchese, G. Perigli, F. Francini, G. Forti, M. Serio, and M. Luconi, "Functional differences in visceral and subcutaneous fat pads originate from differences in the adipose stem cell," *PLoS ONE*, vol. 7, no. 5, p. e36569, May 2012.
[89] S. R. Preis, J. M. Massaro, S. J. Robins, U. Hoffmann, R. S. Vasan, T. Irlbeck, J. B. Meigs, P. Sutherland, R. B. D'Agostino Sr, C. J. O'Donnell, and C. S. Fox, "Abdominal subcutaneous and visceral adipose tissue and insulin resistance in the Framingham heart study," *Obes. Silver Spring Md*, vol. 18, no. 11, pp. 2191–2198, Nov. 2010.
[90] S. Kaul, M. P. Rothney, D. M. Peters, W. K. Wacker, C. E. Davis, M. D. Shapiro, and D. L. Ergun, "Dual-energy x-Ray absorptiometry for quantification of visceral Fat," *Obes. Silver Spring Md*, vol. 20, no. 6, pp. 1313–1318, Jun. 2012.
[91] Y. Jin, C. Z. Imielinska, A. F. Laine, J. Udupa, W. Shen, and S. B. Heymsfield, "Segmentation and evaluation of adipose tissue from whole body MRI scans," in

Medical Image Computing and Computer-Assisted Intervention - MICCAI 2003, R. E. Ellis and T. M. Peters, Eds. Springer Berlin Heidelberg, 2003, pp. 635–642.

[92] S. A. Gronemeyer, R. G. Steen, W. M. Kauffman, W. E. Reddick, and J. O. Glass, "Fast adipose tissue (FAT) assessment by MRI," *Magn. Reson. Imaging*, vol. 18, no. 7, pp. 815–818, 2000.

[93] J. Machann, C. Thamer, B. Schnoedt, M. Haap, H.-U. Haring, C. D. Claussen, M. Stumvoll, A. Fritsche, and F. Schick, "Standardized assessment of whole body adipose tissue topography by MRI," *J. Magn. Reson. Imaging*, vol. 21, no. 4, pp. 455–462, 2005.

[94] S. Bonekamp, P. Ghosh, S. Crawford, S. Solga, A. Horska, F. Brancati, A. Diehl, S. Smith, and J. Clark, "Quantitative comparison and evaluation of software packages for assessment of abdominal adipose tissue distribution by magnetic resonance imaging," *Int. J. Obes. 2005*, vol. 32, no. 1, pp. 100–111, Jan. 2008.

[95] G. Thörmer, H. H. Bertram, N. Garnov, V. Peter, T. Schütz, E. Shang, M. Blüher, T. Kahn, and H. Busse, "Software for automated MRI-based quantification of abdominal fat and preliminary evaluation in morbidly obese patients," *J. Magn. Reson. Imaging*, vol. 37, no. 5, pp. 1144–1150, 2013.

[96] J. Kullberg, H. Ahlström, L. Johansson, and H. Frimmel, "Automated and reproducible segmentation of visceral and subcutaneous adipose tissue from abdominal MRI," *Int. J. Obes. 2005*, vol. 31, no. 12, pp. 1806–1817, Dec. 2007.

[97] A. Zhou, H. Murillo, and Q. Peng, "Novel segmentation method for abdominal fat quantification by MRI," *J. Magn. Reson. Imaging JMRI*, vol. 34, no. 4, pp. 852–860, Oct. 2011.

[98] V. Positano, A. Gastaldelli, A. maria Sironi, M. F. Santarelli, M. Lombardi, and L. Landini, "An accurate and robust method for unsupervised assessment of abdominal fat by MRI," *J. Magn. Reson. Imaging*, vol. 20, no. 4, pp. 684–689, 2004.

[99] E. W. Demerath, W. Shen, M. Lee, A. C. Choh, S. A. Czerwinski, R. M. Siervogel, and B. Towne, "Approximation of total visceral adipose tissue with a single magnetic resonance image," *Am. J. Clin. Nutr.*, vol. 85, no. 2, pp. 362–368, 2007.

[100] U. Vovk, F. Pernus, and B. Likar, "A Review of methods for correction of intensity inhomogeneity in MRI," *IEEE Trans. Med. Imaging*, vol. 26, no. 3, pp. 405–421, 2007.

[101] O. Salvado, C. Hillenbrand, Shaoxiang Zhang, and D. L. Wilson, "Method to correct intensity inhomogeneity in MR images for atherosclerosis characterization," *IEEE Trans. Med. Imaging*, vol. 25, no. 5, pp. 539–552, May 2006.

[102] D. Yang, J. Zheng, A. Nofal, J. Deasy, and I. M. El Naqa, "Techniques and software tool for 3D multimodality medical image segmentation," *J. Radiat. Oncol. Inform.*, vol. 1, no. 1, pp. 1–22, 2009.

[103] T. F. Chan and L. A. Vese, "Active contours without edges," *IEEE Trans. Image Process.*, vol. 10, no. 2, pp. 266–277, Feb. 2001.

[104] K. O. McGraw and S. P. Wong, "Forming inferences about some intraclass correlation coefficients," *Psychol. Methods*, vol. 1, no. 1, pp. 30–46, Mar. 1996.

[105] J. M. Bland and D. G. Altman, “Statistical methods for assessing agreement between two methods of clinical measurement,” *Lancet*, vol. 1, no. 8476, pp. 307–310, Feb. 1986.
[106] O. Addison, R. L. Marcus, P. C. LaStayo, and A. S. Ryan, “Intermuscular fat: a review of the consequences and causes,” *Int. J. Endocrinol.*, vol. 2014, p. e309570, Jan. 2014.
[107] M. A. Bredella, M. Torriani, R. H. Ghomi, B. J. Thomas, D. J. Brick, A. V. Gerweck, C. J. Rosen, A. Klibanski, and K. K. Miller, “Vertebral bone marrow fat is positively associated with visceral fat and inversely associated with IGF-1 in obese women,” *Obesity*, vol. 19, no. 1, pp. 49–53, Jan. 2011.
[108] D. Giavarina, “Understanding Bland Altman analysis,” *Biochem. Medica*, vol. 25, no. 2, pp. 141–151, Jun. 2015.
[109] J. Kullberg, L. Johansson, H. Ahlström, F. Courivaud, P. Koken, H. Eggers, and P. Börnert, “Automated assessment of whole-body adipose tissue depots from continuously moving bed MRI: a feasibility study,” *J. Magn. Reson. Imaging JMRI*, vol. 30, no. 1, pp. 185–193, Jul. 2009.
[110] B. T. Addeman, S. Kutty, T. G. Perkins, A. S. Soliman, C. N. Wiens, C. M. McCurdy, M. D. Beaton, R. A. Hegele, and C. A. McKenzie, “Validation of volumetric and single-slice MRI adipose analysis using a novel fully automated segmentation method,” *J. Magn. Reson. Imaging*, vol. 41, no. 1, pp. 233–241, Jan. 2015.
[111] W. Shen, M. Punyanitya, Z. Wang, D. Gallagher, M.-P. St-Onge, J. Albu, S. B. Heymsfield, and S. Heshka, “Visceral adipose tissue: relations between single-slice areas and total volume,” *Am. J. Clin. Nutr.*, vol. 80, no. 2, pp. 271–278, 2004.
[112] W. Shen, J. Chen, M. Gantz, G. Velasquez, M. Punyanitya, and S. B. Heymsfield, “A single MRI slice does not accurately predict visceral and subcutaneous adipose tissue changes during weight loss,” *Obes. Silver Spring Md*, vol. 20, no. 12, pp. 2458–2463, Dec. 2012.
[113] S. Lee, I. Janssen, and R. Ross, “Interindividual variation in abdominal subcutaneous and visceral adipose tissue: influence of measurement site,” *J. Appl. Physiol.*, vol. 97, no. 3, pp. 948–954, Sep. 2004.
[114] J. Ma, “Dixon techniques for water and fat imaging,” *J. Magn. Reson. Imaging JMRI*, vol. 28, no. 3, pp. 543–558, Sep. 2008.
[115] S. B. Reeder, C. A. McKenzie, A. R. Pineda, H. Yu, A. Shimakawa, A. C. Brau, B. A. Hargreaves, G. E. Gold, and J. H. Brittain, “Water-fat separation with IDEAL gradient-echo imaging,” *J. Magn. Reson. Imaging JMRI*, vol. 25, no. 3, pp. 644–652, Mar. 2007.
[116] M. Borga, E. L. Thomas, T. Romu, J. Rosander, J. Fitzpatrick, O. Dahlqvist Leinhard, and J. D. Bell, “Validation of a fast method for quantification of intra-abdominal and subcutaneous adipose tissue for large-scale human studies,” *NMR Biomed.*, vol. 28, no. 12, pp. 1747–1753, Dec. 2015.
[117] A. Schaudinn, N. Linder, N. Garnov, F. Kerlikowsky, M. Blüher, A. Dietrich, T. Schütz, T. Karlas, T. Kahn, and H. Busse, “Predictive accuracy of single- and multi-

slice MRI for the estimation of total visceral adipose tissue in overweight to severely obese patients," *NMR Biomed.*, vol. 28, no. 5, pp. 583–590, May 2015.
[118] H. H. Hu, J. Chen, and W. Shen, "Segmentation and quantification of adipose tissue by magnetic resonance imaging," *Magn. Reson. Mater. Phys. Biol. Med.*, pp. 1–18, Sep. 2015.
[119] H. Samouda, A. Dutour, K. Chaumoitre, M. Panuel, O. Dutour, and F. Dadoun, "VAT=TAAT-SAAT: Innovative anthropometric model to predict visceral adipose tissue without resort to CT-Scan or DXA," *Obesity*, vol. 21, no. 1, pp. E41–E50, Jan. 2013.
[120] P. Dandona, A. Aljada, A. Chaudhuri, P. Mohanty, and R. Garg, "Metabolic syndrome a comprehensive perspective based on interactions between obesity, diabetes, and inflammation," *Circulation*, vol. 111, no. 11, pp. 1448–1454, Mar. 2005.
[121] R. K. Masters, E. N. Reither, D. A. Powers, Y. C. Yang, A. E. Burger, and B. G. Link, "The impact of obesity on US mortality levels: the importance of age and cohort factors in population estimates," *Am. J. Public Health*, vol. 103, no. 10, pp. 1895–1901, Aug. 2013.
[122] R. K. Masters, D. A. Powers, and B. G. Link, "Obesity and US mortality risk over the adult life course," *Am. J. Epidemiol.*, vol. 177, no. 5, pp. 431–442, Mar. 2013.
[123] J. Cawley and C. Meyerhoefer, "The medical care costs of obesity: an instrumental variables approach," National Bureau of Economic Research, Working Paper 16467, Oct. 2010.
[124] R. J. Kuczmarski and K. M. Flegal, "Criteria for definition of overweight in transition: background and recommendations for the United States," *Am. J. Clin. Nutr.*, vol. 72, no. 5, pp. 1074–1081, Nov. 2000.
[125] Y. Matsuzawa, S. Fujioka, K. Tokunaga, and S. Tarui, "Classification of obesity with respect to morbidity," *Exp. Biol. Med.*, vol. 200, no. 2, pp. 197–201, Jun. 1992.
[126] J. M. Lyznicki, D. C. Young, J. A. Riggs, R. M. Davis, and Council on Scientific Affairs, American Medical Association, "Obesity: assessment and management in primary care," *Am. Fam. Physician*, vol. 63, no. 11, pp. 2185–2196, Jun. 2001.
[127] R. P. Wildman, P. Muntner, K. Reynolds, A. P. McGinn, S. Rajpathak, J. Wylie-Rosett, and M. R. Sowers, "The obese without cardiometabolic risk factor clustering and the normal weight with cardiometabolic risk factor clustering: prevalence and correlates of 2 phenotypes among the US population (NHANES 1999-2004)," *Arch. Intern. Med.*, vol. 168, no. 15, pp. 1617–1624, Aug. 2008.
[128] M. Kanazawa, N. Yoshiike, T. Osaka, Y. Numba, P. Zimmet, and S. Inoue, "Criteria and classification of obesity in Japan and Asia-Oceania," *Asia Pac. J. Clin. Nutr.*, vol. 11, pp. S732–S737, Dec. 2002.
[129] M. E. J. Lean, T. S. Han, and C. E. Morrison, "Waist circumference as a measure for indicating need for weight management," *BMJ*, vol. 311, no. 6998, pp. 158–161, Jul. 1995.
[130] "WHO | Obesity: preventing and managing the global epidemic," *WHO*. [Online]. Available:

http://www.who.int/entity/nutrition/publications/obesity/WHO_TRS_894/en/index.html. [Accessed: 25-Feb-2016].
[131] D. Canoy, B. J. Cairns, A. Balkwill, F. L. Wright, J. Green, G. Reeves, V. Beral, and for the M. W. S. Collaborators, "Coronary heart disease incidence in women by waist circumference within categories of body mass index," *Eur. J. Prev. Cardiol.*, p. 2047487313492631, May 2013.
[132] I. Janssen, S. B. Heymsfield, D. B. Allison, D. P. Kotler, and R. Ross, "Body mass index and waist circumference independently contribute to the prediction of nonabdominal, abdominal subcutaneous, and visceral fat," *Am. J. Clin. Nutr.*, vol. 75, no. 4, pp. 683–688, Apr. 2002.
[133] I. Janssen, P. T. Katzmarzyk, and R. Ross, "Waist circumference and not body mass index explains obesity-related health risk," *Am. J. Clin. Nutr.*, vol. 79, no. 3, pp. 379–384, Mar. 2004.
[134] T. L. Kelly, K. E. Wilson, and S. B. Heymsfield, "Dual energy x-ray absorptiometry body composition reference values from NHANES," *PLoS ONE*, vol. 4, no. 9, Sep. 2009.
[135] R. W. Taylor, I. E. Jones, S. M. Williams, and A. Goulding, "Body fat percentages measured by dual-energy X-ray absorptiometry corresponding to recently recommended body mass index cutoffs for overweight and obesity in children and adolescents aged 3–18 y," *Am. J. Clin. Nutr.*, vol. 76, no. 6, pp. 1416–1421, Dec. 2002.
[136] C.-H. Kim, H. S. Park, M. Park, H. Kim, and C. Kim, "Optimal cutoffs of percentage body fat for predicting obesity-related cardiovascular disease risk factors in Korean adults," *Am. J. Clin. Nutr.*, vol. 94, no. 1, pp. 34–39, Jul. 2011.
[137] N. Macias, A. D. Quezada, M. Flores, M. E. Valencia, E. Denova-Gutiérrez, M. Quiterio-Trenado, K. Gallegos-Carrillo, S. Barquera, and J. Salmerón, "Accuracy of body fat percent and adiposity indicators cut off values to detect metabolic risk factors in a sample of Mexican adults," *BMC Public Health*, vol. 14, no. 1, p. 341, Apr. 2014.
[138] J. J. Lee, S. N. Beretvas, and J. H. Freeland-Graves, "Abdominal adiposity distribution in diabetic/prediabetic and nondiabetic populations: a meta-analysis," *J. Obes.*, vol. 2014, p. e697264, Nov. 2014.
[139] M. Yumi, N. Toru, Y. Shuichiro, T. Yoshihiko, Y. Tetsuji, M. Tetsuya, and N. Mitsuhiko, "Visceral fat area cutoff for the detection of multiple risk factors of metabolic syndrome in Japanese: the Hitachi Health Study," *Obes. Silver Spring Md*, vol. 20, no. 8, pp. 1744–1749, Aug. 2012.
[140] J. A. Kim, C. J. Choi, and K. S. Yum, "Cut-off values of visceral fat area and waist circumference: diagnostic criteria for abdominal obesity in a korean population," *J. Korean Med. Sci.*, vol. 21, no. 6, pp. 1048–1053, Dec. 2006.
[141] B. M. Kaess, A. Pedley, J. M. Massaro, J. Murabito, U. Hoffmann, and C. S. Fox, "The ratio of visceral to subcutaneous fat, a metric of body fat distribution, is a unique correlate of cardiometabolic risk," *Diabetologia*, vol. 55, no. 10, pp. 2622–2630, Oct. 2012.

[142] J. Lin, L. Bardina, W. G. Shreffler, D. A. Andreae, Y. Ge, J. Wang, F. M. Bruni, Z. Fu, Y. Han, and H. A. Sampson, "Development of a novel peptide microarray for large-scale epitope mapping of food allergens," *J. Allergy Clin. Immunol.*, vol. 124, no. 2, p. 315–322.e3, Aug. 2009.
[143] J. C. Bezdek, R. Ehrlich, and W. Full, "FCM: The fuzzy c-means clustering algorithm," *Comput. Geosci.*, vol. 10, no. 2–3, pp. 191–203, 1984.
[144] P. J. Rousseeuw, "Silhouettes: A graphical aid to the interpretation and validation of cluster analysis," *J. Comput. Appl. Math.*, vol. 20, pp. 53–65, Nov. 1987.
[145] L. Kaufman and P. J. Rousseeuw, *Finding Groups in Data: An Introduction to Cluster Analysis*. John Wiley & Sons, 2009.
[146] I. Gat-Viks, R. Sharan, and R. Shamir, "Scoring clustering solutions by their biological relevance," *Bioinformatics*, vol. 19, no. 18, pp. 2381–2389, Dec. 2003.
[147] B. G. Tabachnick and L. S. Fidell, *Using multivariate statistics (5th ed.)*, vol. xxvii. Boston, MA: Allyn & Bacon/Pearson Education, 2007.
[148] C. Cortes and V. Vapnik, "Support-Vector Networks," *Mach. Learn.*, vol. 20, no. 3, pp. 273–297, Sep. 1995.
[149] C.-W. Hsu and C.-J. Lin, "A comparison of methods for multiclass support vector machines," *IEEE Trans. Neural Netw.*, vol. 13, no. 2, pp. 415–425, Mar. 2002.
[150] B. Scholkopf and A. J. Smola, *Learning with kernels: support vector machines, regularization, optimization, and beyond*. Cambridge, MA, USA: MIT Press, 2001.
[151] S. Amari and S. Wu, "Improving support vector machine classifiers by modifying kernel functions," *Neural Netw.*, vol. 12, no. 6, pp. 783–789, Jul. 1999.
[152] S. S. Keerthi and C.-J. Lin, "Asymptotic behaviors of support vector machines with gaussian kernel," *Neural Comput*, vol. 15, no. 7, pp. 1667–1689, Jul. 2003.
[153] F. E. H. Tay and L. Cao, "Application of support vector machines in financial time series forecasting," *Omega*, vol. 29, no. 4, pp. 309–317, Aug. 2001.
[154] C.-C. Chang and C.-J. Lin, "LIBSVM: A library for support vector machines," *ACM Trans Intell Syst Technol*, vol. 2, no. 3, p. 27:1–27:27, May 2011.
[155] R. KOHAVI, "A study of cross-validation and bootstrap for accuracy estimation and model selection," *Int. Jt. Conf. Artif. Intell. 1995*, pp. 1137–1143, 1995.
[156] H. Liu and H. Motoda, *Feature Selection for Knowledge Discovery and Data Mining*. Norwell, MA, USA: Kluwer Academic Publishers, 1998.
[157] I. Guyon and A. Elisseeff, "An introduction to variable and feature selection," *J Mach Learn Res*, vol. 3, pp. 1157–1182, Mar. 2003.
[158] H. Peng, F. Long, and C. Ding, "Feature selection based on mutual information criteria of max-dependency, max-relevance, and min-redundancy," *IEEE Trans. Pattern Anal. Mach. Intell.*, vol. 27, no. 8, pp. 1226–1238, Aug. 2005.
[159] C. Ding and H. Peng, "Minimum redundancy feature selection from microarray gene expression data," *J. Bioinform. Comput. Biol.*, vol. 3, no. 2, pp. 185–205, Apr. 2005.
[160] M.-C. Lee, "Using support vector machine with a hybrid feature selection method to the stock trend prediction," *Expert Syst. Appl.*, vol. 36, no. 8, pp. 10896–10904, Oct. 2009.

[161] H. O, P. S, and A.-O. E, “Metabolic obesity: the paradox between visceral and subcutaneous fat.,” *Curr. Diabetes Rev.*, vol. 2, no. 4, pp. 367–373, Nov. 2006.
[162] G. D. Ruxton and G. Beauchamp, “Time for some a priori thinking about post hoc testing,” *Behav. Ecol.*, vol. 19, no. 3, pp. 690–693, May 2008.
[163] M. B. Brown and A. B. Forsythe, “Robust tests for the equality of variances,” *J. Am. Stat. Assoc.*, vol. 69, no. 346, pp. 364–367, Jun. 1974.
[164] Y. Tang, Y.-Q. Zhang, N. V. Chawla, and S. Krasser, “SVMs modeling for highly imbalanced classification,” *IEEE Trans. Syst. Man Cybern. Part B Cybern.*, vol. 39, no. 1, pp. 281–288, Feb. 2009.
[165] N. Japkowicz, “The class imbalance problem: significance and strategies,” in *In Proceedings of the 2000 International Conference on Artificial Intelligence (ICAI*, 2000, pp. 111–117.
[166] E. Osuna, R. Freund, and F. Girosi, “Support vector machines: training and applications,” Mar. 1997.
[167] V. N. Vapnik, *The Nature of Statistical Learning Theory*. New York, NY, USA: Springer-Verlag New York, Inc., 1995.
[168] P. Jiang, S. Missoum, and Z. Chen, “Optimal SVM parameter selection for non-separable and unbalanced datasets,” *Struct. Multidiscip. Optim.*, vol. 50, no. 4, pp. 523–535, Jul. 2014.
[169] P. Hs, Y. Ys, P. Jy, K. Ys, and C. Jm, “Obesity, abdominal obesity, and clustering of cardiovascular risk factors in South Korea.,” *Asia Pac. J. Clin. Nutr.*, vol. 12, no. 4, pp. 411–418, Dec. 2002.
[170] B. Larsson, K. Svärdsudd, L. Welin, L. Wilhelmsen, P. Björntorp, and G. Tibblin, “Abdominal adipose tissue distribution, obesity, and risk of cardiovascular disease and death: 13 year follow up of participants in the study of men born in 1913.,” *Br Med J Clin Res Ed*, vol. 288, no. 6428, pp. 1401–1404, May 1984.
[171] V. J. Carey, E. E. Walters, G. A. Colditz, C. G. Solomon, W. C. Willet, B. A. Rosner, F. E. Speizer, and J. E. Manson, “Body fat distribution and risk of non-insulin-dependent diabetes mellitus in women the nurses’ health study,” *Am. J. Epidemiol.*, vol. 145, no. 7, pp. 614–619, Apr. 1997.
[172] J. P. Després, S. Moorjani, P. J. Lupien, A. Tremblay, A. Nadeau, and C. Bouchard, “Regional distribution of body fat, plasma lipoproteins, and cardiovascular disease,” *Arterioscler. Dallas Tex*, vol. 10, no. 4, pp. 497–511, Aug. 1990.
[173] A. R. Folsom, R. J. Prineas, S. A. Kaye, and R. G. Munger, “Incidence of hypertension and stroke in relation to body fat distribution and other risk factors in older women.,” *Stroke*, vol. 21, no. 5, pp. 701–706, May 1990.
[174] Rexrode KM, Carey VJ, Hennekens CH, and et al, “Abdominal adiposity and coronary heart disease in women,” *JAMA*, vol. 280, no. 21, pp. 1843–1848, Dec. 1998.
[175] C. M. Shay, M. R. Carnethon, T. R. Church, A. L. Hankinson, C. Chan, D. R. Jacobs, C. E. Lewis, P. J. Schreiner, B. Sternfeld, and S. Sidney, “Lower extremity fat mass is associated with insulin resistance in overweight and obese individuals:

the CARDIA study," *Obes. Silver Spring Md*, vol. 19, no. 11, pp. 2248–2253, Nov. 2011.
[176] D. W. Haupt, L. C. Rosenblatt, E. Kim, R. A. Baker, R. Whitehead, and J. W. Newcomer, "Prevalence and predictors of lipid and glucose monitoring in commercially insured patients treated with second-generation antipsychotic agents," *Am. J. Psychiatry*, vol. 166, no. 3, pp. 345–353, Mar. 2009.
[177] J. Y. Jang, S. D. Shin, E. J. Lee, C. B. Park, K. J. Song, and A. J. Singer, "Use of a comprehensive metabolic panel point-of-care test to reduce length of stay in the emergency department: a randomized controlled trial," *Ann. Emerg. Med.*, vol. 61, no. 2, pp. 145–151, Feb. 2013.
[178] A. L. Garcia, K. Wagner, T. Hothorn, C. Koebnick, H.-J. F. Zunft, and U. Trippo, "Improved prediction of body fat by measuring skinfold thickness, circumferences, and bone breadths," *Obes. Res.*, vol. 13, no. 3, pp. 626–634, Mar. 2005.
[179] J. C. Seidell, A. Oosterlee, M. A. Thijssen, J. Burema, P. Deurenberg, J. G. Hautvast, and J. H. Ruijs, "Assessment of intra-abdominal and subcutaneous abdominal fat: relation between anthropometry and computed tomography.," *Am. J. Clin. Nutr.*, vol. 45, no. 1, pp. 7–13, Jan. 1987.
[180] J. P. T. Higgins, S. G. Thompson, J. J. Deeks, and D. G. Altman, "Measuring inconsistency in meta-analyses," *BMJ*, vol. 327, no. 7414, pp. 557–560, Sep. 2003.
[181] A. M. Nevill, A. D. Stewart, T. Olds, and R. Holder, "Relationship between adiposity and body size reveals limitations of BMI," *Am. J. Phys. Anthropol.*, vol. 129, no. 1, pp. 151–156, Jan. 2006.
[182] J. J. Lee, J. H. Freeland-Graves, M. R. Pepper, M. Yao, and B. Xu, "Predictive equations for central obesity via anthropometrics, stereovision imaging and MRI in adults," *Obesity*, vol. 22, no. 3, pp. 852–862, 2014.
[183] S. Klein, D. B. Allison, S. B. Heymsfield, D. E. Kelley, R. L. Leibel, C. Nonas, and R. Kahn, "Waist circumference and cardiometabolic risk: a consensus statement from shaping America's health: Association for Weight Management and Obesity Prevention; NAASO, the Obesity Society; the American Society for Nutrition; and the American Diabetes Association," *Obesity*, vol. 15, no. 5, pp. 1061–1067, 2007.
[184] S. T. Johnson, J. L. Kuk, K. A. Mackenzie, T. T.-K. Huang, R. J. Rosychuk, and G. D. C. Ball, "Metabolic risk varies according to waist circumference measurement site in overweight boys and girls," *J. Pediatr.*, vol. 156, no. 2, p. 247–252.e1, Feb. 2010.
[185] H. C. McGill, C. A. McMahan, E. E. Herderick, A. W. Zieske, G. T. Malcom, R. E. Tracy, J. P. Strong, and for the P. D. of A. in Y. (PDAY) R. Group, "Obesity accelerates the progression of coronary atherosclerosis in young men," *Circulation*, vol. 105, no. 23, pp. 2712–2718, Jun. 2002.
[186] G. L. Vega, B. Adams-Huet, R. Peshock, D. Willett, B. Shah, and S. M. Grundy, "Influence of body fat content and distribution on variation in metabolic risk," *J. Clin. Endocrinol. Metab.*, vol. 91, no. 11, pp. 4459–4466, Sep. 2006.
[187] K. Goel, N. Gupta, A. Misra, P. Poddar, R. M. Pandey, N. K. Vikram, and J. S. Wasir, "Predictive equations for body fat and abdominal fat with DXA and MRI as

reference in Asian Indians," *Obes. Silver Spring Md*, vol. 16, no. 2, pp. 451–456, Feb. 2008.
[188] S. Demura and S. Sato, "Prediction of visceral fat area in Japanese adults: proposal of prediction method applicable in a field setting," *Eur. J. Clin. Nutr.*, vol. 61, no. 6, pp. 727–735, Dec. 2006.
[189] V. Brundavani, S. R. Murthy, and A. V. Kurpad, "Estimation of deep-abdominal-adipose-tissue (DAAT) accumulation from simple anthropometric measurements in Indian men and women," *Eur. J. Clin. Nutr.*, vol. 60, no. 5, pp. 658–666, May 2006.
[190] M. J. Toth, A. Tchernof, C. K. Sites, and E. T. Poehlman, "Menopause-related changes in body fat distribution," *Ann. N. Y. Acad. Sci.*, vol. 904, no. 1, pp. 502–506, 2000.
[191] N. R. Shah and E. R. Braverman, "Measuring adiposity in patients: the utility of body mass index (BMI), percent body fat, and leptin," *PLoS ONE*, vol. 7, no. 4, p. e33308, Apr. 2012.
[192] A. Myers and J. C. Rosen, "Obesity stigmatization and coping: Relation to mental health symptoms, body image, and self-esteem," *Int. J. Obes.*, vol. 23, no. 3, pp. 221–230, Mar. 1999.
[193] C. M. Grilo, D. E. Wilfley, K. D. Brownell, and J. Rodin, "Teasing, body image, and self-esteem in a clinical sample of obese women," *Addict. Behav.*, vol. 19, no. 4, pp. 443–450, Jul. 1994.
[194] M. B. Schwartz and K. D. Brownell, "Obesity and body image," *Body Image*, vol. 1, no. 1, pp. 43–56, Jan. 2004.
[195] S. A. Porter, J. M. Massaro, U. Hoffmann, R. S. Vasan, C. J. O'Donnel, and C. S. Fox, "Abdominal subcutaneous adipose tissue: a protective fat depot?," *Diabetes Care*, vol. 32, no. 6, pp. 1068–1075, Jun. 2009.
[196] K. S. Park, B. D. Rhee, K.-U. Lee, S. Y. Kim, H. K. Lee, C.-S. Koh, and H. K. Min, "Intra-abdominal fat is associated with decreased insulin sensitivity in healthy young men," *Metabolism*, vol. 40, no. 6, pp. 600–603, Jun. 1991.
[197] T. Hayashi, E. J. Boyko, M. J. McNeely, D. L. Leonetti, S. E. Kahn, and W. Y. Fujimoto, "Visceral adiposity, not abdominal subcutaneous fat area, is associated with an increase in future insulin resistance in Japanese Americans," *Diabetes*, vol. 57, no. 5, pp. 1269–1275, May 2008.
[198] Q. He, E. S. Engelson, and D. P. Kotler, "A comparison of abdominal subcutaneous adipose tissue pattern in obese and lean HIV-infected women," *J. Nutr.*, vol. 135, no. 1, pp. 53–57, Jan. 2005.
[199] G. E. Walker, B. Verti, P. Marzullo, G. Savia, M. Mencarelli, F. Zurleni, A. Liuzzi, and A. M. Di Blasio, "Deep subcutaneous adipose tissue: a distinct abdominal adipose depot," *Obesity*, vol. 15, no. 8, pp. 1933–1943, Aug. 2007.
[200] M. Rahman, J. R. Temple, C. R. Breitkopf, and A. B. Berenson, "Racial differences in body fat distribution among reproductive-aged women," *Metabolism.*, vol. 58, no. 9, pp. 1329–1337, Sep. 2009.
[201] J. F. Carroll, K. G. Fulda, A. L. Chiapa, M. Rodriquez, D. R. Phelps, K. M. Cardarelli, J. K. Vishwanatha, and R. Cardarelli, "Impact of race/ethnicity on the

relationship between visceral fat and inflammatory biomarkers," *Obesity*, vol. 17, no. 7, pp. 1420–1427, Jul. 2009.

[202] U. Lim, T. Ernst, S. D. Buchthal, M. Latch, C. L. Albright, L. R. Wilkens, L. N. Kolonel, S. P. Murphy, L. Chang, R. Novotny, and L. Le Marchand, "Asian women have greater abdominal and visceral adiposity than Caucasian women with similar body mass index," *Nutr. Diabetes*, vol. 1, no. 5, p. e6, May 2011.